FIBER OPTIC PROBES FOR BIOMEDICAL OPTICAL SPECTROSCOPY

Urs Utzinger and Rebecca R. Richards-Kortum

February 2001

Biomedical Engineering and Obstetrics & Gynecology, University of Arizona, Tucson, AZ 85724
Biomedical Engineering, The University of Texas at Austin, Austin, TX 78712

Address for Editorial Correspondence and Reprint Requests:

Urs Utzinger, PhD
Assistant Professor
Arizona Cancer Center, 1968 H
1515 N. Campbell
Tucson, AZ 85724
phone: (520) 626-9281
fax: (520) 626-9287
e-mail: utzinger@u.arizona.edu

Abstract

Fiber optic probes are a key element for biomedical spectroscopic sensing. This paper reviews the use of fiber optic probes for optical spectroscopy, focusing on applications in turbid media, such as tissue. The design of probes for reflectance, polarized reflectance, fluorescence, and Raman spectroscopy will be illustrated. This paper covers universal design principals, as well as technologies for beam deflecting and reshaping.

Keywords

Diffuse reflectance

Elastic scattering spectroscopy

Fiber optic sensors

Fluorescence spectroscopy

Inelastic scattering spectroscopy

Optical diagnosis

Probes

Polarized reflectometry

Raman spectroscopy

Reflectance spectroscopy

Resonance Raman spectroscopy

Spectrophotometry

Introduction

In the clinical environment, optical techniques (microscope, ophthalmoscope, endoscope, and colposcope) have been used for hundreds of years [1-5]. The integration of spectroscopic devices into existing optical examinations has the potential to substantially improve clinical practice. Fiber optic cables provide a flexible solution for an adequate optical interface between the spectroscopic device and the sample to be interrogated *in situ*. Fiber optic probes can be advanced into cavities and tubular structures, put in contact with epithelial surfaces, and inserted into structures that can be punctured by rigid devices such as needles. Fiber optic devices for optical spectroscopy can be manufactured as flexible catheters with an outer diameter of less than 0.5 mm. This paper reviews fiber optic probes for fluorescence, and elastic and inelastic scattering spectroscopy of turbid tissues. After describing the fiber optic interface, we describe probes for reflectance spectroscopy (diffuse reflectance and polarized reflectance), probes for fluorescence measurements, probes which combine fluorescence and reflectance measurements, and probes for Raman spectroscopy. Finally we review optical designs for side looking probes, diffuser tips and refocusing optics. The fiber optic probes discussed in this article have a biomedical application in mind. Probes with sensing elements for indirect measures such as pH and temperature will not be reviewed in this article.

The fiber optic interface

A spectroscopic system incorporates a light source, an optical analyzer with detector, and a light transport conduit which, in many cases, is made of fiber optic cables. A separate illumination and collection channel minimizes background signals produced in the illumination fiber (Fig. 1a). The excitation or illumination light source is typically a laser or a filtered white light source, such as a xenon or mercury lamp. Dielectric bandpass filters, monochromators, or double monochromators, can be used as filters according to the need for spectral purity. For fluorescence excitation with bandpass filters, xenon lamps with more than 150W power consumption require additional mirrors removing infrared (IR) light from the beam path (a cold mirror is used if the mirror deflects the main beam path by 90^{o} degrees) to protect the optical parts from excessive radiation. Pulsed light sources, such as lasers (e.g. nitrogen-pumped dye laser and optical parametric oscillators) or arc lamps release photons in short bursts and, combined with a gated detector

allow measurements under ambient light conditions. The coupling optics adapt the f-number of the light source to the numerical aperture of the fiber and guarantee optimal irradiance into the fiber. Laser radiation can be focused on a small spot compared to the imaging of a lightsource arc onto a fiber bundle. The probe transports the remitted light from the tissue to the spectroscopic system. New techniques, such as holographic transmission gratings (Holospec, Kaiser Optical Systems Inc, Ann Arbor) and back illuminated thinned charge coupled devices (CCDs) with high quantum efficiencies, allow short integration times and sufficient spectral and spatial resolution. Additional filter stages that are placed in front of the spectrograph reduce the influence of stray light originating from the excitation light source. For fluorescence applications, this filter stage holds longpass filters and for Raman spectroscopy holds notch filters.

To achieve the smallest probe diameters, single fiber solutions are used in combination with a dichroic beam splitter and well-aligned coupling optics (Fig. 1b). Single fiber solutions are limited because of the difficulty of reducing back-scattered excitation and illumination light at the fiber coupling site, and the suppression of autofluorescence induced in the fiber optic cable by excitation light. Nevertheless, single fiber-based probes require a minimal amount of components for the probe and can be used to create the smallest illumination spots as well as having excellent light collection efficiency.

Fiber optic lightguides

An optical fiber for spectroscopy consists of a core, a doped cladding, and a protective jacket. Light is transmitted based on the principle of total internal reflection. The half-angle (α) of the light cone that a fiber can accept is characterized by the numerical aperture (NA), which is defined by the difference in the refractive indices (n) of the core and the cladding material (Fig. 2):

$$NA = n_{media} \sin(\alpha) = \sqrt{n_{core}^2 - n_{cladding}^2} \qquad \textbf{Equation 1}$$

For transmission in the visible wavelength range, the optical fiber core is made out of glass or plastic (e.g. acrylic or polystyrene). The doped cladding is usually made of a similar material but with lower refractive index. Since light is not propagating in the cladding, losses due to absorption are less important. As soon as background signals introduced by the fiber itself become critical for the application, or the wavelength

range needs to be extended to the ultraviolet (UV) and infrared (IR), high-grade fused silica are used for the core material. All-silica fibers have a doped silica cladding, while plastic clad fibers have a silicone cladding. Optimized fiber preform manufacturing [6-10] allows transmittance from 200 nm (solarization-resistant-ultraviolet grade fiber, Polymicro Technologies Inc., Phoenix, AZ or Ceramoptec, East Longmeadow, MA) up to 2500 nm (low-hydroxyl fiber) and Sapphire fibers (Saphikon, Milford, NH) extend the transmission in the IR above 3000 nm. This allows the application of fiber optic probes for Ultraviolet Resonance Raman (UVRR) and IR Raman spectroscopies [11]. Due to bending of the fibers and defects in the fibers causing scattering, light may exit the core and hit the jacket. Most plastic jackets, such as Nylon and Tefzel®, produce significant autofluorescence when irradiated with UV light. Polyimide and metal-coated fibers, such as gold and aluminum, exhibit minimal fluorescence. During intense UV irradiation, defects may form in quartz fibers that are accompanied by autofluorescence in a broad band at both 450 and 650 nm [12]. The formation of these defects is partly reversible through diffusion processes occurring in the quartz glass. It is further known that silica produces intrinsic Raman signals at near infrared (NIR) excitation that interfere with *in-vivo* Raman spectroscopy. If background signals in spectroscopic measurements are present, the dynamic range of the detector can become critical [13]. For spectroscopic applications, multimode fibers with a core diameter of 50 μm to 600 μm are usually used. Short pieces (1-2m) of fibers with larger diameters can be produced in custom runs. The bending radius of quartz fibers in which no long-term defects result is approximately 100 times the fiber diameter and the momentary bending radius is approximately 50% of the long-term bending radius.

Fiber packing

In order to manufacture flexible fiber optic cables with a large optically-active area, fibers with a diameter of 100 to 200 μm are packed into bundles. The amount of fibers (n_{fiber}) that can be packed into a round cross section is illustrated in Figure 3. If fibers are packed hexagonally according ring a in Figure 3 the number of fibers is determined with:

$$n_{fiber} = 1 + \sum_{k=0}^{m} 6k \qquad \textbf{Equation 2}$$

Where m is the amount of rings around a central fiber. The total outer diameter (OD) is calculated by

$$OD_{total} = OD_{fiber}(1 + 2m) \qquad \textbf{Equation 3}$$

For hexagonal packing with additional fibers, according to ring b in Figure 3, equation 2 changes to

$$n_{fiber} = 1 + \sum_{k=0}^{m} 6k + 6m \qquad \textbf{Equation 4}$$

and the total OD is calculated by

$$OD_{Total} = OD_{fiber}\left[1 + \sqrt{3}(m + 1)\right] \qquad \textbf{Equation 5}$$

However, this is based on optimal arrangement of fibers which usually is not achieved under real manufacturing conditions. For a given bundle cross section, the dead space (inactive area) in between the fibers increases when the fiber diameter is reduced and reaches an upper value of 25% when more then 3 fiber rings are used. The inactive area additionally includes the area of the cladding and the jacket, which consumes normally more than 30% of the individual fiber cross section. If the jacket is stripped, this inactive area is reduced and the cladding accounts for approximately 17% of the fiber cross section. This leaves a total active area of approximately 60-65% in a tightly packed and optimized fiber bundle with stripped jacket material.

Beveled versus flat exit surface

To ensure optimal coupling, the end of fiber optic cable is cleaved or polished. If the exit surface is polished with an oblique angle in respect to the fiber axis, the output will be deflected (Fig. 4) (beveled fibers). If the critical angle for total internal reflection is reached, the light will leave the fiber through the cylindrical side (Figs. 4d, 4e) [14-16]. The critical angle (Fig. 4d) for the silica-air interface is 43.3^{o} and for the silica-water interface is 66^{o}. A fiber with a combination of a beveled and a flat polished tip [17], (Gaser Technology, Visionex Inc., GA; product no longer available) can also be used for deflection (Fig. 4f) as one part of the beam is exiting in the direction of the fiber axis while another part is guided sideways. To allow a larger range of steering angle, the beveled surface of the fibers can alternatively be coated (e.g. aluminum).

Beveled fiber applications for probe designs have been theoretically and experimentally analyzed by Cooney [18, 19]. The sensitivity and sampling volume of beveled fibers was compared to other designs, such as single fibers (Fig. 4g) flat tipped probes (Fig. 4h), and probes with lenses. The sensitivity and sampling volume was measured in a clear medium and results were reported for the collection of Raman scattered light and are also applicable for fluorescence collection. A probe consisting of two beveled fibers (Fig. 4i) is at least by a factor of 1.5 more efficient than a dual fiber with a flat tip probe (NA=0.22) and the sampling volume is smaller and located closer to the probe tip. A single fiber probe (Fig. 4g) is 1.8 to 4 times more efficient, depending on fiber diameter, than a dual fiber with a flat tip probe (Fig. 4h).

The efficiency of a "Gaser-type" collection fiber (Fig. 4f, 300 μm core) combined with a flat tip illumination fiber (Fig. 4j, 400 μm core) has been measured by Shim et al [17] with a sapphire Raman standard. Two configurations were considered: First, the light deflection angle of the "Gaser" fiber was between 13^{o} and 32^{o} (low deflection) and second, the deflection angle was between 35 and 55^{o} (high deflection). Compared to a flat tip probe, Shim et al found that, in air, a low deflection probe measures a 4 times and the high deflection probe a 16 times increased signal. In water, the factors were 6.5 and 28, respectively. Similar values were found in 0.25% and 0.50% Intralipid™ solution. For a flat tip probe with a 400 μm illumination fiber and a 300 μm pickup fiber, maximal signal was picked up at a distance between 1.7 and 1.4 mm from the tip in water or in the Intralipid™ solution. The low deflection probe received the largest signal at a distance of approximately 0.5 mm, and the high deflection probe at 0.25 mm from the fiber tip in water or the Intralipid™ solution.

The concept of dual fiber arrangement for separate illumination and collection can easily extend to a multifiber design, as shown in Figures 4k and 4l. The sampling volume of a single excitation fiber overlaps with concentric arranged collection fibers. Six collection fibers can be arranged around a single illumination fiber, which is equivalent to six dual fiber arrangements. To construct the probe tip, the fiber bundle is glued together and polished to a cone shape by rotating the probe axially while polishing. This design can be optimized for immersed operation (Fig. 4k) or for the interrogation of a surface (Fig. 4i). For

surface measurements, the tip needs to be enclosed and a quartz or sapphire window placed at the distal end (Fig. 4i). In general, collection and illumination channels are exchangeable.

Material choice and safety considerations

All fiber optic probes reviewed and presented in this study have a biomedical application in mind. The probe tip is either at close distance or in contact with the tissue surface or body fluids and, therefore, should be analyzed for potential hazards. An analysis of potential risks and protection against those risks is a requirement of human subject studies funded by the National Institute of Health (NIH). A guidance document, which is also helpful for the evaluation of hazards of fiber optic probes, was developed by the US Food and Drug Administration (FDA) for electro-optical detection of cervical cancer [20]. The list of potential adverse events which are applicable to the use of fiber optic probes are optical radiation hazards, thermal hazards, electrical shock hazards, clinical hazards (transmission of diseases), and material toxicity hazards. According a general evaluation of medical devices [21], fiber optic probes are most likely categorized as transient surface or transient external communicating devices and their materials should be tested for cytotoxicity, sensitization, and irritation, and depending on the application, for acute systemic toxicity. If the fiber optic probe is made of materials that have been well-characterized in published literature and have a history of safe use, there is adequate justification to not conduct some or all of the suggested tests.

Optical threshold limit values (TLV) or maximum permissible exposure (MPE) have been established to assist in the control of health hazards [22, 23] by the American Conference of Governmental Hygienists (ACGIH) and the American National Standard Institute (ANSI). The biologically-effective radiation (device emission weighted by the action spectrum which is normalized at 270 nm) should not exceed the TLV for skin and eye (which is 3 mJ/cm^2 at 270 nm for non-laser based devices). The TLV for skin and eye has also been recommended for the cervix. Potential temperature increases should be evaluated using endpoints or by potential peak tissue temperature. Since materials (fused silica, acrylic, polystyrene or silicone) used for fiber manufacturing are good electric isolators, a fiber optic probe with minimal shock hazard can be manufactured.

To avoid clinical hazards, such as the transmission of diseases, the fiber optic probe needs to be disinfected or sterilized prior to its use with common clinical practice. If the fiber optic probe cannot be detached from the spectroscopic equipment, the parts which may be in contact with tissue need to be soaked; for example, in a solution based on 2.4% gluteraldehyde (CIDEX, Advanced Sterilization Products, Irvine, CA) or 0.55% orthophthalaldehyde solution (CIDEX OPA). If a fiber optic probe is used during a surgical procedure, it can be covered with sterile drapes developed to cover ultrasound probes. Low temperature sterilization with ethylene oxide or hydrogen peroxide gas can be applied to a detachable probe. Most critical is the compatibility of the probe materials with the disinfectant. CIDEX OPA is a disinfectant that is compatible with most materials used to manufacture fiber optic probes, including adhesives cyanoacrylate (super glue) or Epotek 353 and Epotek 301 (Epoxy Technology, Billerica, MA).

A variety of materials that can be used to enclose the fiber optic probe have been well characterized and their biocompatibility has been previously published in the literature. Safe choices are materials created for implants or materials that were tested for U.S. Pharmacopoeia (USP), class VI. USP, class VI, is a base requirement for medical device manufacturers. A summary of materials that could be used to create fiber optic probes are listed in Table 1. One of the first alloys created for human use was stainless steel Type 302 and the corrosion resistance improved stainless steel Type 316 (hypodermic steel) [24]. A large variety of standard tubing diameters and wall thicknesses are available to enclose fiber optic cables and optical elements. Aluminum oxide Al_2O_3 is an inert bioceramic and, when grown to a crystal (sapphire), is chemically inert and almost insoluble. Sapphire has a high thermal conductivity and is optically transparent between 200 nm and 3 μm. EPOTEK produces a variety of glues with excellent transmission (301-2 and 307) and with low autofluorescence (301-2FL) that can be used to bond optical elements within the fiber optic probe. Several glues from EPOTEK were tested for USP class VI and are autoclavable (e.g. 353 and 375). Many thermoplastic polymers have been used in the body, for example, polyethylene (PE), polytetrafluoroethylene (PTFE, Teflon), polymethylmethacrylate (PMMA), and polyester (PET). These materials can be used to create flexible and heat shrink tubing or plastic enclosures for fiber optic probes.

High temperature resistant polymers include polyimide (220^{o}C), PTFE (230^{o}C), and silicone rubber (200^{o}C).

Reflectance probes

The elastically scattered light that escapes the surface of the sampling volume is called reflectance [25]. The transport mean free path (mfp) length of a photon in a turbid media is defined as:

$$\mathrm{mfp}' = \frac{1}{(\mu_a + \mu_s')} \qquad \textbf{Equation 6}$$

where μ_a is the absorption coefficient and μ_s' is the reduced scattering coefficient, which represents the isotropic approximation of anisotropic scattering.

The reduced scattering coefficient is defined as:

$$\mu_s' = \mu_s(1-g) \qquad \textbf{Equation 7}$$

where g is the average cosine of the scattering angle probability and μ_s is the scattering coefficient. The optical properties μ_s, μ_a and g depend on the chemical and structural composition of the sample. The absorption coefficient is a superposition of individual chromophores. Since the major chromophores in tissue are oxy, deoxygenated hemoglobin [26, 27], and water, as well as other absorbers such as melanin and bilirubin, it is possible to derive diagnostic parameters from the absorption coefficient, such as total blood concentration and average blood oxygenation [28]. The structural composition of the sample is reflected in the shape, structure, size distribution and concentration of the scattering particles. The reduced scattering coefficient shows a linear dependency with wavelength when transformed in double logarithmic space. The power constant (slope in double log space) is related to the average scattering size [29, 30], and the average scattering size may be related in tissue to the ratio of the nucleus to cytoplasm. All these characteristics vary spatially and are wavelength dependent.

There are several methods to measure absorption and scattering properties in the time domain, frequency domain and steady state by analyzing reflected or transmitted light. Here, we focus on steady-state spatially resolved measurements of a reflectance profile from a point source or a narrow collimated light beam. This profile can be measured with a contact fiber optic probe. Measurements with fiber optic probes are simple and inexpensive, however, they require contact to the tissue which can induce variations because the applied pressure affects local blood content in tissue [31].

Diffuse reflectance probes

Several recent studies have suggested that differences in the optical properties assessed using diffuse reflectance spectroscopy can be used to discriminate normal and abnormal human tissues *in vivo* in the urinary bladder [32, 33], pancreas [34], esophagus [35, 36] , colon [37, 38], ovaries [39], breast [40] and the skin [41], using simple fiber optic probes.

In order to extract absorption and scattering properties from reflectance measurements, spatially resolved reflectance intensities need to be obtained. This data is then fitted to an analytic expression, which is based on diffusion theory with the assumption that the sample is homogenous and semi-infinite [28, 31, 42, and 43]. When this approximation is compared with Monte Carlo based photon propagation simulations [44-46], it can shown

that at source detector separations smaller than $\frac{1}{\mu_s'}$ [42] to $\frac{1.5}{\mu_s'}$ [43], significant deviations occur.

Therefore, optical properties are normally derived from reflectance profiles measured at six to nine source detector separated locations. For tissue, the separation distances are in the range of 2 – 20 mm. The fiber optic probes used for these studies consist of a single excitation source and several spatially distributed collection fibers (Fig. 5a, b, c). A probe with linear alignment was constructed by Wang et al [47-48] and places the detection fibers over a range of 1 to 10 mfp' (Fig. 5a). Bays et al [49] used a scanning approach with a side deflected illumination fiber and collection fiber that can be translated axially (Fig. 5b). A black mask was printed on the measurement window and defined measurement locations. The scanning range was 27 mm. Alternatively, a circular fiber arrangement (Fig. 5c) by Nichols et al [50] allows a simple

calibration of the system by placing a source fiber in the center of all fibers. Measuring the spectrally-resolved reflectance of all fibers simultaneously requires a dynamic range of 4 orders of magnitude. Neutral density filters in the fiber optic path reduce the required dynamic range of the detector. Our approach to measure reflectance with a source-detector separation from 200 μm to 3 mm requires three different integration time settings (150ms, 2s and 9s), and sufficient spacing in between the fibers on the CCD detector to prevent blooming, and an increased number of detection fibers for larger source-detector separations. Fiber tracks are electronically binned on the CCD to detect lower light levels [51]. Wang et al [48, 52] modified their linear probe design with an oblique incident source fiber and measured the shift of the reflectance profile. This removes the necessity of measuring in absolute units. All fiber optic probes that measure reflectance profiles in the diffusion regime have a diameter of approximately 2 cm and the assumption is made that the optical properties do not vary over this range. However, the optical properties of currently investigated target areas (e.g. cervix, ovaries, and oral cavity) vary over orders of millimeters (lesion size) and the organ size is similar to the diameter of the proposed probes. Therefore, an accurate measurement of optical properties from small, premalignant lesions requires other approaches.

To overcome limitations of the diffusion theory, heuristic approaches, such as Monte Carlo trained neural networks [31, 53, and 54] have been investigated to obtain optical properties. Accurate numerical light-propagation can be modeled outside the diffusion regime with various forms of multivariate analyses [55]. Also hybrid approaches [56, 57] were proposed that combine diffusion theory and Monte Carlo calculations to predict reflectance profiles over a wide range of source-detector separations. Recently, Dam et al [58] presented a probe design with 6 short source-detector separations between 0.6 and 7.8 mm. The probe measures at 4 different wavelengths. Using a multiple polynomial regression model, absorption and scattering could be predicted with an error of roughly 3% for absorption and 1.5% for scattering. Bevilacqua et al [59, 60] have investigated short source-detector separated reflectance measurements and explained their sensitivity to the scattering phase function. Their probe diameter is 2.5 mm and incorporates eight linearly-aligned 300 μm diameter fibers. He found that for source detector separations between $\frac{0.5}{\mu_s'}$ and $\frac{10}{\mu_s'}$, the reflectance profile is not only depending on the average cosine of the

scattering phase function, but also on the second momentum of the phase function. It is still difficult to determine absorption accurately if only reflectance profiles are available [59], however, if the ratio of second and first momentum is known, absorption and scattering can be derived accurately from the reflectance intensity and the spatial slope of the reflectance intensity profile.

Mourant et al [61, 62] have shown that for certain source-detector separations, the path length of the collected photons does not depend on scattering parameters. For experimentally verified μ_a of 0–0.86 cm^{-1} a source-detector separation of approximately 1.75 mm is mainly sensitive to changes in absorption. Scattering parameters for this investigation were in the tissue relevant range for visible light ($7.5 < \mu_a' < 15\ cm^{-1}$ and $0.8 < g < 0.95$). The NA (0.2 or 0.34) of the fibers did not affect these findings. Drezek et al [63] found that changes in neoplastic cells mainly affect high scattering angles which can best be detected with a source-detector separation smaller than 500 μm and an NA of the fibers smaller than 0.4.

Both scattering and absorption properties of tissue can contain diagnostic information relevant to tissue pathology. Variations in scattering are due to inhomogeneities in the refractive index; recent results [63, 64] have shown that tissue backscattering is altered as the size of the nucleus increases and the nuclear texture becomes coarser. In case of spherical scatterers, a periodic structure in the reflectance spectrum is characteristic and depends on relative scattering size and collection and illumination geometry [36, 65]. This periodic structure can be theoretically derived by evaluating the scattering phase function at the angle corresponding with the angle between illumination and collection direction for every wavelength.

A probe to collect data which measures reflectance at a single point is shown in Figure 5d. A wedge is put in front of a fiber bundle to reduce specular reflection in the detection path [66]. Reflected light from the glass tissue interface is absorbed on the sides of the wedge (black paint or glue mixed with carbon powder). If the angle of the wedge is chosen carefully, light that is specularly reflected back onto the fiber bundle will reach it with an angle that is larger than the acceptance angle of the fibers and will therefore not be transported to the detector.

Polarization reflectometry probes

Polarization techniques have been successfully used to gate detection depth in reflectometry. This is particularly interesting because the origin of epithelial neoplastic changes is within the first 100-300 micrometers of tissue and neovascularization is originating in deeper tissue layers. Reflectance measured in a parallel-polarized fashion contains mainly light scattered from upper tissue layers, since light from the deeper tissue layers is multiple scattered which randomized the polarization status. Light loses its original polarization status after approximately 20 scattering mfp lengths ($1/\mu_s$) and becomes unpolarized in the diffusing regime [67, 68]. Cross polarized reflectance originates from deeper tissue layers since the polarized illumination light needs to undergo several scattering events until significant components are created in perpendicular polarization direction. Subtracting the perpendicular polarized reflectance from the parallel polarized, removes 90% of light originating from deeper tissue layers [69]. Dividing this subtracted reflectance by the sum of the parallel and perpendicular polarized reflectance cancels common attenuation and the spectral characteristics of the light source and detector. Jacques et al [69] used this technique for polarization imaging to detect basal cell carcinoma in highly pigmented tissues. Syris Scientific, LLC (Gray, ME) and Cytometrics Inc. (Philadelphia, PA) use an orthogonal polarized imaging technique to enhance signal from deeper tissue layers and to reduce surface specular reflections. [70]

Fiber optic probes which measure polarized reflectance consist of a polarization filtered white light source and a polarization filtered detection system with an optical multichannel analyzer (Fig. 5e). Since multimode fibers do not conserve the polarization status of light, the polarization filters need to be placed at the fiber optic probe tip. Johnson et al [71] presented a system which measures reflected light at four positions though a linear polarizer. Linear polarizing laminated film (Edmund Scientific, Barrington, NJ) was placed in front of the fibers. Suppression of different polarization modes was in the order of 98-99%. Ideally, in a polarization filtered probe, two or more pieces of polarization film are placed on the probe tip (as shown in Figure 5f and 5g). It is expected that light from fibers (b) and (c) do not return the same intensities. Also fiber positions (d) and (e) will collect less light than locations (b) and (c). This is illustrated in Fig. 5h for the case of one small scattering particle. It can be deducted that parallel polarized

location (b) will exhibit highest intensity. In this simplified model, location (c) should receive $\sin^2(\theta)$ less light and locations (d) and (e) would require several other scattering events until the scattering plane is aligned with the polarizing filter. The light intensities detected in these fibers can be calculated with Monte Carlo simulations that consider the propagation of polarized light [72, 73]. The probe design from Johnson et al [71] incorporates a single polarization film covering all 5 fibers. For diagnostic purposes, the polarization ratio of light collected from fiber (b) and (c) was formed. This design is similar to Fig. 5g, with fibers (d) and (e) covered with the same polarization film as fibers (b) and (c). The distance between the fibers is critical for such measurements, as described by Gurjar et al [74] and Backman et al [75]. It is desirable to keep the angle between the axis of the illumination and collection path small. This prevents photons from entering the detection channel after one scattering event in a cross-polarized setup. If the angle is larger, after one scattering event, the projection of the field vector can result in a component that pass the polarization filter. Small source-detector fiber separations are most sensitive to changes in the scattering phase function at high angles [63]. Sokolov et al [76] presents *in-vitro* results with a system similar to Fig. 5e. Data from phantoms and cell suspensions was represented in a linear combination of forward and backward scattering components which were determined by the Mie theory. A fiber optic probe was designed based on this study (Fig. 5i and 5j) and characterized *in vivo.* [77] A laminated polarization film was mounted with microscope guidance onto a fixture holding three 200 μm diameter fibers. Clear tape with adhesive on both sides was very useful in mounting the filters, because the tape is transparent and the filters could be visualized with a light microscope. A glass cover and rigid tubing encapsulate the construction. If the measurement and illumination spot have to overlap on the sample surface, the shield thickness could be increased. An increased shield thickness results in specular reflections from the shields exit surface. Tilting the reflective surface, in respect to the optical axis, prevents reflected light from coupling back into the fibers. Alternatively, an optical lens can be placed in front of the probe similar to Fig. 14a (section Refocusing), or a conical reflector (Fig. 5k) could align the beam path. If reflectors are used to align the illumination and measurement path, linear polarized light will be converted into elliptical polarized light if the light is not purely linear polarized. This will make construction with mirrors challenging.

Fluorescence probes

A growing number of clinical studies have demonstrated that fluorescence spectroscopy can be used to distinguish normal from abnormal human tissues *in vivo* in the head and neck [78-88], cervix [89-99], skin [83,100-105], bladder [106-112], bronchus [113-116], esophagus [116-122], colon [116, 119-138], breast [139-145], brain [146-151] and artery 78, 151-162]. Recent reviews [86, 91, 120, 127, 128, 130, 145, 163-171] provide an overview of studies using fluorescence spectroscopy. It is well known that fluorescence intensity and line shape are a function of both the excitation and emission wavelength in samples such as human tissue containing multiple chromophores. Major fluorescence contributors are structural proteins such as elastin and collagen, pyridine nucleotide (NAD(P)H), flavoprotein (FAD), tryptophan, and porphyrins [164, 171].

Single pixel measurements

The classic fiber optic probe to measure fluorescence consists of at least one excitation and one collection fiber (Fig. 4h or 6a). A quartz shield placed at the distal end of the fibers (Fig. 6a item (f)) allows the illuminated and probed area to overlap. The fraction of overlapping increases with an enlargement of the numerical aperture of the fibers and the thickness of the shield. A larger shield thickness requires a larger diameter shield. A typical shield thickness is 1 mm – 7 mm. If a shield is omitted, fluorescence can still be detected but will originate from deeper layers because the average photon path length is increased. Such a design has been used to measure skin fluorescence [105].

The collection efficiency β_t for a fiber optic probe describe in Figure 6a can be described as:

$$\beta_t = \frac{\beta_0}{(z + \text{shield}_t)^2} \qquad \textbf{Equation 8}$$

where z is the position along the optical axis of the probe and β_0 is a constant which includes the detector efficiency [97]. Previous studies performed in arterial tissue have demonstrated empirically that tissue does not emit isotropically as a result of highly forward scattering [172, 173]. For arterial specimens, tissue fluorescence power decreases with the shield thickness as $\frac{1}{shield_t^{\,n}}$, where n is approximately 1.1.

Pfefer et al [174] have shown the influence of the fiber diameter and shield thickness to probing depth and remittance at 337 nm excitation, 450 nm emission, and at 400 nm excitation, 630 nm emission. The simulation consisted of a single fiber delivering excitation and collecting fluorescence (Figs. 4g and 6b). The Monte Carlo simulations assumed typical optical properties for esophageal tissue. The remittance (337 nm excitation, 450 nm emission) increased with increasing fiber diameter and was 0.11% for 0.1 mm fiber diameter and was 0.4% for 1 mm fiber diameter when the fibers were placed in direct contact with the tissue. 80% of the fluorescence signal originated between the tissue surface and a depth of 0.175 mm when a 0.1 mm diameter fiber was used. A 1 mm diameter fiber collected from deeper tissue layers and 80% of the fluorescence signal originated between the tissue surface and a depth of 0.375 mm. Placing a shield in front of the fibers increased the probing depth further. With a 5 mm thick shield, 80% of the fluorescence was collected between the surface and 0.425 mm for fibers with 0.2 - 1 mm diameter, while the collected fluorescence dropped by a factor of 20 for the 0.2 mm fiber and a factor of 5 for the 0.6 mm diameter fiber. Similar results were found at 400 nm excitation wavelength with the probing depth increased by approximately 20%. This indicates that by varying the excitation and emission aperture one may be able to identify depth variations in fluorophore concentrations.

A typical probe with the design presented in Fig. 6a consists of excitation fibers, collection fibers, carbon filled or low fluorescent epoxy, and tubing. A rigid type uses metallic tubing and a flexible type uses shrink tubing (Zeus Industrial Products, Inc). A probe with an outer diameter of 4 mm, as presented in Fig. 6c has been successfully used by Ramanujam et al [94] in a study with more than 100 patients. The shield and a sleeve are detachable to disinfect the probe. With the classical design, a probe based on seven 200 μm fibers has a diameter of at least 1.5 mm.

Minimizing the outer diameter

For an improved detection and illumination spot overlap, the shield in front of the probe is replaced with a coated glass rod or a thick piece of optical fiber (Fig. 7a). It acts as a mixing element, homogenizing the output of the probe, with two major benefits: During manufacturing, illumination and collection fibers can be randomly mixed and the outer diameter of a probe is reduced and limited by the number of excitation

and emission fibers only. Simple probes with minimal diameter can be assembled by stripping the jacket from the excitation and emission fibers, bundling the fibers with glue, and attaching a glass rod with shrink tubing (Fig. 7b). The length of this rod should exceed $\frac{2R_{fiber}}{NA}$ to allow a uniform illumination.

Innova Quart (Phoenix, AZ) has successfully manufactured fiber optic tips using CO_2 laser micro-machining. Melting and compressing fibers in a fiber bundle eliminates the dead space in between the fibers. An increase of power density and almost complete overlap in between illumination and collection areas was reported. However, this technique is currently limited to fiber bundles with a few fibers only.

Multi-pixel measurements

With a single pixel measurement one can obtain spectroscopic information of a small tissue volume and, based on the performed analysis, a classification of the measurement location is possible. However, for many biomedical applications, a tissue surface area needs to be investigated, either to determine the extent of a lesion or to identify the location of potential lesions. Pitris et al [175] and Agrawal et al [176] have successfully adopted the principle of a single pixel fluorescence spectroscopy measurement to a measurement that interrogates 31 locations simultaneously (Fig. 8a, b). For that purpose, the traditional single pixel measurement is conducted in parallel and data is obtained from a static pattern of pixel locations. Several spectroscopic measurements can be conducted simultaneously with modern aberration corrected imaging spectrographs. Combined with a large focal plane CCD detector (e.g. 30 x 12 mm), these spectrographs can disperse up to 30 and more input channels with minimal cross-talk. The average pre-cancerous lesion size, for example, of the cervical epithelium is between 1 and 2 mm. This means that for the screening of the cervix one does not need a high spatial resolution and can use fiber optic multi-pixel probes. The outer diameter of the probe in Fig. 8b is 1 inch and the shield thickness is ¼ inch. In order to cover the whole cervix (which is approximately 3 cm in diameter), this probe was placed onto 4 quadrants separately [177]. Figure 8a shows a schematic arrangement of a multi-pixel probe consisting of several 6 around 1 single pixel probes, while Fig. 8b shows the actual implementation with a single excitation and collection fiber. As proposed in Fig. 8a, using several excitation fibers for each collection fiber increases the illumination intensity. An estimation based on commonly-used equipment and the

previously-introduced formula for hexagonal packing shows that more than 500 fibers with a core diameter of 200 μm can be successfully located in a spot created by a standard 300W xenon lamp. The focal spot size of the excitation source at the coupling site is determined by the arc size, which is typically in the order of 0.5-3 millimeters. A 300W xenon lamp with a parabolic reflector (Compact Illuminator 6000CI, ORC) produces a spot diameter of approximately 7 mm when a lens with a focal length of 50 mm is used.

Fiber optic multi-pixel systems have been recently presented by the private sector [178, 179]. An advanced system that can measure fluorescence and reflectance spectra at 120 locations was introduced by Nordstrom et al [178]. This system incorporates imaging optics and a laser scanning device that can simultaneously illuminate 6 excitation channels out of 120 rectilinear aligned fibers. In order to investigate even larger surface areas, researchers have proposed systems that do not rely on fiber optic probes, such as a flying spot scanner [180], or the use of imaging techniques [181].

Influence of illumination and detection spot separation

Keijzer et al [157] described scattering and detection of fluorescence from arterial tissue outside the illumination spot experimentally and theoretically (Fig. 8c). β and α absorption bands of oxygenated hemoglobin alter the fluorescence spectra. Avrillier et al [182] described the same effect and called the fluorescence distortions “media function”. In experiments with a separate excitation and fluorescence collection fiber (200 μm in diameter), they showed that when brain is excited at 308 nm, the fluorescence ratio at 360 nm and 440 nm emission decreases with increased fiber separation (2.8 for 250 μm, 2.5 for 500 μm, and 2.4 for 750 μm. Pfefer et al [174] have investigated the average probing depth in esophageal tissue when fluorescence is collected outside the excitation spot. They simulated an excitation fiber with a diameter of 100 μm and found that inside the excitation fiber area, the collected fluorescence was very sensitive to superficial layers, however the first 50 μm outside the excitation area, the detected fluorescence, is mainly originating from a depth of 125 μm, while the intensity dropped by approximately a factor of 2.5 compared to the intensity within the excitation area. Absorption in the fluorescence distortion function and, hence, the spectral shape variations are enhanced when the excitation and collection fibers

are separated further [182]. This may be useful to detect neovascularization with fluorescence spectroscopy. In contrast, when multi-pixel fluorescence measurements are conducted in parallel, the spacing of the collection spots and the shield thickness have to be chosen carefully to minimize cross-talk between the measurement channels.

Combined probes fluorescence and reflectance spectroscopy

It is well known that the absorption and scattering properties of tissues *in vivo* affect both the intensity and lineshape of measured fluorescence spectra [164]. Furthermore, measuring both fluorescence and diffuse reflectance spectra may provide additional information of diagnostic value [183]. Durkin et al [183] have described a probe that combines the measurement of fluorescence and optical properties. Scattered light is collected with a white light "transmission" measurement. This light travels through the same tissue volume which is excited for fluorescence measurements. The probe, as illustrated in Fig. 9a and 9b, consists of a total of 21 optical fibers (200 μm diameter, NA=0.2) arranged in concentric bundles. The center bundle contains seven fluorescence excitation fibers and twelve fluorescence collection fibers. At the distal end of the probe, the fibers which excite and collect fluorescence are sealed with a quartz shield. This shield is placed in contact with the sample surface and ensures that the area from which fluorescence is collected is the same as that illuminated for reflectance measurements. The reflectance fibers are flush with the tip of the central shield. Similar attempts have been described in the literature [168, 184].

The authors attempt [50, 185] to measure combined fluorescence and reflectance resulted in a probe with a mixing element for the fluorescence channel, 4 different source-detector separations and visual illumination for probe placement (Fig. 9c). The current probe consists of 46 fibers: 25 for fluorescence excitation, 12 for fluorescence, and 9 for reflectance collection. Reflectance is measured in a circular fashion with fibers placed at 200 μm, 1.1, 2.1 and 3 mm distance to the source fiber (Fig. 9d). The detection fibers are linearly aligned in the spectrograph ferrule (Fig. 9e). For fluorescence measurements, all emission collection fibers are binned on the CCD chip, while for reflectance measurements all fibers are imaged with appropriate resolution. The outer diameter is smaller than 5 mm which allows to measure through a trocar shaft in the peritoneal cavity (Fig. 9f).

Probes for Raman spectroscopy

Near-infrared Raman scattering can be used as a tool to perform *in situ* histochemical analysis [11, 13, 186-205]. In biological applications, approximately 10^{-10} of the incident light is Raman scattered and the Raman signal is normally 6 orders of magnitude weaker than typical fluorescence signals. The amount of light that can be delivered to the sample area is limited due to heating hazards. The design of a fiber optic probe for Raman spectroscopy is driven by maximal light collection. Additionally, background signal originating from the laser source, the fibers and all optical components can fill the dynamic range of the detector and overwhelm the Raman signal [13, 206]. These signals must be reduced with filters to accomplish sensitive *in-vivo* measurements. The dynamic range of the detector can also be enlarged with multiple readings that reduce the noise by the square root of the number of readings. Currently, Raman spectra of tissues are recorded *in-vivo* in less than 5 seconds [207].

A design developed by Myrick and Angel (Fig. 10a) [208, 209] is based on GRIN lenses. Filters are placed in the excitation and emission path and allowed remote analysis with fiber optic cables. The light source is bandpass filtered to eliminate signals produced in the fibers, and a longpass filter reduces specular reflections and elastically scattered light that enters into the collection fibers.

A similar approach is shown in Figure 10b. A probe developed by Savannah River Technology Center (Aiken, SC) [210] consists of dielectric filters placed in between fibers that are held together with spring-loaded SMA connectors. Six collection fibers are arranged around an excitation fiber. They are arranged according to the drawings in Figure 4l. A sapphire window isolates the probe from the surrounding environment.

Berger et al [188] and Tanaka et al [211] have developed a design for improved signal collection to allow spectral acquisition in a short time. A compound parabolic concentrator (CPC) was used at the distal end of the probe. They produced a hollow shell, based on a mandrel, electrolytically. The mandrel followed an optimized parabolic form that was cut with a numerically controlled lathe. Small CPC dimensions with an

input aperture of 0.57, an exit aperture of 2.1 mm, and a length of 4.1 mm, were achieved (Fig. 10c). The probe design with the CPC improved the collection efficiency six-fold. This system incorporates a 500 mW tunable 830 nm-diode laser that was coupled with a mirror and a dichroic beam splitter onto the sample site. Inelastic scattered light exiting the CPC is further collimated with a lens and filtered by the dichroic mirror and additional filters. Field lenses prevent vignetting of the signal. The last lens images the output onto two hundred 100 μm fibers, which illuminate a f/1.8 spectrograph. The signal is detected with a back illuminated liquid nitrogen (LN)-cooled CCD. Spectral resolution is 13 cm^{-1}.

Mahadevan-Jansen et al [193, 194, 212] have successfully measured Raman spectra on the cervix with a fiber optic probe in less than 3 minutes (Fig. 10d) [193, 194, 212]. A diode laser is coupled into a single 200 μm fiber. A small diameter dielectric filter (3 - 4 mm) rejects out of band light (OD5) and a gold mirror deflects the focused beam onto the specimen site. The beam has to pass a quartz window which is a part of the housing. Scattered light from the same spot area is imaged with two biconvex lenses on a fiber bundle. Elastically scattered and specular reflected light is rejected with a beam aperture stop and a holographic notch filter (OD6). The optics in the detection arm are 8 mm in diameter and the whole probe diameter is less than 2 cm. A similar spectroscopic detection system is used, as described in Fig. 10c: The spectrograph with the holographic transmission grating (Holospec, Kaiser Optical Systems, Ann Arbor, MI) and the deep depletion, back illuminated, LN-cooled CCD allow optimal system performance. A similar two-legged probe is commercially available by InPhotonics (Norwood, MA). The design is further optimized by inserting a dichroic mirror that combines the excitation and collection light before focusing it onto the sample.

Kaiser Optical Systems has presented a commercially available fiber optic Raman probe (Fig. 10e) [213]. Excitation light is filtered though a transmission grating and can be monitored outside the probe head. The sample spot is imaged with two microscope objectives onto a fiber optic cable. Two Raman notch filters remove excitation light in the collimated beam path. The filters are arranged symmetrically to remove interference signals.

All of the described Raman probes include imaging optics to enhance the collection efficiency. This makes it difficult to correct the spectral throughput of the system with standardized light sources such as the tungsten filament lamp. The NA of the probe should be filled with light similar to tissue measurements. Therefore, the calibration light source has to be placed in focus of the imaging optics of the probe. This can be accomplished by measuring the diffuselyscattered light from a reflectance standard placed at the tissue location. If the calibration light source is not placed at the location of the measured tissue, light passes the probe optics differently than during tissue measurement conditions. This may result in the transmission of light outside the designed blocking areas of band pass filters or in increased scattering of light on non-optical surfaces inside the probe. The reflectance standard can be flat Spectralon disk or an integrating sphere with an entrance port for the calibration light source and an exit port for the probe.

Visionex Inc. developed a biomedical Raman probe based on fibers with beveled and flat tips (Fig. 4j). A central flat delivery fiber (400 μm diameter) is surrounded by seven beveled collection fibers (300 μm diameter). Furthermore, filters are incorporated onto the core of the fibers approximately 2.5 cm from the probe tip: a bandpass filter is placed in line with the delivery fibers and a longpass filter in line with the collection fibers. The fibers have a NA of 0.22. Small probe diameters and excellent collection efficiency has been reported from this probe [17]. It can easily be configured for fluorescence and reflectance measurements.

The scattering cross section for Raman interactions is increased dramatically if excitation is in resonance with the electronic transitions of the chromophore involved in the vibration. For many biologically relevant chromophores, these transitions are in the UV. Resonance enhancements are on the order of $10^4 – 10^5$ for UV absorption bands [11]. To measure these phenomena with fiber optic probes, the inherent signals produced in the delivery and collection system are problematic. The Raman group [16] at the University of British Columbia has successfully built a fiber optic probe for UV resonance Raman spectroscopy (Fig. 10f). UV-grade and solarization-resistant UV-grade optical fibers [9] are used for the collection and excitation path, respectively. Their design incorporates an excitation fiber and an oblique polished fiber

with a larger diameter to collect the scattered light (600 μm). This configuration minimizes inner filtering (sample self-absorbance). Because solutions are investigated, a reflective surface based on a metallic coating is needed on the collection fiber. Aluminum reflects more than 90% at 250 nm.

Side looking probes and their application

As described earlier, oblique polishing of individual fibers deflects the output of the fiber in respect to the fiber axis (Fig. 4b-e). At the critical angle for total internal reflection, light will leave the fiber through the cylindrical side which focuses the beam in an angular direction resulting in an elliptical focal spot close to the fiber surface. In order to permit the light to leave the fiber sideways at the tip, the jacket needs to be stripped. Depending on the jacket material, it can be dissolved in acid, mechanically abraded, or burned away with a lighter.

Illumination analysis software ASAP (Breault Research Organization Inc., Tucson, AZ) shows maximal irradiance at a polishing angle of 40 degrees in air as surrounding media [214]. The distance between the focal spot and the fiber wall is 1.3 times the cladding radius. In water, this distance increases to 3.17 times the cladding radius. Since the critical angle for total internal reflection on the silica-water interface is 66^{o}, a 40^{o} polishing angle is not sufficient. For a side deflection with this geometry, the beveled fiber end surface needs to be coated with a reflective material. The increase of irradiance is 2.4 in air and 1.6 in water (Fig. 11a and 11b).

Enclosing a single oblique polished fiber into a glass capillary tube allows the production of minimal diameter deflecting probes. These off-the-shelf products (Innova Quartz, Phoenix, AZ) are manufactured for vaporization and coagulation of tissue but can also be used for spectroscopic applications (Fig. 11c).

If separate illumination and collection fibers are needed, the alignment of these fibers will be a tedious task. An example of separate illumination and collection fibers is shown in Fig. 11d. In order to produce this probe, fiber pairs are mounted in a cylindrical tube with grooves. A simultaneous investigation of sites

along the circumference of the probe is possible (ring probe). The fiber pairs need to be aligned flush and rotated so that the illumination and collection spot overlap. Shrink tubing or elastic bands could assist in this task.

Diffuser tips

With the approval of photosensitive drugs such as Photofrin® (QLT Photo Therapeutics Inc., Vancouver, Canada) by the FDA and clinical trials of many others, there is a need for fiber optic probes which provide a homogeneous illumination of large areas in canals and on surfaces. Diffusely scattering elements mounted at the end of fibers or fiber bundles distribute light over large areas. In addition to therapeutic applications, such as photodynamic therapy [215-228] and coagulation [229], diffuse light delivery systems can also be used for illumination during spectral measurements.

The scattering particles included in the diffuser elements are titanium (TiO_2) or aluminum oxide (Al_2O_3) which are embedded in a transparent matrix such as optical glue (Epotek 307, Epoxy Technology, Inc. Billerica, MA). Flexible containment is produced with micro-tubing based on fluorpolymers (PTFE, FEP from Zeus, Orangeburg, SC). Rigid tips are based on ceramics or materials similar to Spectralon (Labsphere, North Sutton, NH). If these materials are used in the UV wavelength range to deliver fluorescence excitation, the autofluorescence and transmission is of importance. FEP tubing (0.3 mm wall thickness) shows good transmission from 250 nm up to 2 μm (40%@250 nm, VIS 80-90%), while autofluorescence is an order of magnitude lower than tissue fluorescence. Some oxides such as Al_2O_3 or $BaSO_4$ emit fluorescence in the UV-VIS and can contribute to background signals.

An example diffuser is presented in Fig. 12a. Light exits the fiber optic bundle and enters a turbid cylindrical volume. Scattered light leaves this volume in a radial direction. A uniform light distribution along the optical axis is achieved with a reflector mounted at the end of the scattering volume. Light that would leave the probe in an axial direction is reflected back into the scattering material and undergoes further scattering events [229]. The length of the probe determines the concentration of scatterers (Fig. 12a and 12 b). Figure 12b illustrates a diffuser with a length of 30 mm and a diameter of less than 2 mm.

A probe to measure fluorescence spectra inside the endocervical canal was proposed by the authors and consists of a diffuser element and side looking fibers. In addition to the diffuser described above (Fig. 12a, and 12b), a reflective foil (aluminum or gold) placed around a diffuser tip restricts illumination in an angular direction. The foil is attached to the diffuser with thin-walled shrink tubing (Fig. 12c). For spectroscopic measurements inside the canal, oblique polished fibers probe the light emitted from the sample area. The collection fibers are bundled and, in order to probe different positions along the axis, each beveled fiber is retracted to a different axial position. The diffuser and the bundle with the collection fibers are placed adjacent. Since the illumination light exits the diffuser and needs to pass collection fibers, the absorbing jacket of the fibers needs to be removed.

A sapphire tip based ring probe

Sampling along the circumference of the probe is useful to identify the angular position of obstructions in tubes (e.g. arteriosclerosis) or for identification of lesions in tubular structures (e.g. dysplasia in the endocervical canal). A probe initially designed for radial ablation and simultaneous spectroscopic analysis [214] is illustrated in Fig. 13a and 13b. The fibers are glued onto a metallic ring (OD 2.4 mm, ID 2.05 mm). A hollow plug attaches internal flexible tubing for flushing and a guide wire. A custom made sapphire prism (Swiss Jewel, Tenero, Switzerland) is attached to the plug. The output of the fibers with a NA of 0.22 is totally deflected at the back surface of the prism. An outer flexible silicone tube seals the tip from the liquid environment. Two different outer diameters were realized: 1.4 and 2.8 mm. Fig. 13b shows the individual parts partially assembled. In the upper picture the outer tubing is not completely mounted. For spectroscopic measurements, smaller 100 μm fibers were integrated in between the ablation fibers (lower picture). The sealing of such a tip is a tedious task since only small amounts of glue can be used. Similar tips can be produced with vee-, ring-, orifice-, cup- and chisel-jewels (Swiss Jewel, Tenero, Switzerland; Sapphire Engineering Inc., Pocasset, MA; SWIP, Biel, Switzerland).

Refocusing

Refocusing the illumination or collection beam paths can serve several purposes: 1) to decrease the sample volume if the target is placed in focus, or 2) to increase the illuminated area if the target is placed outside the focus. A focused beam samples a smaller area and leads to increased illumination intensity. If light is collected through a focusing optic, it will encompass a larger solid angle. In contrast, if the area to be illuminated is large, a rapidly diverging beam is desirable. This can be accomplished by placing the sample behind the focal spot where light diverges. Concave and convex optical surfaces can be placed between the fiber exit and the tissue. Following, we present three different solutions with increasing complexity to refocus the beam of a fiber optic cable. First, the fiber tip is altered into a spherical shape, which is equivalent to adding a plano convex lens in front of the fiber. Second, spherical lenses image and concentrate the fiber output. Lastly, mirrors are used to redirect and focus the fiber output.

Spherical fiber tips

Melting the end of the fiber shapes the exit surface of optical fibers. An almost spherical surface will be created by the surface tension of liquid quartz [230]. Its form is determined by the volume of melted quartz which is related to the amount of absorbed thermal energy. A number of techniques are used to achieve this deformation: micro furnace, Bunsen micro-burner, electrical arc, and a CO_2 laser beam [231].

The smallest possible surface curvature is a hemisphere. Theoretical results of a beam exiting a hemispherical fiber tip in air and water are shown in Fig. 14a and b (modified from [14]). Because the refractive index of silica is 1.46, the focusing power is limited in aqueous media. Figure 14c illustrates the focusing of a fiber with a 200 μm core diameter and a NA of 0.22 in water. The beam in water is reduced to a quasi-parallel beam. A light intensity concentration was found at a distance 3 times the distal radius of curvature from the vertex. In simulations [214] the maximal irradiance was found to be 3 times the irradiance within the fiber. A fiber optic probe for spectroscopic measurements could be manufactured with a single fiber (Fig. 1b). The sampling area would be smaller then the fiber diameter and the solid angle of collected light larger than the NA of the fiber.

Ball lenses

Spherical ball lenses have been used as collimators in fiber optic connectors [232]. Sapphire spheres with a high refractive power are industrially produced in a wide range of diameters (Sandoz SA, Cugy, Switzerland; Rubis Precis, Charquemont, France). Light emitted from a fiber can be focused with this lens type onto the sample site (Fig. 15a and 15 b). Rol et al [14] found a maximal illumination intensity when the ratio of the back surface distance to the fiber and the radius of the sphere is in between 1.8 and 2.8 in water and air. Illumination analysis shows a maximal increase of the irradiance by a factor of 4.8 in water (Fig. 15c) and 5.7 in air (Fig. 15d). With increased fiber diameter, spherical aberrations will degrade the focusing of the beam because light will propagate outside the paraxial regime.

An example fiber optic probe (Fig. 15a) with a 200 μm core diameter fiber and a sphere with a radius of 0.4 mm will not exceed an outer diameter of 0.9mm (modified from [15]). The sphere and fiber can be held in a cylinder with a conic inner shape. For side looking applications, the same principle is used with a half sphere. If the plane is inclined by 45 degrees and the step in the refractive index is equivalent to sapphire-air, the beam will be deflected with total internal reflection at the interface and leave the probe at 90 degrees in respect to the probe axis. A micro quartz tube encloses the half sphere and provides air as refractive media. For spectroscopic measurements a setup as described in Fig 15(b) would be needed.

Spherical and parabolic reflectors

Mirrors can concentrate light [233]. The complex refractive index of a dielectric material defines the absorption and the reflectance of a mirror. An example of a non-imaging parabolic light concentrator is presented in Fig. 9c. For side looking applications, parabolic or spherically polished mirrors focus the output of several fibers onto the same area (Fig. 16a and 16b). Best performance is achieved with a parabolic surface (Fig. 16b). The manufacturing of such mirrors requires a high-precision, numerically-controlled lathe. Surfaces with optical quality can be manufactured with single-point, diamond-cutting machines.

An example of a probe illuminating a ring is shown in Fig. 16c and 16d [214]. Multiple fibers are glued into a metallic ring. A plug with the optimized polished surface is centered into the ring and deflects the axial fiber output in a radial direction. A quartz tube shields the reflective surface. Illumination analysis shows that the output of 5 fibers (2 fibers were arranged on an inner concentric ring and 3 on an outer location) overlaps on the circumference of the probe (Fig. 16e and 16f). The rotational symmetric design spreads the light from the fibers in an elliptical spot around the circumference. The inner ring of fibers could be used as collection fibers and the outer ring as illumination fibers. This design confines the sampling volume close to the probe surface since the light diverges rapidly outside the focal spot (Fig. 16f).

Summary

A large variety of optical designs allows optimal illumination and light collection for spectroscopic applications. Specific solutions for fluorescence, reflectance and Raman spectroscopy are available and the possibility of combining them in a single probe is feasible. Future technology development will lead to integrated, multifunctional, and highly optimized fiber optic probes.

Table

Table 1: Materials suitable for fiber optic probe enclosures and references for biocompatibility. A literature reference is equivalent to a paragraph in The Biomedical Engineering Handbook [24]. An implant reference means that the material has been used as body implant. USP class VI testing is the basis for medical device manufacturers and a reference to this class means that material with this certification is available.

Figures

Figure 1a: A fiber optic based spectroscopy system with separate illumination and collection path is based on an excitation source, which is a laser, a white light source (reflectometry), or a monochromator filtered arc lamp (fluorescence). Optical elements couple the excitation light into the flexible probe. A probe collects the emitted light. Coupling optics adapt the numerical aperture of the probe to the spectrograph or filter system. An optical detector (CCD, photodiode array, or photo multiplier tube) is read out and digitized [234].

Figure 1b: A fiber optic spectroscopy system with a probe that incorporates *one optical fiber* needs a dichroic beam splitter and well-aligned optics to separate excitation and fluorescence light [234].

Figure 2: A fiber optic cable for spectroscopy consists of a core and a cladding with a lower refractive index and a rugged supportive jacket. Light is transported by total internal reflection. The light acceptance angle of the fiber (α) is defined by the refractive indices of the media, core and cladding (n_{media}, n_{core}, $n_{cladding}$).

Figure 3: Hexagonal packing of fibers into the smallest possible cross section.

Figure 4a: The output of an optical fiber is described by the opening half angle (α), or the numerical aperture (NA).

Figure 4b,and 4c: Oblique polishing of the fiber tip deflects the output beam.

Figure 4d: When total internal reflection is achieved for a part of the light, the output will be split into two parts, one exiting in axial direction and the other in radial direction.

Figure 4e: When all light is totally internally reflected at the fiber end surface or the beveled end surface is reflectively coated, light leaves the fiber through the side wall.

Figure 4f: A fiber based on a combination of a beveled and flat polished surface has a partially deflected output beam.

Figure 4g: A fiber optic probe that illuminates and collects through the same fiber has the highest collection efficiency.

Figure 4h: A dual fiber bundle is used for many spectroscopy application. This concept can be easily extended to hexagonal packed fiber bundles.

Figure 4i: A dual fiber probe based on beveled fibers achieves a better collection efficiency compared to the flat tip dual fiber configuration, while collection and illumination channels are still separated.

Figure 4j: Fiber probes based on a fiber with a combination of a flat tip and a beveled surface have excellent collection efficiencies.

Figure 4k, and 4l: Two probe designs for submersion k) and measurements on surfaces l): A central fiber (a) illuminates the sampling volume or the surface. Six surrounding fibers (b) collect the emitted light. Collection and illumination channels are interchangeable. Housing with a thin shield (quartz, sapphire) permits a constant sampling distance for surface measurements [234].

Figure 5a: A fiber optic probe for reflectometry: The light scattered from a single excitation fiber is detected by a linearly arranged array of collection fibers. Tilting the excitation fiber shifts the profile along the surface by an amount which is determined by the sample optical properties. The distance between the source and detector fibers needs to be adjusted for the expected intensity profile sampling [234].

Figure 5b: Scanning fiber optic probe for reflectance measurements: a) illumination fiber, b) SELFOC lens, c) deflecting prism, and d) photo mask on exit surface (with permission from 48).

Fig. 5c: A fiber optic probe with a circular fiber arrangement for reflectometry: A 2cm probe head consists of a central calibration fiber, an illumination fiber, and non-equally spaced fibers. A variable neutral density filter adapts the light intensity in a transfer array to a smaller dynamic range (with permission from

[50] and suggestions from M. Patterson and coworkers). Parts are: illumination fiber (a), circular probe head (b), calibration fiber (c), detection fibers (d), linear transfer array (e) + (f), neutral density filter (g), and a spectrograph input ferrule (h).

Figure 5d: A fiber optic probe for single point reflectance measurements: Hexagonal packed fibers are randomly assigned for collection (a) and illumination (b). An outer tubing (c) combines the fiber bundle (d) with a spacing wedge (e). An absorbing coating (f) based on carbon powder or black paint absorbs specular reflected light from the tissue glass interface.

Figure 5e: Polarized reflectance system: White light is transported from the light source with a fiberoptic cable, collimated (a) and passes a polarizer. Reflectance is collected (b) with an imaging system. In the collimated beam path, reflectance is filtered with rotatable polarizer (c) for parallel or cross polarization.

Figure 5f: Frontal view of a fiber optic polarized reflectance probe: A simple probe consisting of one illumination channel (a), two detection channels for parallel (b) and cross-polarized (c) light detection.

Figure 5g: Frontal view of a fiber optic polarized reflectance probe: Ideally all four possible polarization combinations are measured. This can be achieved when the illumination fiber (a) and two detector fibers (b) and (c) covered with the parallel polarization filter and two fibers (d) and (e) with the cross polarized filter. Note that the intensity of channel (c) will be lower than channel (b).

Figure 5h: Schematic of a back scattering event on a small particle and the intensities associated with various pick up geometries. The scattering probability is indicated by the mesh surface and the distance from the center (particle) to the surface is equivalent with the scattering probability in that direction. Incident light is polarized in vertical direction. Detectors are positioned at the same location as in Figure 5f.

Figure 5i: A simple polarized reflectance probe consists of optical fibers (a), a mechanical placeholder for the fibers (b), the polarization filter (c), a cover glass (d) and a housing (e). Two fibers are covered with the same polarization filter while the other fiber is covered with a 90 degrees rotated filter.

Figure 5j: An assembled version of the probe described in Figure 5i. The probe tip consists of three 200 μm diameter fibers. The gap formed by the two perpendicular oriented polarization filters can be identified in both pictures.

Figure 5k: In order to measure the same spot of a surface a polarized reflectance probe could be constructed with a conical reflector. There is a large difference in angle of incidence and angle of collection with this design and the polarization state changes at the reflecting surface.

Figure 6a: The classic fiber optic probe for fluorescence spectroscopy is based on two or more fibers. Hexagonal packing is a dense arrangement and allows the selection of multiple fibers for different excitation sources and collection channels. A quartz shield permits the overlap of excitation and collection areas. Parts include: excitation fibers (a), collection fibers (b), tubing (c), carbon filled glue (d), sleeve (e), and shield (f) [234].

Figure 6b: A single fiber fluorescence probe with a spacer (optical shield).

Figure 6c: A typical fluorescence probe for single point sampling (legend according to Figure 6a) [234].

Figure 7a: Reduced outer diameter is achieved with a mixing element instead of a quartz shield. The mixing element consists of a coated quartz rod or a thick piece of optical fiber. The outer diameter does not exceed the diameter of the hexagonal packing. The parts are: excitation fibers (a), collection fibers (b), tubing (c), epoxy (d), and coated glass rod (mixing element) (e).

Figure 7b: Assembling of a reduced diameter fiber probe: Illumination and collection fibers (a), (b) are packed hexagonally and glued together (c). The glass rod (d) is placed in front of the polished fiber bundle and held in place with shrink tubing (e).

Figure 8a: A multi-pixel fiber optic design based on the design of Figure 6a (frontal view): At each sample spot one collection fiber is surrounded by one to six illumination fibers. Cross-talk in between sample spots can be influenced by the separation distance of the collection and emission fibers [234].

Figure 8b: A typical fluorescence probe for simultaneous multi-pixel measurements with 32 sampling locations: Black shrink tubing holds the quartz shield. Emission and collection fiber pairs are arranged hexagonally [234].

Figure 8c: Separated illumination and collection spot: Fluorescence generated in a 1mm spot area spreads by scattering inside the tissue and is also detectable outside the illumination area. Since the average path

length of the light detected outside the illumination spot is larger, absorption processes are increased and can be observed at increased oxyhemoglobin absorption valleys at 540 and 580 nm (adapted from [157]).

Figure 9a: A fiber optic probe that combines fluorescence and reflectance measurements: White light scatters through the volume interrogated during fluorescence measurements. Parts include: excitation fibers (a), fluorescence collection fibers (b), carbon filled glue (c), outer tubing (d), quartz shield (e), reflectance collection (f), and white light illumination (g) [234].

Figure 9b: Manufactured probe according to the design of Figure 9a. Parts included: Same as Figure 8a.

Figure 9c: Combined fluorescence and reflectance probe: Illumination of the area around the measured spot allows visual feedback during measurements (a). Fluorescence fibers (b) and reflectance fibers (c) are arranged in the center of the probe. An integrated glass rod minimizes the outer diameter (d) of the fluorescence channel. The reflectance fibers (c) are flush with the tissue.

Figure 9d: A frontal view of the probe and its connectors from Figure 9c: Fluorescence excitation and collection fibers (b) are randomly arranged behind the quartz rod. Reflectance illumination (E) is facilitated with one fiber, and reflectance is collected at 4 different source-detector separations (0, 1, 2, and 3).

Figure 9e: Fluorescence excitation fibers from the design represented in Figure 9c and 9d are arranged in two lines and coupled to the output of a monochromator filtered xenon light source. Fluorescence and reflectance collection fibers are linearly arranged for the imaging spectrograph ferrule. Sufficient spacing between the fibers eliminates blooming on the CCD detector, while measuring low light levels with fiber position 2 and 3.

Figure 9f: Compatibility of probe with laparoscopic equipment: A trocar shaft (a) allows the passage of probe with a diameter smaller than 5 mm for measurements during abdominal surgery. The probe (b) and shaft are sealed with a flexible lip (c). Illumination fibers (d) allow a remote controlled illumination of the measured spot while endoscopic illumination is dimmed. A second trocar needs to be placed for endoscopic supervision.

Figure 10a: A fiber optic probe for Raman spectroscopy based on separate illumination and collection fibers. The output of the fibers is collimated and filtered and then projected onto the same area on the

sample. Bandpass filters (a) are used for the excitation fibers and longpass filters (b) for the collection fibers. GRIN lenses (c) are assembled into the probe in order to maintain small diameters (adapted from [209]).

Figure 10b: A fiber optic probe based on the design in Figure 4l.: In line filters (a) and (b) are mounted into spring-loaded SMA connectors. The fiber length in between the tip and the filters is kept short (adapted from [210]).

Figure 10c: A CPC Raman collection system: Parts include NIR diode laser (a), collimating lens (b), reflective mirror (c), dichroic mirror (d), focusing lens (e), parabolic concentrator (f), field lenses (g, h) to prevent vignetting, a focusing lens (i) to couple the Raman signal into a collection fiber bundle (j), and a high efficiency spectrograph with a LN cooled CCD (k) (with permission from [13,211]).

Figure 10d: Raman probe: The excitation light is transported through a single fiber (a) and imaged with a biconvex lens (b) through a dielectric bandpass filter via a mirror (c) onto the sample area. The inelastic scattered light is collected behind a quartz window (d) and imaged with two plano convex lenses (e), (f) through an aperture stop (g), and a holographic notch filter onto a flexible fiber bundle (h) (with permission from [193]).

Figure 10e: Commercial Raman probe: Excitation light (a) is collimated (b) and bandpass filtered through a transmission grating (c) and aperture stop (d). The excitation intensity can be monitored (e). Raman scattered light is collected with a microscope objective and imaged on a collection fiber bundle (f). Two holographic notch filters (g) are placed in the collimated beam path to remove reflected excitation light. (adapted from [213]).

Figure 10f: The UVRR spectroscopy probe incorporates a smaller diameter solarization resistant UV grade quartz fiber for excitation and an oblique polished fiber to collect scattered light close to the excitation fiber. The oblique polished fiber is coated with aluminum (R) to achieve side looking in liquid samples (with permission from [16]).

Figure 11a: Illumination analysis of beveled fibers with a uniform spatial and angular light distribution inside the fiber shows a focusing in air. When light leaves the fiber through the cylindrical wall, it is

focused. In air the irradiance increases to a factor of 2.4 in the focal spot compared to the intensity within the fiber. The focus spot has an elliptical shape.

Figure 11b: Illumination analysis of a beveled fiber in water: The refractive power of the cylindrical surface is reduced compared to the silica-air interface in Figure 11a and the irradiance in the focal spot is 1.6 times larger than in the fiber core.

Figure 11c: An oblique polished fiber (a) is enclosed in quartz capillary tubing (b) for minimal diameter side looking probes (Innova Quartz). A two-fiber arrangement for separate illumination and collection path can also be manufactured [234].

Figure 11d: A circular arrangement of oblique polished fibers allows the fabrication of a ring probe with separate illumination and excitation channels. Alignment is a tedious task [234].

Figure 12a: A diffuser is mounted on the tip of a fiber bundle which allows uniform illumination along the probe axis (CardioFocus Inc., formerly Rare Earth Medical, Inc.). A reflector (a) at the diffuser end and the local concentration of scattering particles (b) determine the intensity profile. Tubing (c) made of fluorpolymers has a high transmission and good heat resistance [234].

Figure 12b: A “Lightstick” manufactured according the design in Figure 12a with a length of 3 cm and a reflector allows radial illumination with a relatively flat intensity profile along the axis.

Figure 12c: This line-sampling probe is based on a combination of a diffuser illuminator (a) and oblique polished fibers (b). The light emitted by the diffuser passes the collection fibers which have the jacket striped. A metallic foil (c) restricts the illumination to a reduced angle [234].

Figure 13a: A sapphire prism deflects the output of a fiber ring into a radial direction. The probe consists of a plug (a) holding the prism (b) and inner tubing. Fibers (c) are glued into a metallic ring (d). Outer tubing (e) and glue seals the fiber tip [234].

Figure 13b: In the upper picture, the sapphire prism and the fibers are partially assembled. The lower picture represents a cross-sectional view and shows the arrangement of illumination and smaller collection fibers in a metallic ring (d) [234].

Figure 14a and 14b: Hemispherically shaped ends of fibers focus the output beam in air (Fig. 14a) and collimate the output beam in water (Fig. 14b) [234].

Figure 14c: Maximal irradiance is found at a distance of 3 times the fiber radius in water for quartz fibers with a NA of 0.22. The irradiance increases by a factor of 3 [234].

Figure 15a: Ball lenses image the output of a fiber and focus it. The ball lens is centered and placed at a fixed distance to the fiber with metallic holder .If this probe is used in a fluid, focusing is limited.

Figure 15b: A side deflecting probe can be manufactured with a half sphere. The flat surface is inclined to the probe axis. If this surface is a sapphire-air interface, total internal reflection will occur. The flat surface could also be coated with aluminum to achieve a similar effect. The deflecting optic is housed in quartz tube. Focusing in water is not affected, since the beam path is determined inside the probe [234].

Figure 15c and 15d: Illumination analysis demonstrates an up to five-fold increase of irradiance in the focal spot in water c) and air d) [234].

Figure 16a and 16b: A spherical (Fig. 16a) or parabolic (Fig. 16b) mirror focuses and deflects the fiber output. Rotationally symmetric mirrors with optical surface quality can be manufactured with numerically controlled diamond-turning machines [234].

Figure 16c and 16d: A fiber optic ring probe with a parabolic reflector according Figure 16b: A plug with the reflective surface (Fig. 16d) is mounted into a ring of fibers and flexible tubing. A short piece of a quartz tube isolates the mirror from the probe environment [234].

Figure 16e: Illumination analysis of the output from 5 fibers was performed with a reflector according the design of Figure 16c. The analysis shows a good overlap of the fibers on the exit surface (B) of the probe. The spot diagram on the exit surface (B) shows that the output of the optical fibers is spread in a circumferential direction [234].

Figure 16f: The flux density profile was measured at the exist surface (B) and the 5 fibers produced an increase of a factor of 2 compared to the intensity inside a single fiber. A ray trace projection (A) shows that the output is focused to a small spot in radial direction [234].

Support

Research on fiber optic devices was supported in part by the Swiss National Science Foundation (Laser Coronary Angioplasty, 32-27888.89) and the Swiss National Science Foundation (fiber optic probes for *in vivo* spectroscopy, Postdoctoral fellowship 1995/96).

This work would not have been possible without Pascal Rol [1956-2000] (University of Zurich, Department of Ophthalmology, Switzerland).

Citations

1. M. Malpighi, *Microscopical Anatomy,* University of Bologna, University of Pisa, University of Messina, Chief physician to Pope Innocent XII at Rome, 1628-1694.
2. H. L. F. von Helmholtz, *Handbook of Physiological Optics,* 1867.
3. A. J. Desormeaux, *Inventor of first effective endoscope,* 1853.
4. B. Bernheim, "Organoscopy," *Ann Surg,* 53:764, (1911).
5. H. Hinselman, "Verbesserung der Inspektionsmoeglichkeiten von Vulva, Vagina und Portio," *Muenchner Medizinische Wochenschrift* 73, 1733 (1925).
6. V. P. Pashinin, N. Konstantinov, V. G. Artjushenko, V. I. Konov, A. S. Silenok, G. Muller, B. Schaldach and R. Ulrich, "Mechanism of UV laser-induced absorption in fused silica fibers," *Fiber & Integrated Optics* 10:4, 365-72 (1991).
7. V. G. Artjushenko, A. A. Lerman, E. G. Litvinenko, A. O. Nabatov, V. I. Konov, R. I. Kuznetsov, V. G. Plotnichenko, I. L. Pylnov, V. A. Shtein-Margolina, A. A. Urusovskaja, V. V. Vojtsekhovsky, N. D. Zaharov, W. Neuberger and K. Moran, "Mechanisms of optical losses in polycrystalline fibers," *Proc. SPIE,* 1591, 83-9 (1992).
8. H. Fabian, U. Grzesik, K. H. Worner, H. Henschel, O. Kohn and H. U. Schmidt, "Radiation resistance of optical fibers: correlation between UV attenuation and radiation-induced loss," *Proc. SPIE,* 1791, 297-305 (1993).
9. J. Vydra and G. F. Schoetz, "Improved all-silica fibers for deep-UV applications," *Proc. SPIE.,* 3596, 165-75 (1999).
10. L. Grant, G. Schoetz, J. Vydra and D. G. Fabricant, "Optical fiber for UV-IR broadband spectroscopy," *Proc. SPIE,* 3355, 884-891 (1998).
11. P. R. Carey, *Biochemical Applications of Raman and Resonance Raman Spectroscopy,* Academic Press, New York (1982).
12. G. Muller, H. Kar, K. Dorschel and H. Ringelhan, "Transmission of short pulsed high power UV laser radiation through depending on pulse length, intensity and long term behavior," *Proc. SPIE,* 906, 231-5 (1988).

13. J. F. Brennan, III, W. Yang, R. R. Dasari and M. S. Feld, "Near-infrared Raman spectrometer systems for human tissue studies," *Appl. Spectrosc,*. 51:2, 201-8 (1997).

14. P. Rol and P. Niederer, "High-power laser transmission through optical fibers: Applications to ophthalmology," In: *Laser applications in medicine and biology,* M. Wolbarsht Ed., pp. 141-198, Plenum Press, New York (1991).

15. P. Rol, U. Utzinger, D. Beck and P. Niederer, "Fiber beam shaping and ophthalmic applications," *Proc. SPIE,* 2330, 56-62 (1995).

16. L. Greek, H. Schulze, M. Blades, C. Haynes, K. Klein and R. Turner, "Fiber-optic probes with improved excitation and collection efficiency for deep-UV Raman and Raman resonance spectroscopy," *Appl. Optics,* 37:1, 170-80 (1998).

17. M. G. Shim, B. C. Wilson, E. Marple and M. Wach, "Study of fiber-optic probes for *in vivo* medical Raman spectroscopy," *Appl. Spectrosc,* 53:6, 619-627 (1999).

18. T. F. Cooney, H. Trey Skinner and S. M. Angel, "Comparative study of some fiber-optic remote Raman probe designs. I. Model for liquids and transparent solids," *Appl. Spectrosc.,* 50:7, 836-48 (1996).

19. T. F. Cooney, H. Trey Skinner and S. M. Angel, "Comparative study of some fiber-optic remote Raman probe designs. II. Tests of single-fiber, lensed, and flat- and bevel-tip multi-fiber probes," *Appl. Spectrosc.,* 50:7, 849-60 (1996).

20. Center for Devices and Radiological Health, *Electro-optical Sensors for the In Vivo Detection of cervical cancer and its precursors: Submission guidance – not for implementation*, U.S. Food and Drug Administration (1997).

21. Center for Devices and Radiological Health, *Required biocompatibility training and toxicology profiles for evaluation of medical devices (G95-1*), U.S. Food and Drug Administration, (1995)

22. American Conference of Governmental Industrial Hygienists (ACGIH®), *Threshold Limit Values for Chemical Substances and Physical Agents, Biological Exposure Indices* (1996).

23. American National Standards Institute, *American National Standard for Safe Use of Lasers, ANSI Z1361*, Laser Institute of America, Orlando (2000).

24. J. B. Park, Biomaterials, Chap IV in *The Biomedical Engineering Handbook*, J. D. Bronzino, Ed., pp 529-798, CRC & IEEE Press (1995).

25. A. J. Welch, M. J. C. van Gemert, W. M. Star and B. C. Wilson, "Definition and overview of tissue optics," in *Optical-Thermal Response of Laser-Irradiated Tissue,* A. J. Welch and M. J. C. van Gemert, Eds., pp. 15-46, Plenum Press, New York (1995).

26. W. G. Zijlstra, A. Buursma and W. P. Meeuwsen-van der Roest, "Absorption spectra of human fetal and adult oxyhemoglobin, de-oxyhemoglobin, carboxyhemoglobin, and methemoglobin," *Clin. Chem.,* 37:9, 1633-8 (1991).

27. W. G. Zijlstra, A. H. Maas and R. F. Moran, "Definition, significance and measurement of quantities pertaining to oxygen carrying properties of human blood," *Scan. J. Clin. Lab. Invest.,* 224, 27-45 (1996).

28. R. M. P. Doornbos, R. Lang, M. C. Aalders, F. W. Cross and H. J. C. M. Sterrenborg, "The determination of in vivo human tissue optical properties and absolute chromophore concentrations using spatially resolved steady-state diffuse reflectance spectroscopy," *Phys. Med. Biol.,* 44, 967-81 (1999).

29. A. M. K. Nilsson, C. Sturesson, D. L. Liu and S. Anderson-Engels, "Changes in spectral shape of tissue optical properties in conjunction with laser-induced thermography," *Appl. Opics,* 28, 2331-6 (1997).

30. J. R. Mourant, T. Fuselier, J. Boyer, T. M. Johnson and I. J. Bigio, "Prediction and measurements of scattering and absorption over broad wavelength ranges in tissue phantoms," *Appl. Optics,* 36, 949-57 (1997).

31. A. Kienle, L. Lilge, M. S. Patterson, R. Hibst, R. Steiner and B. C. Wilson, "Spatially resolved absolute diffuse reflectance measurements for noninvasive determination of the optical scattering and absorption coefficients of biological tissue," *Appl. Optics,* 35:13, 2304-14 (1996).

32. J. R. Mourant, I. J. Bigio, J. Boyer, R. L. Conn, T. Johnson and T. Shimada, "Spectroscopic diagnosis of bladder cancer with elastic light," *Lasers Surg. Med.,* 17:4, 350-7 (1995).

33. F. Koenig, R. Larne, H. Enquist, F. J. McGovern, K. T. Schomacker, N. Kollias and T. F. Deutsch, "Spectroscopic measurement of diffuse reflectance for enhanced detection of bladder carcinoma," *Urology,* 51:2, 342-5 (1998).

34. W. T. Knoefel, N. Kollias, D. W. Rattner, N. S. Nishioka and A. L. Warshaw, "Reflectance spectroscopy of pancreatic microcirculation," *J. Appl. Physiol.,* 80:1, 116-23 (1996).

35. M. B. Wallace, L.T. Perelman, V. Backman, J. M. Crawford, M. Fitzmaurice, M. Seiler, K. Badizadegan, S. J. Shields, I. Itzkan, R. R. Dasari, J. Van Dam and M. S. Feld, "Endoscopic detection of dysplasia in patients with Barrett's esophagus using light-scattering spectroscopy," *Gastroenterology,* 119, 677-82 (2000).

36. L. T. Perelman, V. Backman, M. Wallace, G. Zonios, R. Manoharan, A. Nusrat, S. Shields, M. Seiler, C. Lima, T. Hamano, I. Itzkan, J. Van Dam, J. M. Crawford and M. S. Feld, "Observation of periodic fine structure in reflectance from biological tissue: a new technique for measuring nuclear size distribution," *Phys. Rev. Ltrs.,* 80:3, 627-30 (1998).

37. Z. Ge, K. Schomacker and N. Nishioka, "Identification of colonic dysplasia and neoplasia by diffuse reflectance spectroscopy and pattern recognition techniques," *Appl. Spectrosc.,* 52:6, 833-45 (1998).

38. G. Zonios, L. T. Perelman, V. Backman, R. Manahoranm M. Fitzmaurice, J. Van Dam and M. S. Feld, "Diffuse reflectance spectroscopy of human adenomatous colon polyps in vivo," *Appl. Optics,* 38, 6628-37 (1999).

39. U. Utzinger, M. Brewer, E. Silva, D. Gershenson, R. C. Bast, M. Follen and R. R. Richards-Kortum, "Reflectance spectroscopy for in vivo characterization of ovarian tissue," *Lasers Surg. Med.*. 28, 56-66, 2001.

40. I. J. Bigio, S.G. Brown, C. Kelley, S. Lakhani, D. Pickard, P. M. Ripley and C. Saunders, "Diagnosis of breast cancer using elastic-scattering spectroscopy: preliminary clinical results," *J. Biomed. Optics,* 5, 221-228 (2000).

41. C. J. Lynn, I. S. Saidi, D. G. Oelberg and S. L. Jacques, "Gestational age correlates with skin reflectance in newborn infants of 24-42 weeks gestation," *Biol Neonate,* 64:2-3, 69-75 (1993).

42. T. J. Farrell, M. S. Patterson and B. Wilson, "A diffusion theory model of spatially resolved, steady-state diffuse reflectance for the noninvasive determination of tissue optical properties in vivo," *Med. Physics,* 19:4, 879-88 (1992).

43. A. Kienle and M. S. Patterson, "Improved solutions of the steady-state and the time-resolved diffusion equations for reflectance from a semi-infinite turbid medium," *J. Optics, Soc. Am., A* 14:1, 246-254 (1997).

44. S. T. Flock, M. S. Patterson, B. C. Wilson and D. R. Wyman, "Monte Carlo modeling of light propagation in highly scattering. I. Model predictions and comparison with diffusion theory," *IEEE Trans. Biomed. Eng.,* 36:12, 1162-8 (1989).

45. S. T. Flock, B. C. Wilson and M. S. Patterson, "Monte Carlo modeling of light propagation in highly scattering II. Comparison with measurements in phantoms," *IEEE Trans. Biomed. Eng.,* 36:12, 1169-73 (1989).

46. L. H. Wang and S. L. Jacques, *Monte Carlo Modeling of Light Transport in Multi-layered Tissues in Standard C*, The University of Texas M.D. Anderson Cancer Center, Houston, TX (1992).

47. L. Wang and S. L. Jacques, "Use of a laser beam with an oblique angle of incidence to measure the reduced scattering coefficient of a turbid medium," *Appl. Optics,* 34:13, 2362-6 (1995).

48. S.-P. Lin, L. Wang, S. L. Jacques and F. K. Tittel, "Measurement of tissue optical properties by the use of oblique-incidence optical fiber reflectometry," *Appl. Optics,* 36:1, 136-43 (1997).

49. R. Bays, G. Wagnières, D. Robert, D. Braichotte, J.F. Savary, P. Monnier and H. van den Bergh, "Clinical determination of tissue optical properties by endoscopic spatially resolved reflectometry," *Appl. Optics,* 35:10, 1756-66 (1996).

50. M. G. Nichols, E. L. Hull and T. H. Foster, "Design and testing of a white-light, steady-state diffuse reflectance spectrometer for determination of optical properties of highly scattering systems," *Appl. Opt*ics, 36:1, 93-104 (1997).

51. H. Fuchs, U. Utzinger, A. F. Zuluaga, A. Gillenwater, R. Jacob, B. Kemp and R. Richards-Kortum, "Combined fluorescence and reflectance spectroscopy: in vivo assessment of oral cavity epithelial neoplasia," *Proc. CLEO*, 6, 306-7, 1998.

52. G. Marquez and L. V. Wang, "White light oblique incidence reflectometer for measuring absorption reduced scattering spectra of tissue-like turbid media," *Optics Exp.,* 1:13, 454-460 (1997).

53. T. J. Farrell, B. C. Wilson and M. S. Patterson, "The use of a neural network to determine tissue optical properties spatially resolved diffuse reflectance measurements," *Phys. Med. Biol.,* 37:12, 2281-6 (1992).

54. V.P. Wallace, J.C. Bamber, D. C. Crawford, R. J. Ott, P. S. Mortimer, "Classification of reflectance spectra from pigmented skin lesions, a comparison of multivariate discriminant analysis and artificial neural networks," *Phys. Med. Biol,* 45:10, 2859-71 (2000)

55. J. S. Dam, P.E. Andersen, T. Dalgaard and P.E. Fabricius, "Determination of tissue optical properties from diffuse reflectance profiles by multivariate calibration," *Appl. Optics,* 37:4, 772-8 (1998).

56. S. T. Flock, B. C. Wilson and M. S. Patterson, "Hybrid Monte Carlo-diffusion theory modeling of light distributions tissue," *Proc. SPIE,* 908, 20-8 (1988).

57. L. Wang and S. L. Jacques, "Hybrid model of Monte Carlo simulation and diffusion theory for light reflectance by turbid media," *J. Optics, Soc. Am., A* 10:8, 1746-52 (1993).

58. J. S. Dam, C.B. Pedersn, T. Dalgaard, P.A. Fabricius, P. Aruna and S Anderson Engles, "Fiber optic probe for noninvasive real-time determination of tissue optical properties at multiple wavelengths," *Appl. Optics*, 40:7, 1155-64 (2001).

59. F. Bevilacqua, D. Piguet, P. Marquet, J.D. Gross, B. J. Tromberg and C. Depeursinge, "*In vivo* local determination of tissue optical properties: Applications to human brain," *Appl. Opt*ics, 38:22, 4939-50 (1999).

60. F. Bevilacqua and C. Depeursinge, "Monte Carlo study of diffuse reflectance at source-detector separations close to one transport mean free path," *J. Optics, Soc. Am. A,* 16:12, 2935-45 (1999).

61. J. R. Mourant, I. J. Bigio, D. A. Jack, T. M. Johnson and H. D. Miller, "Measuring absorption coefficients in small volumes of highly media: source-detector separations for which path lengths do not depend on scattering properties," *Appl. Opics,*. 36:22, 5655-61 (1997).

62. J. R. Mourant, J. P. Freyer, A. H. Hielscher, A. A. Eick, A. Shen and T. M. Johnson, "Mechanisms of light scattering from biological cells relevant to noninvasive optical-tissue diagnostics," *Appl. Optics,* 37:16, 3586-93 (1998).

63. R. Drezek, A. Kamath, C. MacAulay and R. Richards-Kortum, "Light scattering from normal and neoplastic cells: FDTD modeling based on quantitative cytology," *Proc. OSA: Biomed Topical Mtg.,*, 326-28 (2000).

64. A. K. Dunn, C. Smithpeter, A. J. Welch and R. Richards-Kortum, "Sources of contrast in confocal reflectance imaging," *Appl. Optics,* 35:19, 3441-6 (1996).

65. H. C. Van de Hulst, *Light Scattering by Small Particles,* Dover, New York (1957).

66. R. A. Zangaro, L. Silveira, Jr., R. Manoharan, G. Zonios, I. Itzkan, R. R. Dasari, J. Van Dam and M. S. Feld, "Rapid multiexcitation fluorescence spectroscopy system for *in vivo* tissue diagnosis," *Appl. Optics,* 35:25, 5211-19 (1996).

67. G. Jarry, E. Steimer, V. Damaschini, M. Epifanie, M. Jurczak and R. Kaiser, "Coherence and polarization of light propagating through scattering and biological tissues," *Appl. Optic,.,* 37:31, 7357-67 (1998).

68. G. Jarry, E. Steimer, V. Damaschini, M. Jurczak and R. Kaiser, "Coherent components of forward light propagation through scattering media," *J. Optics*, 28:2, 83-9 (1997).

69. S. L. Jacques, M. R. Ostermeyer, L. Wang and D. V. Stephens, "Polarized light transmission through skin using video reflectometry: toward optical tomography of superficial tissue layers," *Proc. SPIE,* 2671, 199-210, 1996.

70. W. Groner, J. W. Winkelman, A. G. Harris, C. Ince, G. J. Bouma, K. Messmer and N. R.G., "Orthogonal polarization spectral imaging: A new method for study of the microcirculation.," *Nat. Med.,* 5:10, 1209-13 (1999).

71. T. Johnson and J. Mourant, "Polarized wavelength-dependent measurements of turbid media.," *Optics Exp.,* 4:6, 200-216 (1999).

72. S. Bartel and A. H. Hielscher, "Monte Carlo simulations of the diffuse backscattering Mueller matrix for highly scattering media," *Appl. Optics,* 39:10, 1580-8 (2000).

73. L. Wang and G. Yao, "Propagation of polarized light in turbid media: simulated animation sequences," *Optics Exp.,* 7:5, 198-203 (2000).

74. R. Gurjar, V. Backman, K. Badizadegan, R. Dasari, I. Itzkan, L. T. Perelman and M. S. Feld, " Imaging human epithelia properties with polarized light-scattering spectroscopy," *Nat Med.,* 7:11, 1245-8 (2001).

75. V. Backman, R. Gurjar, K. Badizadegan, I. Itzkan, R. Dasari, L. Perelman and M. Feld, "Polarized light scattering spectroscopy for quantitative measurement of epithelial cellular structures in situ.," *IEEE J. Sel. Topi. Quantum Electron,.* 5:4, 1019-26 (1999).

76. K. Sokolov, R. Drezek, K. Gossage and R. Richards-Kortum, "Reflectance spectroscopy with polarized light: is it sensitive to cellular and nuclear morphology?," *Optics Exp.,* 5:13, 302-17 (1999).

77. A. Myakov, L. Nieman, L. Wicky, U. Utzinger, R. Richards-Kortum, and K. Sokolov, "Fiber optic probe for polarized reflectance spectroscopy *in vivo*: design and performance." *J. Biomed. Optics,* in press (2002).

78. L. I. Deckelbaum, I. J. Sarembock, M. L. Stetz, O. B. KM, F. W. Cutruzzola, A. F. Gmitro and M. D. Ezekowitz, "In-vivo fluorescence spectroscopy of normal and atherosclerotic arteries.," *Proc. SPIE,* 906: 314-19, 1988.

79. D. Yang and C. Zeng, "Analysis on the clinical applicability of laser excited autofluorescence spectra for oral cancer diagnosis," *Zhongguo Jiguang/Chinese J. Lasers,* 18:2, 144-8 (1991).

80. V. R. Kolli, H. E. Savage, T. J. Yao and S. P. Schantz, "Native cellular fluorescence of neoplastic upper aerodigestive mucosa," *Arch. Otolaryn.Head Neck Surg.,* 121:11, 1287-92 (1995).

81. J. K. Dhingra, D. F. Perrault, Jr., K. McMillan, E. E. Rebeiz, S. Kabani, R. Manoharan, I. Itzkan, M. S. Feld and S. M. Shapshay, "Early diagnosis of upper aerodigestive tract cancer by autofluorescence," *Arch. Otolaryn. Head Neck Surg.,* 122:11*,* 1181-6 (1996).

82. C. T. Chen, C. Y. Wang, Y. S. Kuo, H. H. Chiang, S. N. Chow, I. Y. Hsiao and C. P. Chiang, "Light-induced fluorescence spectroscopy: a potential diagnostic tool for oral neoplasia," *Proc. Nat. Sci. Council, Rep. China - Part Life Sciences,* 20:4, 123-30 (1996).

83. E. W. J. van der Breggen, A. I. Rem, M. M. Christian, C. J. Yang, K. H. Calhoun, H. Sterenborg and M. Motamedi, "Spectroscopic detection of oral and skin tissue transformation in a model for squamous cell carcinoma: autofluorescence versus systemic aminolevulinic acid-induced fluorescence," *IEEE J. Sel. Top. Quantum Electron.,* 2:4, 997-1007 (1996).

84. D. R. Ingrams, J. K. Dhingra, K. Roy, D. F. Perrault, Jr., I. D. Bottrill, S. Kabani, E. E. Rebeiz, M. M. Pankratov, S. M. Shapshay, R. Manoharan, I. Itzkan and M. S. Feld, "Autofluorescence characteristics of oral mucosa," *Head & Neck,* 19:1, 27-32 (1997).

85. A. Fryen, H. Glanz, W. Lohmann, T. Dreyer and R. M. Bohle, "Significance of autofluorescence for the optical demarcation of field cancerisation in the upper aerodigestive tract," *Acta Oto-Laryngologica,* 117:2, 316-9 (1997).

86. K. Svanberg, C. af Klinteberg, A. Nilsson, I. Wang, S. Andersson-Engels and S. Svanberg, "Laser-based spectroscopic methods in tissue characterization," *Ann. N. Y. Acad. Sci.* 838,123-9 (1998).

87. A. Gillenwater, R. Jacob, R. Ganeshappa, B. Kemp, A. K. El-Naggar, J. L. Palmer, G. Clayman, M. F. Mitchell and R. Richards-Kortum, "Noninvasive diagnosis of oral neoplasia based on fluorescence spectroscopy and native tissue autofluorescence," *Archives of Otolaryngology Head & Neck Surgery,* 124:11, 1251-8 (1998).

88. C. T. Chen, H. K. Chiang, S. N. Chow, C. Y. Wang, Y. S. Lee, J. C. Tsai and C. P. Chiang, "Autofluorescence in normal and malignant human oral tissues and in DMBA-induced hamster buccal pouch carcinogenesis," *J. Oral Path. Med.* 27:10, 470-4 (1998).

89. A. Mahadevan, M. F. Mitchell, E. Silva, S. Thomsen and R. R. Richards-Kortum, "Study of the fluorescence properties of normal and neoplastic human cervical tissue," *Lasers Surg. Med.,* 13:6, 647-55 (1993).

90. N. Ramanujam, M. F. Mitchell, A. Mahadevan, S. Warren, S. Thomsen, E. Silva and R. Richards-Kortum, "In vivo diagnosis of cervical intraepithelial neoplasia using 337-nm-excited laser-induced fluorescence," *Proc. Nat. Acad. Sci. USA,* 91:21, 10193-7 (1994).

91. R. Richards-Kortum, M. F. Mitchell, N. Ramanujam, A. Mahadevan and S. Thomsen, "In vivo fluorescence spectroscopy: potential for non-invasive, diagnosis of cervical intraepithelial neoplasia and use as a surrogate endpoint biomarker," *J. Cell. Biochem.Suppl.,* 19, 111-9 (1994).

92. N. Ramanujam, M. F. Mitchell, A. Mahadevan, S. Thomsen, E. Silva and R. Richards-Kortum, "Fluorescence spectroscopy: a diagnostic tool for cervical intraepithelial neoplasia (CIN)," *Gynecol. Oncol.,* 52:1, 31-8 (1994).

93. E. N. Atkinson, M. F. Mitchell, N. Ramanujam and R. Richards-Kortum, "Statistical techniques for diagnosing CIN using fluorescence spectroscopy: SVD and CART," *J. Cell. Biochem. - Suppl.* 23, 125-30 (1995).

94. N. Ramanujam, M. F. Mitchell, A. Mahadevan-Jansen, S. L. Thomsen, G. Staerkel, A. Malpica, T. Wright, N. Atkinson and R. Richards-Kortum, "Cervical precancer detection using a multivariate statistical algorithm based on laser-induced fluorescence spectra at multiple excitation wavelengths," *Photochem. Photobiol,.* 64:4, 720-35 (1996).

95. C. K. Brookner, A. Agrawal, E. V. Trujillo, M. F. Mitchell and R. R. Richards-Kortum, "Safety analysis: relative risks of ultraviolet exposure from fluorescence spectroscopy and colposcopy are comparable," *Photochem. Photobiol.,* 65:6, 1020-5 (1997).

96. E. V. Trujillo, D. Sandison, N. Ramanujam, M. Follen-Mitchell, S. Cantor and R. Richards-Kortum, "Development of a cost-effective optical system for detection of cervical pre-cancer," *Proc. IEEE Eng. Med. Biol.,* 1, 191-3 (1997).

97. E. V. Trujillo, D. R. Sandison, U. Utzinger, N. Ramanujam, M. F. Mitchell and R. Richards-Kortum, "Method to determine tissue fluorescence efficiency in vivo and predict signal-to-noise ratio for spectrometers," *Appl. Spectros.* 52:7, 943-51 (1998).

98. K. Tumer, N. Ramanujam, J. Ghosh and R. Richards-Kortum, "Ensembles of radial basis function networks for spectroscopic of cervical precancer," *IEEE Trans. Biomed. Eng.,* 45:8, 953-61 (1998).

99. S. B. Cantor, M. F. Mitchell, G. Tortolero-Luna, C. S. Bratka, D. C. Bodurka and R. Richards-Kortum, "Cost-effectiveness analysis of diagnosis and management of cervical squamous intraepithelial lesions," *Obstet. Gynecol,.* 91:2, 270-7 (1998).

100. S. R. Utts, P. Sinichkin Yu and E. A. Pilipenko, "Laser fluorescence spectroscopy of human skin in vivo: the effect of erythema," *Optika i Spektroskopiya* 76:5, 864-8 (1994).

101. S. R. Utz, J. Bart and P. Knuschke, "Fluorescence spectroscopy in dermatology," *Rossiiskoi Akademii Nauk* 59, 174-8 (1995).

102. H. J. Sterenborg, A. E. Saarnak, R. Frank and M. Motamedi, "Evaluation of spectral correction techniques for fluorescence measurements on pigmented lesions in vivo," *J. Photochem. Photobiol.. ,B* 35:3, 159-65 (1996).

103. N. Kollias, R. Gillies, C. Cohen-Goihman, S. B. Phillips, J. A. Muccini, M. J. Stiller and L. A. Drake, "Fluorescence photography in the evaluation of hyperpigmentation in photodamaged skin," *J. Am. Acad. Dermatol.,.* 36:2, 226-30 (1997).

104. P. Siniehkin Yu, S. R. Utz, A. H. Mavliutov and H. A. Pilipenko, "In vivo fluorescence spectroscopy of the human skin: experiments and models," *J. Biomed. Optics,* 3:2, 201-11 (1998).

105. N. Kollias, R. Gillies, M. Moran, I. E. Kochevar and R. R. Anderson, "Endogenous skin fluorescence includes bands that may serve as quantitative markers of aging and photoaging," *J. Invest. Dermatol.,* 111:5, 776-80 (1998).

106. R. R. Alfano, D. B. Tata, J. J. Cordero, P. Tomashefsky, F. W. Longo and M. A. Alfano, "Laser induced fluorescence spectroscopy from native cancerous and normal tissue," *IEEE J. Quantum Electron.* QE-20:12, 1507-11 (1984).

107. M. D. Hallewin, L. Baert and H. Vanherzeele, "In vivo fluorescence detection of human bladder carcinoma without sensitizing agents," *J. Am. Paraplegia Soc.,* 17:4, 161-4 (1994).

108. K. T. Schomacker, T. J. Flotte and T. F. Deutsch, "Laser-induced fluorescence detection of dysplasia in rat urinary bladder," *Proc. CLEO,* 8: 69-70, 1994.

109. M. Anidjar, D. Ettori, O. Cussenot, P. Meria, F. Desgrandchamps, A. Cortesse, P. Teillac, A. Le Duc and S. Avrillier, "Laser induced autofluorescence diagnosis of bladder tumors: dependence on the excitation wavelength," *J. Urol.,* 156:5, 1590-6 (1996).

110. F. Koenig and F. J. McGovern, "Fluorescence detection of bladder carcinoma," *Urology*, 50:5, 778-9 (1997).

111. F. Koenig, F. J. McGovern, H. Enquist, R. Larne, T. F. Deutsch and K. T. Schomacker, "Autofluorescence guided biopsy for the early diagnosis of bladder carcinoma," *J. Urol.,* 159:6, 1871-5 (1998).

112. M. Anidjar, O. Cussenot, S. Avrillier, D. Ettori, P. Teillac and A. Le Duc, "The role of laser-induced autofluorescence spectroscopy in bladder tumor detection. Dependence on the excitation wavelength," *Ann. N. Acad. Sci.*, 838,130-42 (1998).

113. O. J. Balchum, A. E. Profio, D. R. Doiron and G. C. Huth, "Imaging fluorescence bronchoscopy for localizing early bronchial cancer and carcinoma in situ," *Prog. Clin. Biol. Res.* 170, 847-61 (1984).

114. J. Hung, S. Lam, J. C. LeRiche and B. Palcic, "Autofluorescence of normal and malignant bronchial tissue," *Lasers Surg. Med.,* 11:2, 99-105 (1991).

115. J. Qu, C. MacAulay, S. Lam and B. Palcic, "Laser-induced fluorescence spectroscopy at endoscopy: tissue optics, Monte Carlo modeling, and in vivo measurements," *Opt. Eng.,* 34:11, 3334-43 (1995).

116. G. A. Wagnieres, A. P. Studzinski and H. E. van den Bergh, "An endoscopic fluorescence imaging system for simultaneous visual examination and photo-detection of cancers," *Rev. Scient. Instr*., 68:1, 203-12 (1997).

117. M. Panjehpour, B. F. Overholt, J. L. Schmidhammer, C. Farris, P. F. Buckley and T. Vo-Dinh, "Spectroscopic diagnosis of esophageal cancer: new classification improved measurement system," *Gastroint. Endosc.,* 41:6, 577-81 (1995).

118. M. Panjehpour, B. F. Overholt, T. Vo-Dinh, R. C. Haggitt, D. H. Edwards and F. P. Buckley 3rd, "Endoscopic fluorescence detection of high-grade dysplasia in Barrett's esophagus," *Gastroenterology,* 111:1, 93-101 (1996).

119. Z. Haishan, A. Weiss, C. E. MacAulay, N. MacKinnon, R. Cline and R. Dawson, "Development of a fluorescence video endoscopy imaging system for the early detection of cancer in the gastrointestinal tract," *Proc. SPIE,* 2976, 291-6, 1997.

120. H. Stepp, R. Sroka and R. Baumgartner, "Fluorescence endoscopy of gastrointestinal diseases: basic principles, techniques, and clinical experience," *Endoscop,y* 30:4, 379-86 (1998).

121. H. Zeng, A. Weiss, R. Cline and C. E. MacAualy, "Real-time endoscopic fluorescence imaging for early cancer detection in the gastrointestinal tract," *Bioimagin,* 6:4, 151-65 (1998).

122. H. Messmann, R. Knuchel, W. Baumler, A. Holstege and J. Scholmerich, "Endoscopic fluorescence detection of dysplasia in patients with Barrett's esophagus, ulcerative colitis, or adenomatous polyps after 5-aminolevulinic acid-induced protoporphyrin IX sensitization," *Gastroint. Endosc.,* 49:1, 97-101 (1999).

123. W. Chen and G. Wei, "Multivariate discriminating algorithm for analyzing laser-induced fluorescence spectra of human gastrointestinal cancer," *Proc SPIE.,* 3414: 2-10, 1998.

124. T. McKechnie, A. Jahan, I. Tait, A. Cuschieri, W. Sibbett and M. Padgett, "An endoscopic system for the early detection of cancers of the gastrointestinal tract," *Rev. Scient. Instr,.* 69:6, 2521-3 (1998).

125. B. Banerjee, B. Miedema and H. R. Chandrasekhar, "Emission spectra of colonic tissue and endogenous fluorophores," *Am. J. Med. Sci.,* 316:3, 220-6 (1998).

126. M. A. Mycek, K. T. Schomacker and N. S. Nishioka, "Colonic polyp differentiation using time-resolved autofluorescence spectroscopy," *Gastroint. Endosc.,* 48:4, 390-4 (1998).

127. N. E. Marcon and B. C. Wilson, "The value of fluorescence techniques in gastrointestinal endoscopy--better than the endoscopist's eye? II: The North American experience," *Endoscopy* 30:4, 419-21 (1998).

128. J. Haringsma and G. N. Tytgat, "The value of fluorescence techniques in gastrointestinal endoscopy: better than the endoscopist's eye? I: The European experience," *Endoscopy* 30:4, 416-8 (1998).

129. T. D. Wang, G. S. Janes, Y. Wang, I. Itzkan, J. Van Dam and M. S. Feld, "Mathematical model of fluorescence endoscopic image formation," *Appl. Optics,.* 37:34, 8103-11 (1998).

130. A. G. Bohorfoush, "Tissue spectroscopy for gastrointestinal diseases," *Endoscopy* 28:4, 372-80 (1996).

131. G. I. Zonios, R. M. Cothren, J. T. Arendt, W. Jun, J. Van Dam, J. M. Crawford, R. Manoharan and M. S. Feld, "Morphological model of human colon tissue fluorescence," *IEEE Trans. Biomed. Eng,.* 43:2, 113-22 (1996).

132. T. J. Romer, M. Fitzmaurice, R. M. Cothren, R. Richards-Kortum, R. Petras, M. V. Sivak, Jr. and J. R. Kramer, Jr., "Laser-induced fluorescence microscopy of normal colon and dysplasia in colonic adenomas: implications for spectroscopic diagnosis," *Am. J. Gastroenterol.,* 90:1, 81-7 (1995).

133. G. Bottiroli, A. C. Croce, D. Locatelli, R. Marchesini, E. Pignoli, S. Tomatis, C. Cuzzoni, S. Di Palma, M. Dalfante and P. Spinelli, "Natural fluorescence of normal and neoplastic human colon: a comprehensive "ex vivo" study," *Lasers Surg. Med.,* 16:1, 48-60 (1995).

134. Y. Yang, G. C. Tang, M. Bessler and R. R. Alfano, "Fluorescence spectroscopy as a photonic pathology method for detecting colon cancer," *Lasers in the Life Sciences* 6:4, 259-76 (1995).

135. R. Marchesini, M. Brambilla, E. Pignoli, G. Bottiroli, A. C. Croce, M. Dal Fante, P. Spinelli and S. di Palma, "Light-induced fluorescence spectroscopy of adenomas, adenocarcinomas and non-neoplastic mucosa in human colon. I. In vitro measurements," *J. Photochem. Photobiol. B,* 14:3, 219-30 (1992).

136. R. Richards-Kortum, R. P. Rava, R. E. Petras, M. Fitzmaurice, M. Sivak and M. S. Feld, "Spectroscopic diagnosis of colonic dysplasia," *Photochem. Photobiol.* 53:6, 777-86 (1991).

137. C. R. Kapadia, F. W. Cutruzzola, O. B. KM, M. L. Stetz, R. Enriquez and L. I. Deckelbaum, "Laser-induced fluorescence spectroscopy of human colonic mucosa. Detection of adenomatous transformation," *Gastroenterology* 99:1, 150-7 (1990).

138. R. M. Cothren, R. Richards-Kortum, M. V. Sivak Jr., M. Fitzmaurice, R. P. Rava, G. A. Boyce, M. Doxtader, R. Blackman, T. B. Ivanc, G. B. Hayes and et al., "Gastrointestinal tissue diagnosis by laser-induced fluorescence spectroscopy at endoscopy," *Gastroint. Endosc.* 36:2, 105-11 (1990).

139. R. R. Alfano, G. C. Tang, A. Pradhan, W. Lam, D. S. J. Choy and E. Opher, "Fluorescence spectra from cancerous and normal human breast and lung tissues," *IEEE J. Quantum Electron.* QE-23:10, 1806-11 (1987).

140. R. R. Alfano, A. Pradhan, G. C. Tang and S. J. Wahl, "Optical spectroscopic diagnosis of cancer and normal breast tissues," *J. Opt. Soc. Am. B* 6,1015-23 (1989).

141. G. C. Tang, A. Pradhan, S. Wenling, J. Chen, C. H. Liu, S. J. Wahl and R. R. Alfano, "Pulsed and CW laser fluorescence spectra from cancerous, normal, and chemically treated normal human breast and lung tissues," *Appl. Opt.* 28:12, 2337-42 (1989).

142. Y. Yang, A. Katz, E. J. Celmer, M. Zurawska-Szczepaniak and R. R. Alfano, "Optical spectroscopy of benign and malignant breast tissues," *Lasers in the Life Sciences* 7:2, 115-27 (1996).

143. P. K. Gupta, S. K. Majumder and A. Uppal, "Breast cancer diagnosis using N2 laser excited autofluorescence spectroscopy," *Lasers Surg. Med.,,* 21(5):417-22 (1997).

144. Y. Yuanlong, E. J. Celmer, M. Zurawska-Szczepaniak and R. R. Alfano, "Excitation spectrum of malignant and benign breast tissues: a potential optical biopsy approach," *Lasers in the Life Sciences* 7:4, 249-65 (1997).

145. S. Thomsen and D. Tatman, "Physiological and pathological factors of human breast disease that influence optical diagnosis," *Ann. NY Acad. Sci,* 838, 171-93 (1998).

146. J. H. Dowson and S. J. Harris, "Quantitative studies of the autofluorescence derived from neuronal lipofuscin," *J. Microscopy,* 123:3, 249-58 (1981).

147. S. Montan and L. G. Stromblad, "Spectral characterization of brain tumors utilizing laser-induced fluorescence," *Lasers in the Life Sciences* 1:4, 275-85 (1987).

148. Y. Yang, L. Li, Y. Ye, Q. Zhu and H. Zhang, "Laser excited autofluorescence of brain tumour and accumulation of endogenous porphyrin," *Zhongguo Jiguang/Chinese J. Lasers* 17:5, 318-20, 304 (1990).

149. S. Andersson-Engels, J. Johansson and S. Svanberg, "Medical diagnostic system based on simultaneous multispectral fluorescence imaging," *Appl. Optics,* 33:34, 8022-9 (1994).

150. H. A. Ward, "New laser techniques for diagnosis and treatment of deep-seated brain lesions," *J. Laser Applic.,* 10:5, 224-8 (1998).

151. C. Kittrell, R. L. Willett, C. de los Santos-Pacheo, N. B. Ratliff, J. R. Kramer, E. G. Malk and M. S. Feld, "Diagnosis of fibrous arterial atherosclerosis using fluorescence," *Appl. Optics,* 24:15, 2280-1 (1985).

152. M. P. Sartori, R. A. Sauerbrey, S. Kubodera, F. K. Tittel, R. Roberts and P. D. Henry, "Autofluorescence maps of atherosclerotic human arteries-a new technique in medical imaging," *IEEE J. Quantum Electronics,* QE-23:10, 1794-7 (1987).

153. R. Richards-Kortum, R. P. Rava, R. Cothren, A. Metha, M. Fitzmaurice, N. B. Ratliff, J. R. Kramer, C. Kittrell and M. S. Feld, "A model for extraction of diagnostic information from laser induced fluorescence spectra of human artery wall," *Spectrochimica Acta Part A. Molecular Spectroscopy* 45A:1, 87-93 (1989).

154. R. Richards-Kortum, R. P. Rava, M. Fitzmaurice, L. L. Tong, N. B. Ratliff, J. R. Kramer and M. S. Feld, "A one-layer model of laser-induced fluorescence for diagnosis of disease in human tissue: applications to atherosclerosis," *IEEE Trans. Biomed. Eng.,* 36:12, 1222-32 (1989).

155. K. O. Brien, A. F. Gmitro, G. R. Gindi, M. L. Stetz, F. W. Cutruzzola, L. I. Laifer and L. I. Deckelbaum, "Development and evaluation of spectral classification algorithms for fluorescence guided laser angioplasty," *IEEE Trans. Biomed. Eng,.* 36:4, 424-31 (1989).

156. G. H. Pettit, R. Pini, F. K. Tittel, R. Sauerbrey, M. P. Sartori and P. D. Henry, "Excimer laser induced autofluorescence from atherosclerotic human arteries," *Lasers in the Life Sciences* 3:4, 205-15 (1990).

157. M. Keijzer, R. R. Richards-Kortum, S. L. Jacques and M. S. Feld, "Fluorescence spectroscopy of turbid media: autofluorescence of the human aorta," *Appl. Opt*ics, 20, 4286-92 (1990).

158. T. G. Papazoglou, T. Papaioannou, K. Arakawa, M. Fishbein, V. Z. Marmarelis and W. S. Grundfest, "Control of excimer laser aided tissue ablation via laser-induced fluorescence monitoring," *Appl. Optics,* 29:33, 4950-5 (1990).

159. G. R. Gindi, C. J. Darken, O. B. KM, M. L. Stetz and L. I. Deckelbaum, "Neural network and conventional classifiers for fluorescence-guided angioplasty," *IEEE Trans. Biomed. Eng.,* 38:3, 246-52 (1991).

160. S. Andersson-Engels, A. Gustafson, J. Johansson, U. Stenram, K. Svanberg and S. Svanberg, "Investigation of possible fluorophores in human atherosclerotic," *Lasers in the Life Sciences* 5:1-2, 1-11 (1992).

161. S. Warren, K. Pope, Y. Yazdi, A. J. Welch, S. Thomsen, A. L. Johnston, M. J. Davis and R. Richards-Kortum, "Combined ultrasound and fluorescence spectroscopy for physico-chemical imaging of atherosclerosis," *IEEE Trans. Biomed. Eng.,* 42:2, 121-32 (1995).

162. R. T. Strebel, U. Utzinger, M. Peltola, J. Schneider, P. F. Niederer and O. M. Hess, "Excimer laser spectroscopy: Influence of tissue ablation on vessel wall fluorescence," *J. Laser Applics.,* 10:1, 34-40 (1998).

163. D. W. Hochman, "Intrinsic optical changes in neuronal tissue. Basic mechanisms," *Neurosurg.Clinics N Amer.,* 8:3, 393-412 (1997).

164. R. Richards-Kortum, "Fluorescence spectroscopy of turbid media," in *Optical thermal response of laser-irradiated tissue,* A. J. Welch and M. J. C. van Gemmert, Eds., pp. 667-706, Plenum Press, New York (1995).

165. R. Richards-Kortum and E. Sevick-Muraca, "Quantitative optical spectroscopy for tissue diagnosis," *Ann Rev Phys Chem*., 47:555-606 (1996).

166. A. Gillenwater, R. Jacob and R. Richards-Kortum, "Fluorescence spectroscopy: a technique with potential to improve the early detection of aerodigestive tract neoplasia," *Head & Neck,* 20:6, 556-62 (1998).

167. S. Andersson-Engels, C. Klinteberg, K. Svanberg and S. Svanberg, "In vivo fluorescence imaging for tissue diagnostics," *Phys. Med. Biol.,* 42:5, 815-24 (1997).

168. I. J. Bigio and J. R. Mourant, "Ultraviolet and visible spectroscopies for tissue diagnostics: fluorescence spectroscopy and elastic-scattering spectroscopy," *Phys. Med. Biol.,* 42:5, 803-14 (1997).

169. T. G. Papazoglou, "Malignancies and atherosclerotic plaque diagnosis--is laser induced fluorescence spectroscopy the ultimate solution?," *J. Photochem. Photobiol.. B*, 28:1, 3-11 (1995).

170. N. S. Nishioka, "Laser-induced fluorescence spectroscopy," Gastroent. Endosc. Clinics N Amer.*,,* 4:2, 313-26 (1994).

171. G. A. Wagnieres, W. M. Star and B. C. Wilson, "In vivo fluorescence spectroscopy and imaging for oncological applications," *Photochem. Photobiol*., 68:5, 603-32 (1998).

172. K. Pope, S. Warren, Y. Yazdi, J. Johnston, M. Davis and R. Richards-Kortum, "Dual imaging of arterial walls: Intravascular ultrasound and fluorescence spectroscopy," *Proc. SPIE,* 1878, 42-50 (1993).

173. S. Warren, K. Pope, Y. Yazdi, A. Johnston and R. Richards-Kortum, "Monte Carlo fluorescence verification of experimental results for the combined ultrasound and spectroscopic imaging of coronary artery disease," *Proc. 30th Ann. Rocky Mt. Bioeng. Symp.,* 29, 457-458, 1993.

174. J. T. Pfefer, K. T. Schomacker and N. S. Nishioka, "Effect of fiber optic probe design on fluorescent light propagation in tissue," *Proc SPIE,* 4257, 410-416 (2001).

175. C. Pitiris, *Fluorescence imaging instrumentation and clinical study for the diagnosis of cervical pre-cancer and cancer,* Thesis, The University of Texas at Austin (1995).

176. A. Agrawal, *Multi-pixel fluorescence spectroscopy for the diagnosis of cervical precancer,* Thesis, The University of Texas at Austin (1998).

177. A. Agrawal, U. Utzinger, C. Brookner, C. Pitris, M. F. Mitchell and R. Richards-Kortum, "Fluorescence spectroscopy of the cervix: influence of acetic acid, cervical mucus, and vaginal medications," *Lasers Surg. Med.,* 25:3, 237-49 (1999).

178. R. J. Nordstrom, L. Burke, J. M. Niloff, J. F. Myrtle, "Identification of cervical intraepithelial neoplasia (CIN) using UV-excited fluorescence and diffuse-reflectance tissue spectroscopy," *Lasers Surg. Med.,* 29, 118-127 (2001).

179. D. G. Ferris, R. A. Lawhead, E. D. Dickman, N. Holtzapple, J. A. Miller, S. Grogan, S. Bambot, A. Agrawal and M. L. Faupel, "Multimodal hyperspectral imaging for the noninvasive diagnosis of cervical neoplasia," *J. Lower Genital Tract Dis.,* 5:2, 65-72, 2001.

180. N. Ramanujam, J. Chen, K. Gossage, R. Richards-Kortum and B. Chance, "Fast and noninvasive fluorescence imaging of biological tissues in vivo using a flying-spot scanner," *IEEE Trans. Biomed. Eng,*. 48:9, 1034-1041 (2001).

181. A. K. Dattamajumdar, D. Wells, J. Parnell, J. T. Lewis, D. Ganguly, T. C. Wright Jr., "Preliminary experimental results from multi-center clinical trials for detection of cervical precancerous lesions using the Cerviscan system: a novel full field evoked fluorescence based imaging instrument," *Proc. IEEE, Eng. Med. Biol.,* 23, (2001).

182. S. Avrillier, E. Tinet, D. Ettori, J. M. Tualle, B Gélébart, "Influence of the emission-reception geometry in laser-induced fluorescence spectra from turbid media," *Appl. Optics,* 37:13, 2781-7 (1998).

183. A. Durkin, *Quantitative fluorescence spectroscopy of turbid samples,* Dissertation, The University of Texas at Austin (1995).

184. J.A. Zuclich, T Shimada, T.R. Loree, I. Bigio, K. Strobl, N. Shuming, "Rapid noninvasive optical characterization of the human lens," *Lasers in the Life Sciences* 6:1, 39-53 (1994).

185. A. F. Zuluaga, U. Utzinger, A. Durkin, H. Fuchs, A. Gillenwater, R. Jacob, B. Kemp, J. Fan and R. Richards-Kortum, "Fluorescence excitation emission matrices of human tissue: a system for *in vivo* measurement and method of data analysis," *Appl. Spectrosc.,*. 53:3, 302-11 (1999).

186. J. J. Baraga, M. S. Feld and R. P. Rava, "In situ optical histochemistry of human artery using near infrared Fourier transform Raman spectroscopy," *Proc. Nat. Acad. Sci. USA*, 89:8, 3473-7 (1992).

187. A. J. Berger, Y. Wang and M. S. Feld, "Rapid, noninvasive concentration measurements of aqueous biological analytes by near-infrared Raman spectroscopy," *Appl. Optics,* 35:1, 209-12 (1996).

188. A. J. Berger, I. Itzkan and M. S. Feld, "Feasibility of measuring blood glucose concentration by near-infrared Raman spectroscopy," *Spectrochimica Acta Part A-Molecular Spectroscopy* 53A:2, 287-92 (1997).

189. C. J. Frank, D. C. Redd, T. S. Gansler and R. L. McCreery, "Characterization of human breast biopsy specimens with near-IR Raman spectroscopy," *Analyt. Chem.,* 66:3, 319-26 (1994).

190. C. J. Frank, R. L. McCreery and D. C. Redd, "Raman spectroscopy of normal and diseased human breast tissues," *Analyt. Chem*., 67:5, 777-83 (1995).

191. M. Gniadecka, H. C. Wulf, N. N. Mortensen, O. F. Nielsen and D. H. Christensen, "Diagnosis of basal cell carcinoma by Raman spectroscopy," *J. Raman Spectrosc.* 28:2-3, 125-9 (1997).

192. K. Kneipp, H. Kneipp, V. B. Kartha, R. Manoharan, G. Deinum, I. Itzkan, R. R. Dasari and M. S. Feld, "Detection and identification of a single DNA base molecule using surface-enhanced Raman scattering (SERS)," *Phys. Rev. E,* 57:6, R6281-4 (1998).

193. A. Mahadevan-Jansen, M. F. Mitchell, N. Ramanujam, U. Utzinger and R. Richards-Kortum, "Development of a fiber optic probe to measure NIR Raman spectra of cervical tissue in vivo," *Photochem. Photobiol.,* 68:3, 427-31 (1998).

194. A. Mahadevan-Jansen, M. F. Mitchell, N. Ramanujam, A. Malpica, S. Thomsen, U. Utzinger and R. Richards-Kortum, "Near-infrared Raman spectroscopy for in vitro detection of cervical precancers," *Photochem. Photobiol.,* 68:1, 123-32 (1998).

195. R. Manoharan, J. J. Baraga, M. S. Feld and R. P. Rava, "Quantitative histochemical analysis of human artery using Raman spectroscopy," *J. Photochem. Photobiol. B*, 16:2, 211-33 (1992).

196. R. Manoharan, Y. Wang, R. R. Dasari, S. S. Singer, R. P. Rava and M. S. Feld, "Ultraviolet resonance Raman spectroscopy for detection of colon cancer," *Lasers in the Life Sciences* 6:4, 217-27 (1995).

197. R. Manoharan, W. Yang and M. S. Feld, "Histochemical analysis of biological tissues using Raman spectroscopy," *Spectrochimica Acta,* 52A:2, 215-49 (1996).

198. R. Manoharan, K. Shafer, L. Perelman, J. Wu, K. Chen, G. Deinum, M. Fitzmaurice, J. Myles, J. Crowe, R. R. Dasari and M. S. Feld, "Raman spectroscopy and fluorescence photon migration for breast cancer diagnosis and imaging," *Photochem. Photobiol.,* 67:1, 15-22 (1998).

199. A. Mizuno, T. Hayashi, K. Tashibu, S. Maraishi, K. Kawauchi and Y. Ozaki, "Near-infrared FT-Raman spectra of the rat brain tissues," *Neurosc. Letters* 141:1, 47-52 (1992).

200. R. P. Rava, J. J. Baraga and M. S. Feld, "Near infrared Fourier transform Raman spectroscopy of human artery," *Spectrochimica Acta Part* 47A:3-4, 509-12 (1991).

201. T. J. Romer, J. F. Brennan, 3rd, T. C. Schut, R. Wolthuis, R. C. van den Hoogen, J. J. Emeis, A. van der Laarse, A. V. Bruschke and G. J. Puppels, "Raman spectroscopy for quantifying cholesterol in intact coronary artery wall," *Atherosclerosis,* 141:1, 117-24 (1998).

202. T. J. Romer, J. F. Brennan, 3rd, M. Fitzmaurice, M. L. Feldstein, G. Deinum, J. L. Myles, J. R. Kramer, R. S. Lees and M. S. Feld, "Histopathology of human coronary atherosclerosis by quantifying its chemical composition with Raman spectroscopy," *Circulation,* 97:9, 878-85 (1998).

203. H. P. Buschman, E. T. Marple, M. L. Wach, B. Bennett, T. C. Schut, H. A. Bruining, A. V. Bruschke, A. van der Laarse and G. J. Puppels, "In vivo determination of the molecular composition of artery wall by intravascular Raman spectroscopy," *Analyt. Chem.,* 72:16, 3771-5 (2000).

204. E. B. Hanlon, R. Manoharan, T. W. Koo, K. E. Shafer, J. T. Motz, M. Fitzmaurice, J. R. Kramer, I. Itzkan, R. R. Dasari and M. S. Feld, "Prospects for in vivo Raman spectroscopy," *Phys. Med. Biol.,* 45:2, R1-59 (2000).

205. T. R. Hata, T. A. Scholz, I. V. Ermakov, R. W. McClane, F. Khachik, W. Gellermann and L. K. Pershing, "Non-invasive raman spectroscopic detection of carotenoids in human skin," *J. Invest. Dermatol*., 115:3, 441-8 (2000).

206. C. J. de Lima, S. Sathaiah, L. Silveira, R. A. Zangaro and M. T. Pacheco, "Development of catheters with low fiber background signals for Raman spectroscopic diagnosis applications," *Artificial Organs,* 24:3, 231-4 (2000).

207. M. G. Shim, L. M. Song, N. E. Marcon and B. C. Wilson, "In vivo near-infrared Raman spectroscopy: demonstration of feasibility during clinical gastrointestinal endoscopy," *Photochem. Photobiol.,* 72:1, 146-50 (2000).

208. M. L. Myrick, S. M. Angel and R. Desiderio, "Comparison of some fiber optic configurations for measurement of luminescence and Raman scattering," *Appl. Optics,* 29:9, 1333-44 (1990).

209. M. Myrick and S. Angel, "Elimination of background in fiber-optic Raman measurements," *Appl. Spectrosc.,* 44:4, 758-63 (1990).

210. S. Nave, P. O'Rourke and W. Tool, Sampling probes enhance remote chemical analysis, *Laser Focus World,* December, 83-8 (1995).

211. K. Tanaka, M. T. T. Pacheco, J. F. Brennan, III, I. Itzkan, A. J. Berger, R. R. Dasari and M. S. Feld, "Compound parabolic concentrator probe for efficient light collection in spectroscopy of biological tissue," *Appl. Optics,* 35:4, 758-63 (1996).

212. A. Mahadevan-Jansen and E. Richards-Kortum, "Raman spectroscopy for cancer detection: A Review," *J. Biomed. Optics,* 1:1, 31-70 (1998).

213. H. Owen, D. Battey, M. Pelltier and J. Slater, "New spectroscopic instrument based on volume holographic optical elements," *Proc. SPIE,* 2406, 260-267 (1995).

214. U. Utzinger, *Selective coronary excimer laser angioplasty,* Dissertation, Swiss Federal Institute of Technology (1995).

215. S. Lam, "Bronchoscopic, photodynamic, and laser diagnosis and therapy of lung neoplasms," *Current Opinion In Pulmonary Medicine* 2:4, 271-6 (1996).

216. M. A. Biel, "Photodynamic therapy and the treatment of head and neck cancers," *J. Clin. Laser Med. Surg*., 14:5, 239-44 (1996).

217. E. A. Popovic, A. H. Kaye and J. S. Hill, "Photodynamic therapy of brain tumors," *J. Clin. Laser Med. Surg*., 14:5, 251-61 (1996).

218. J. M. Nauta, H. L. van Leengoed, W. M. Star, J. L. Roodenburg, M. J. Witjes and A. Vermey, "Photodynamic therapy of oral cancer. A review of basic mechanisms and clinical applications," *Eur. J. Oral Sci.,* 104:2 (Pt 1), 69-81 (1996).

219. G. Wagnieres, S. Cheng, M. Zellweger, N. Utke, D. Braichotte, J. P. Ballini and H. van den Bergh, "An optical phantom with tissue-like properties in the visible for use in PDT and fluorescence spectroscopy," *Phys. Med. Biol.* 42:7, 1415-26 (1997).

220. R. Bissonnette and H. Lui, "Current status of photodynamic therapy in dermatology," *Dermatology Clinics,* 15:3, 507-19 (1997).

221. J. Moan, Q. Peng, R. Sorensen, V. Iani and J. M. Nesland, "The biophysical foundations of photodynamic therapy," *Endoscopy,* 30:4, 387-91 (1998).

222. H. van den Bergh, "On the evolution of some endoscopic light delivery systems for photodynamic therapy ," *Endoscopy*, 30:4, 392-407 (1998).

223. J. F. Savary, P. Grosjean, P. Monnier, C. Fontolliet, G. Wagnieres, D. Braichotte and H. van den Bergh, "Photodynamic therapy of early squamous cell carcinomas of the esophagus: a review of 31 cases," *Endoscopy,* 30:3, 258-65 (1998).

224. R. R. Allison, T. S. Mang and B. D. Wilson, "Photodynamic therapy for the treatment of nonmelanomatous cutaneous malignancies," *Seminars in Cutaneous Medicine & Surgery* 17:2, 153-63 (1998).

225. N. L. Oleinick and H. H. Evans, "The photobiology of photodynamic therapy: cellular targets and mechanisms," *Radiation Res.,* 150:5 , S146-56 (1998).

226. H. Kato, "Photodynamic therapy for lung cancer--a review of 19 years' experience," *J. Photochem. Photobiol. B* 42:2, 96-9 (1998).

227. C. Fritsch, G. Goerz and T. Ruzicka, "Photodynamic therapy in dermatology," *Arch. Dermatol.,* 134:2, 207-14 (1998).

228. M. A. Biel, "Photodynamic therapy and the treatment of head and neck neoplasia," *Laryngoscope* 108:9, 1259-68 (1998).

229. E. Sinfosky, "High power diffusion tip fibers for photocoagulation," *Proc. IEEE LEOS* 9, (1996).

230. P. Rol, *Optics for Transscleral Laser Applications,* Dissertation, Swiss federal institute of technology (1992).

231. H. Ward, "Molding of laser energy by shaped optic fiber tips," *Laser Surg. Med.,* 7:405-13 (1987).

232. A. Nica, "Lens coupling in fiber-optic devices: efficiency limits," *Appl. Optics* 20:18, 3136-45 (1981).

233. A. Rabl, "Concentrating Collectors, Solar Energy Conversion. An introductory course," in *Solar energy conversion : an introductory course : selected lectures from the 5th Course on Solar Energy Conversion,* A. Dixon and J. Leslie (Eds.), pp. 185-252, Pergamon, Toronto (1979).

234. U. Utzinger and R. Richards-Kortum, "Fiber optic probes for optical spectroscopy, clinical applications," in *Encyclopedia of Spectroscopy and Spectrometry,* J. C. Lindon, G. E. Tranter and J. L. Holmes, Eds., pp. 513-527, Academic Press, (2000).

TABLE 1: Materials suitable for fiberoptic probe enclosures.

	Fiberoptic application	*Reference medical application*	*Biocompatibility*	*Useful properties*
Metals, Alloys				
stainless steel 302	tubing, housing	needle tubing	literature	
stainless steel 316	tubing, housing	needle tubing	literature implants	• increased acid resistant
Titanium and Titanium alloys	tubing housing		literature implants	
Amalgam		dental filling material	literature dental implants	
Ceramics				
Aluminum Oxide, Sapphire	scattering particles optical window		literature implants	• transmission 200nm - 3μm • high thermal conductivity • almost insoluble
Polymers				
Polyethylene PE	tubing, housing	pharmaceutical bottles, catheter	literature hip implants	
PVC	tubing	blood bags, cannulae	USP VI	
Teflon, PTFE	tubing	catheter, vascular grafts	USP VI	• temperature resistant, 230^{o}C
PMMA	optical components	bone cement, blood pump	literature optical implants	• transparent in the visible
Polyester, PET		suture, mesh, vascular grafts	literature implants	
Polyimide	tubing		USP VI	• temperature resistant 220^{o}C
Silicone rubber	catheters, coatings, tubing		literature implants	• temperature resistant 200^{o}C • flexible
Cycloolefin copolymer, Topas	optical components	micro plates for cell culture	USP VI	• 93% transmission visible • UV transparent below 300 nm
Glue				
Cyanoacrylate (superglue)		surgical adhesive	USP VI	• fast bonding
EPOTEK 301	bonding of optical elements		USP VI	• transparent in the UV and visible • low autofluorescence
EPOTEK 353, 375	sealing		USP VI	• autoclavable
2-TON DevCon	sealing		suggestive for low skin carcinogenicity	• high tensile strength • water resistant • transparent

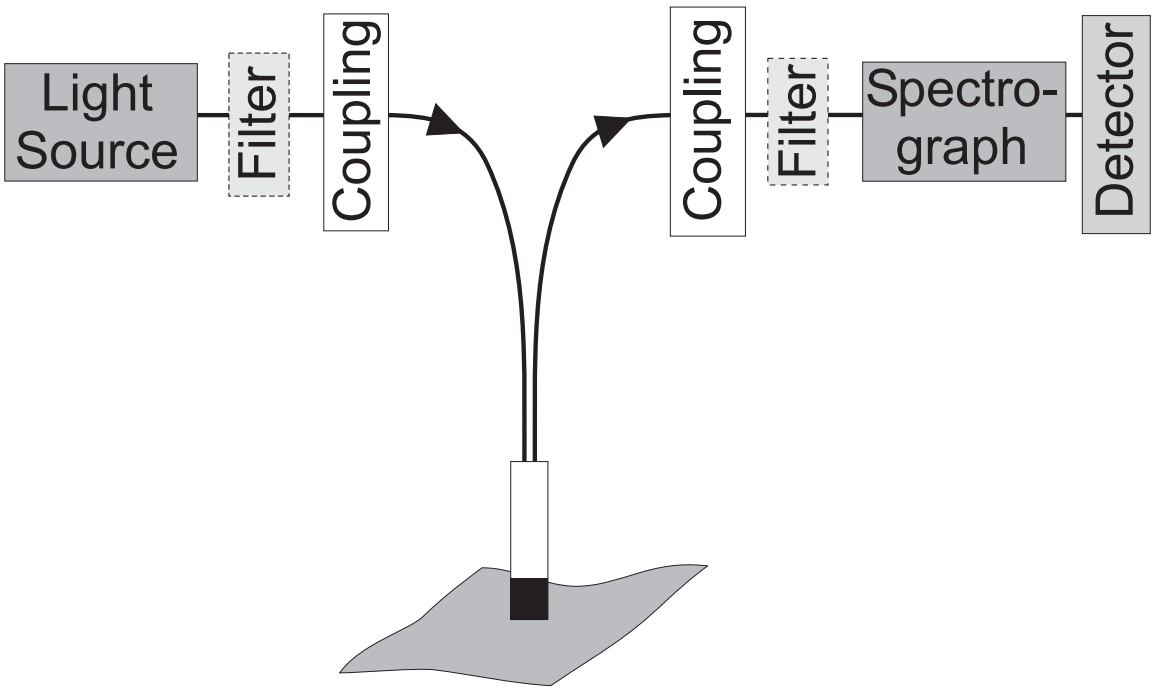
Light Source
Filter
Coupling
Coupling
Filter
Spectro-graph
Detector

Figure 1 a)

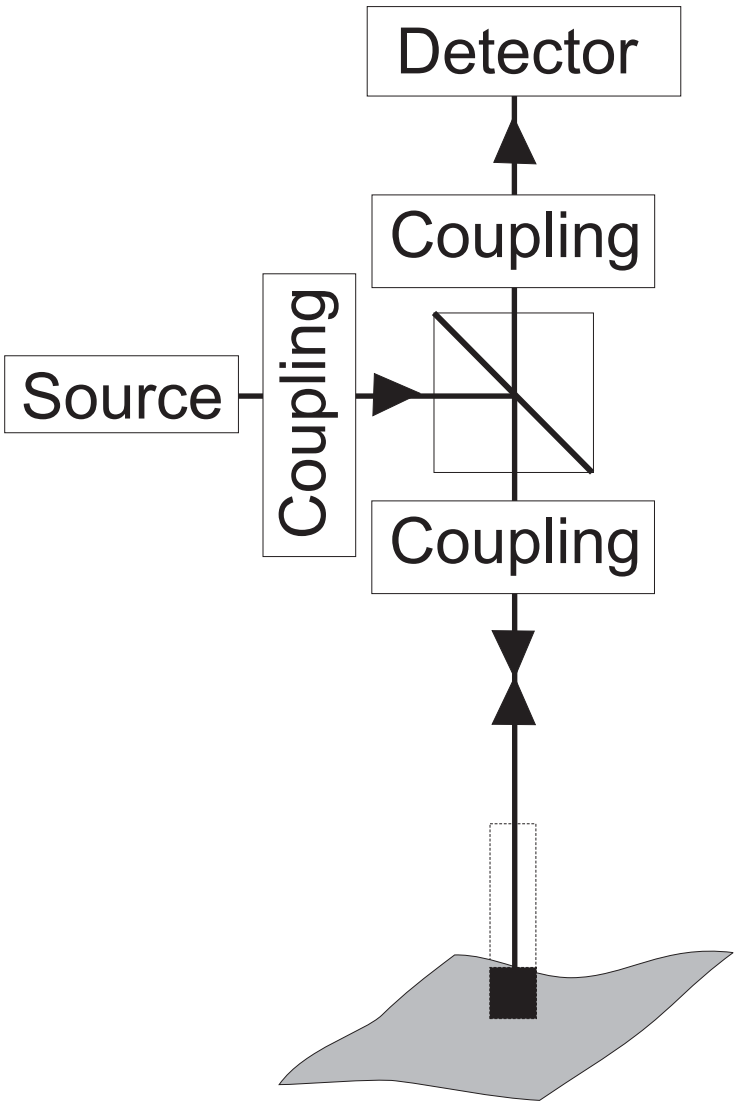

Figure 1 b)

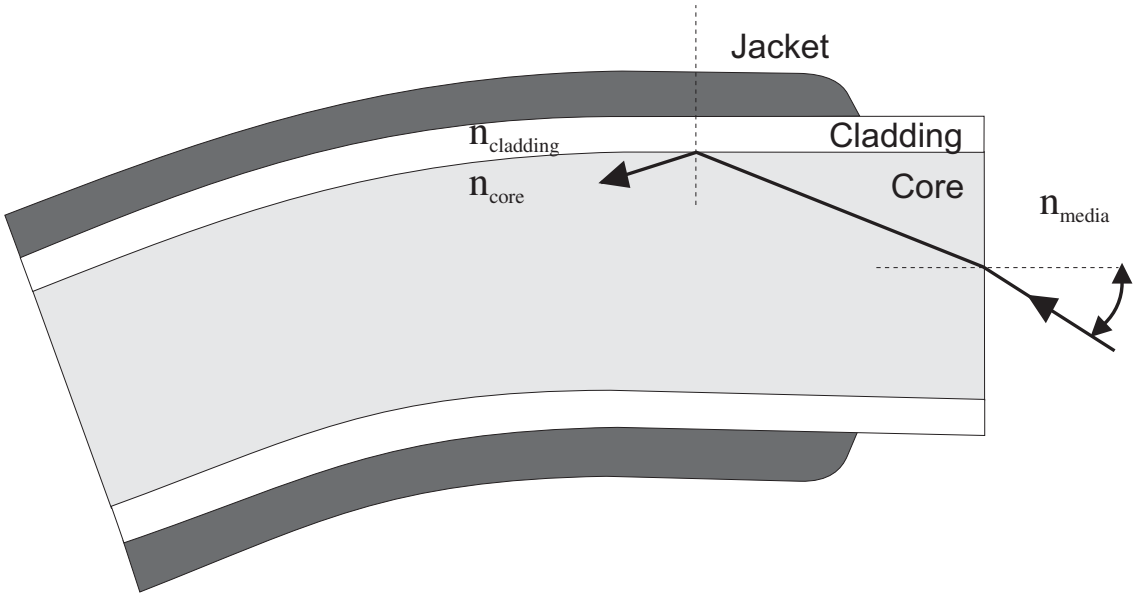

Figure 2)

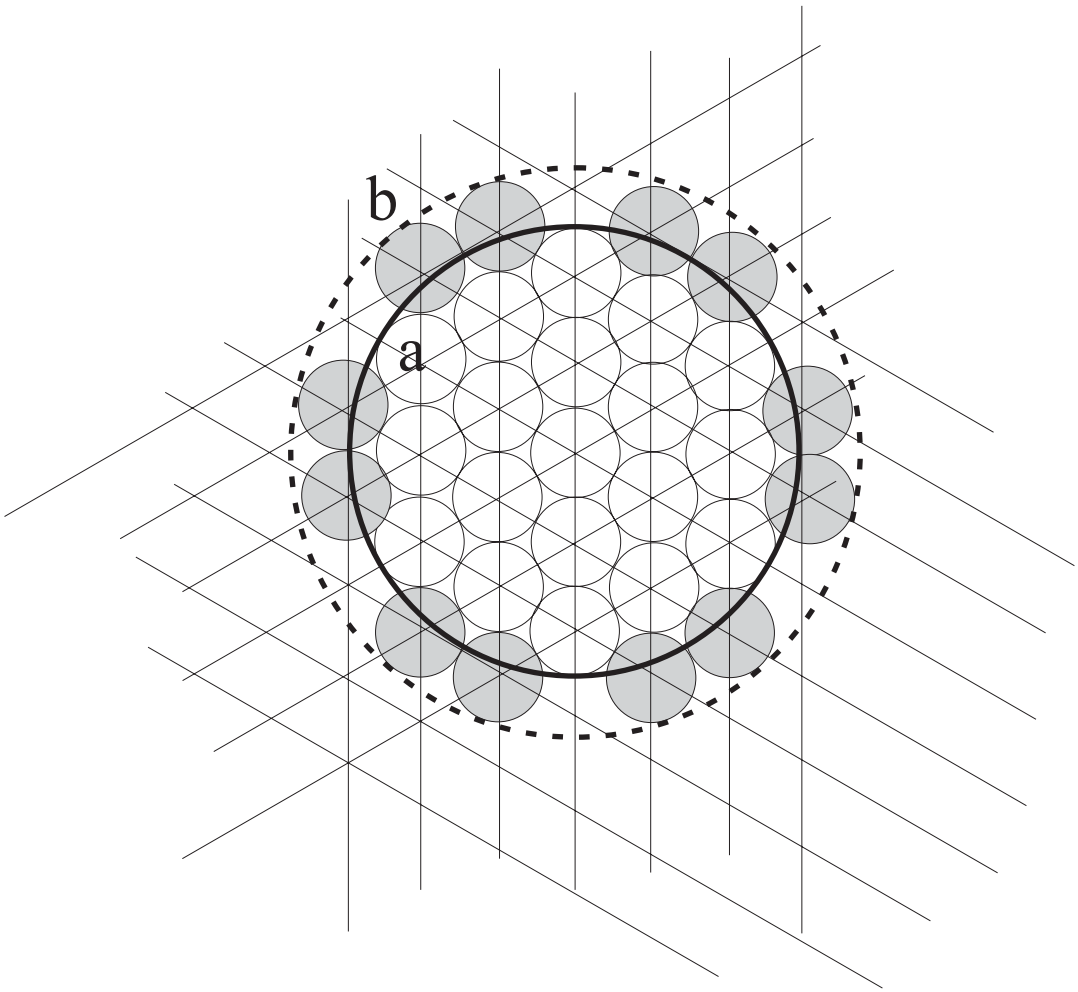

Figure 3)

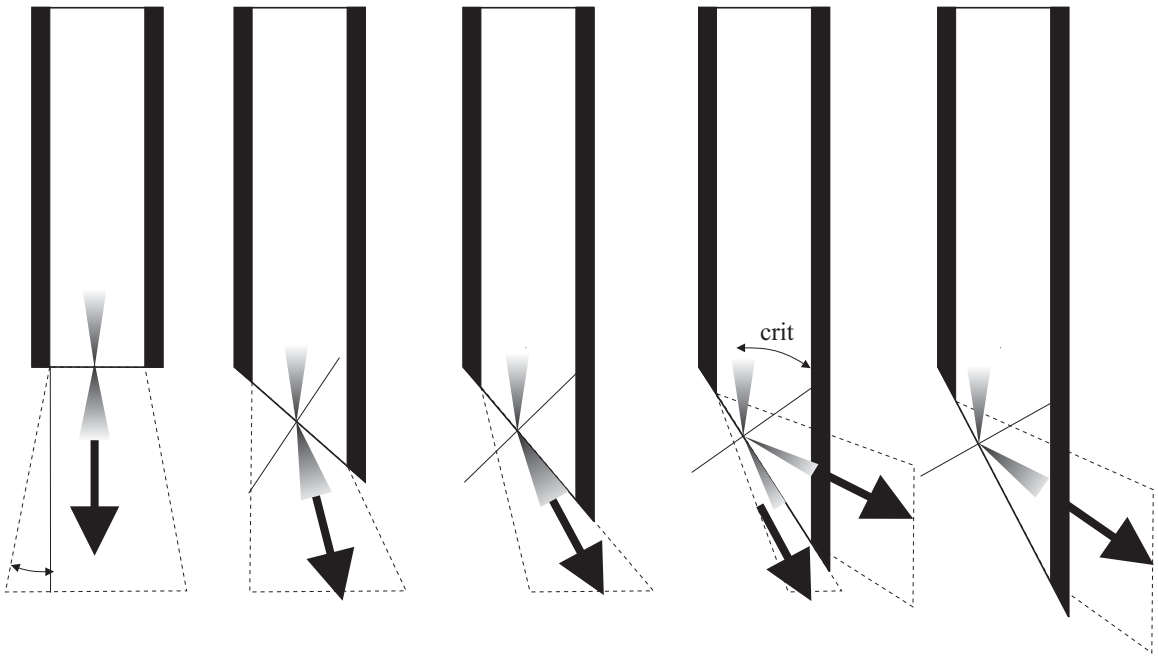

Figure 4 a,b,c,d,e)

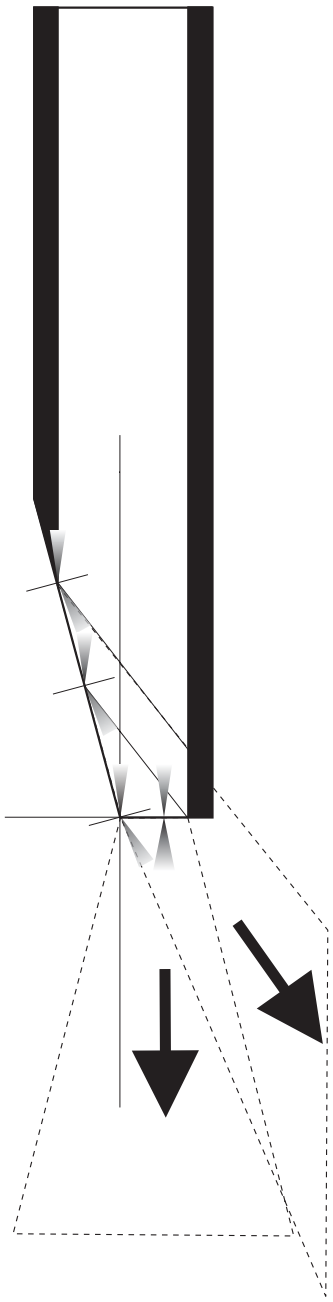

Figure 4 f)

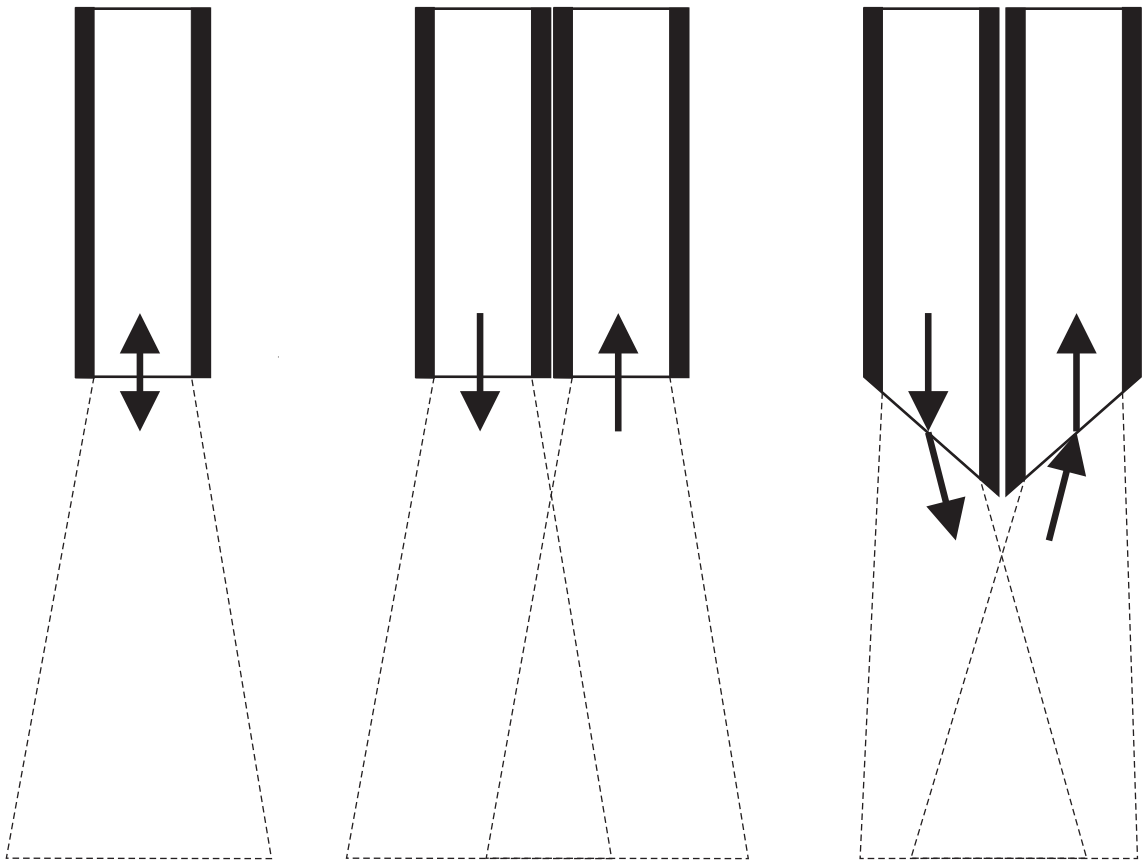

Figure 4 g,h,i)

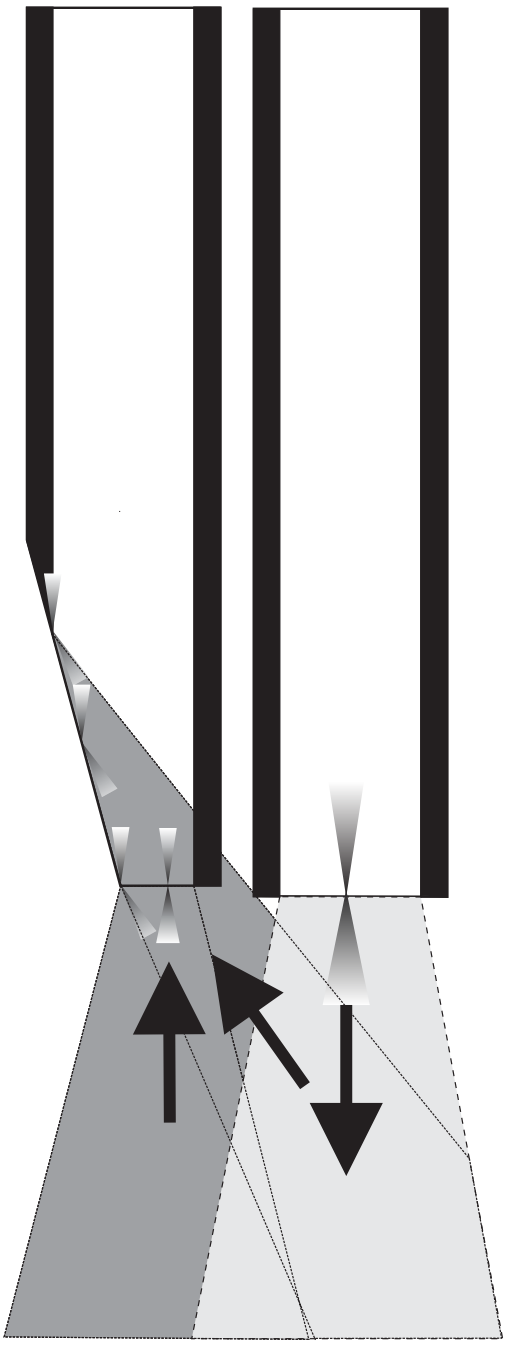

Figure 4 j)

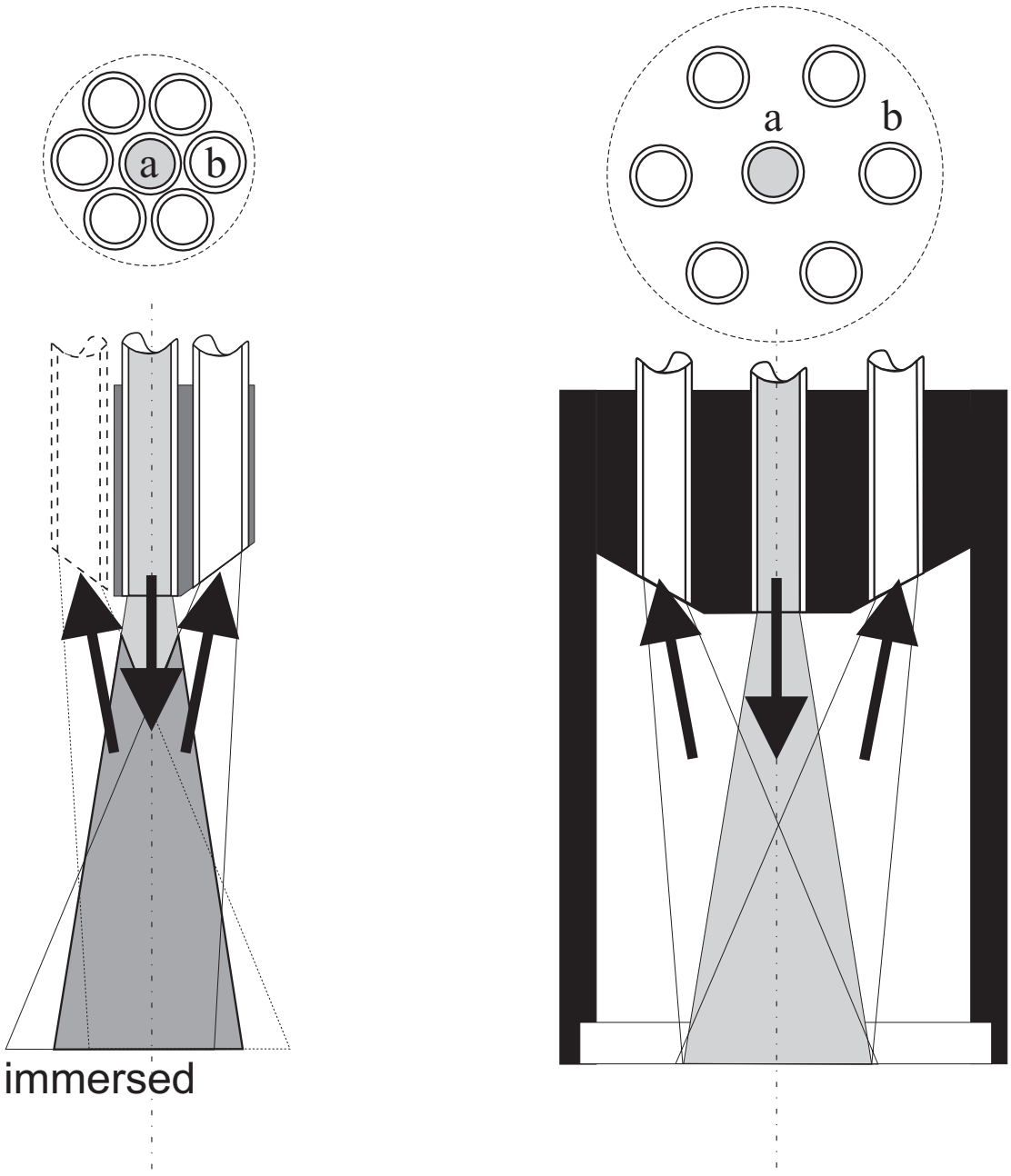

Figure 4 k, l)

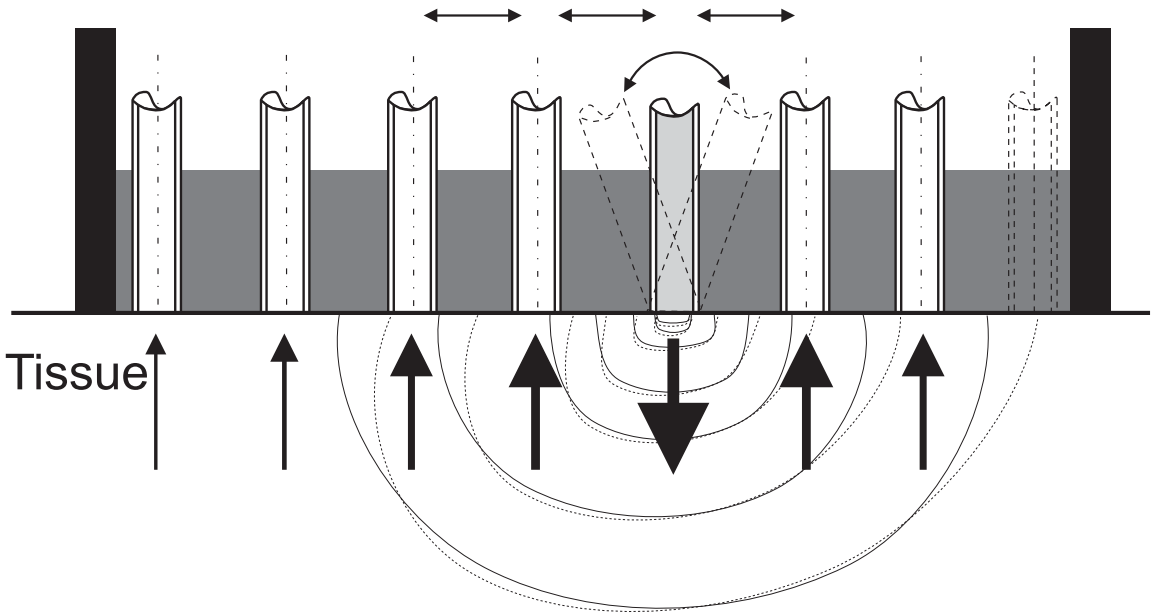

Figure 5 a)

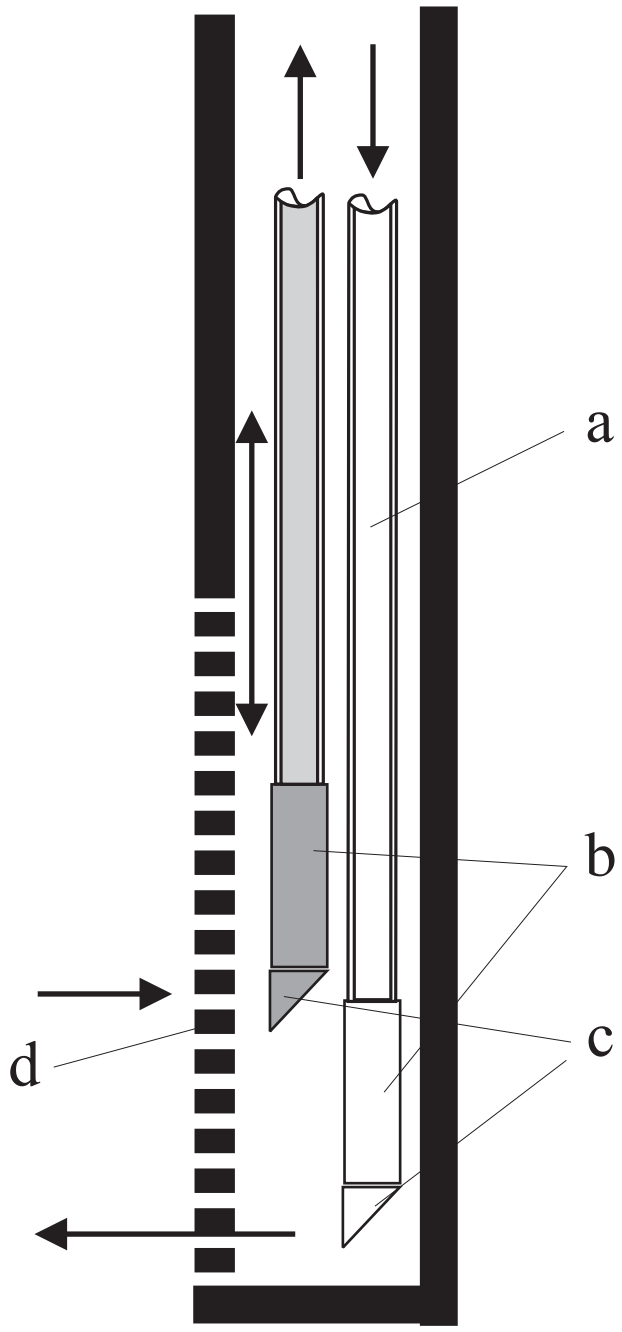

Figure 5b)

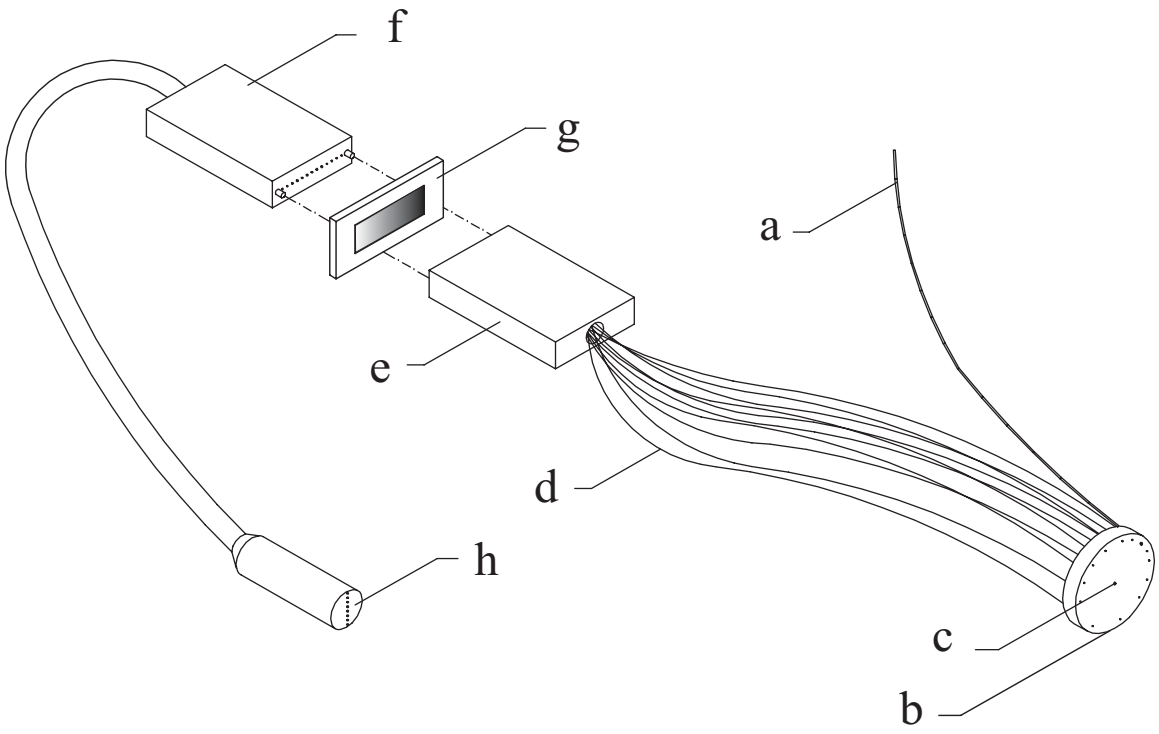

Figure 5 c)

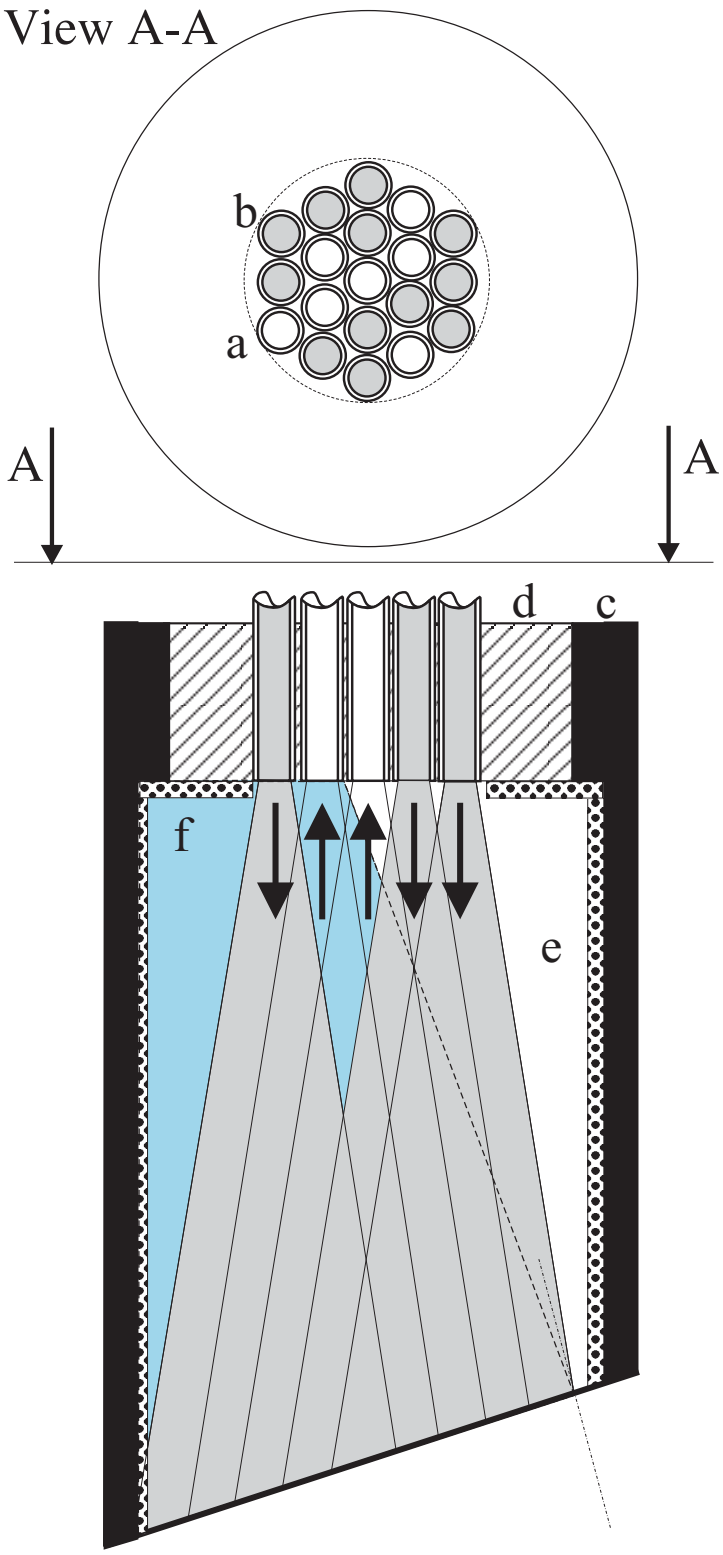

Figure 5 d)

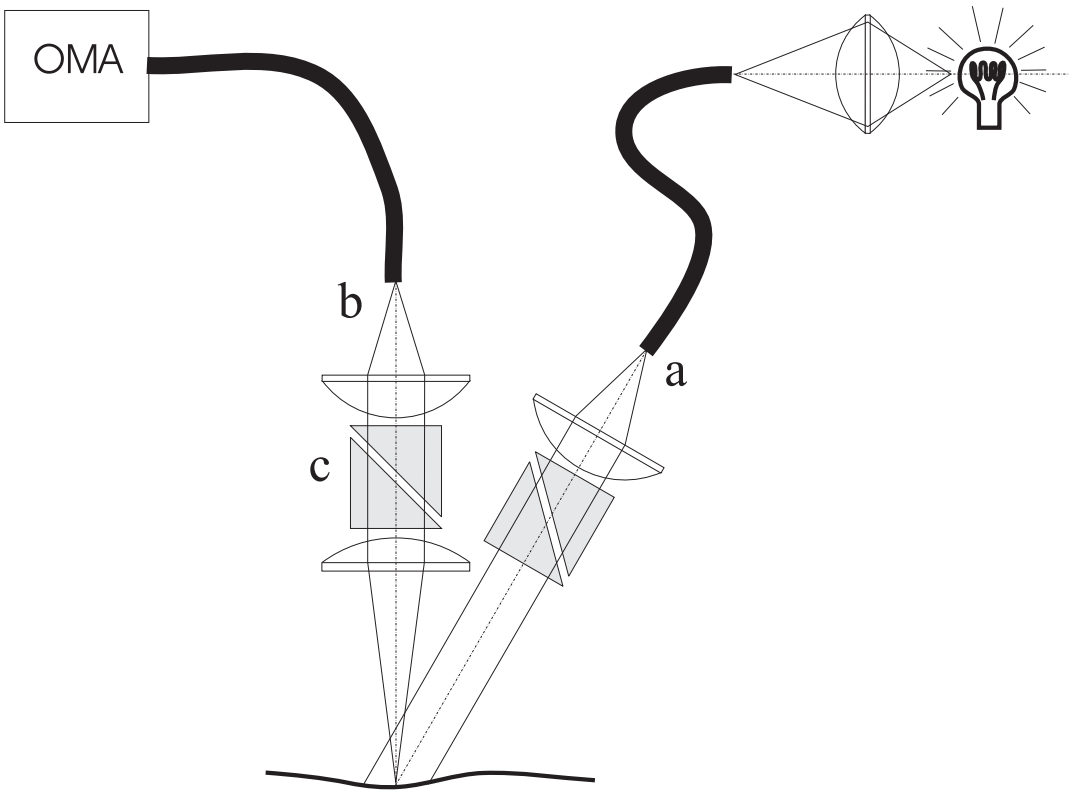

Figure 5 e)

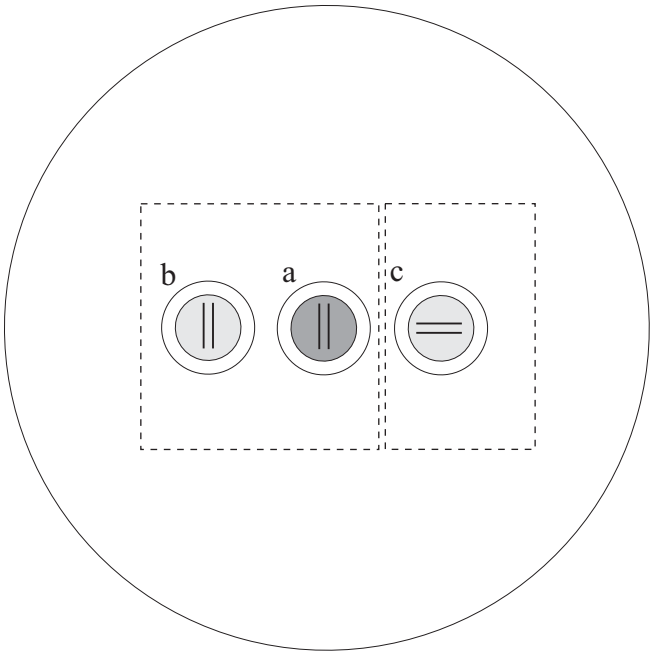

Figure 5 f)

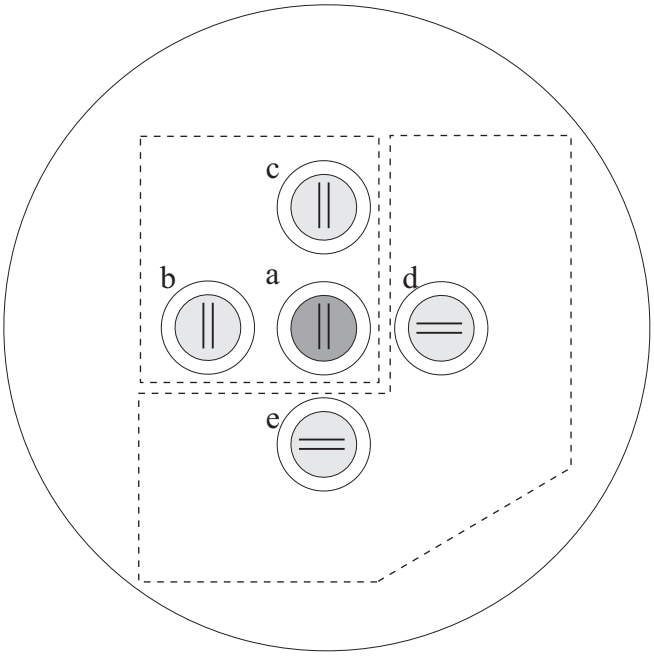

Figure 5 g)

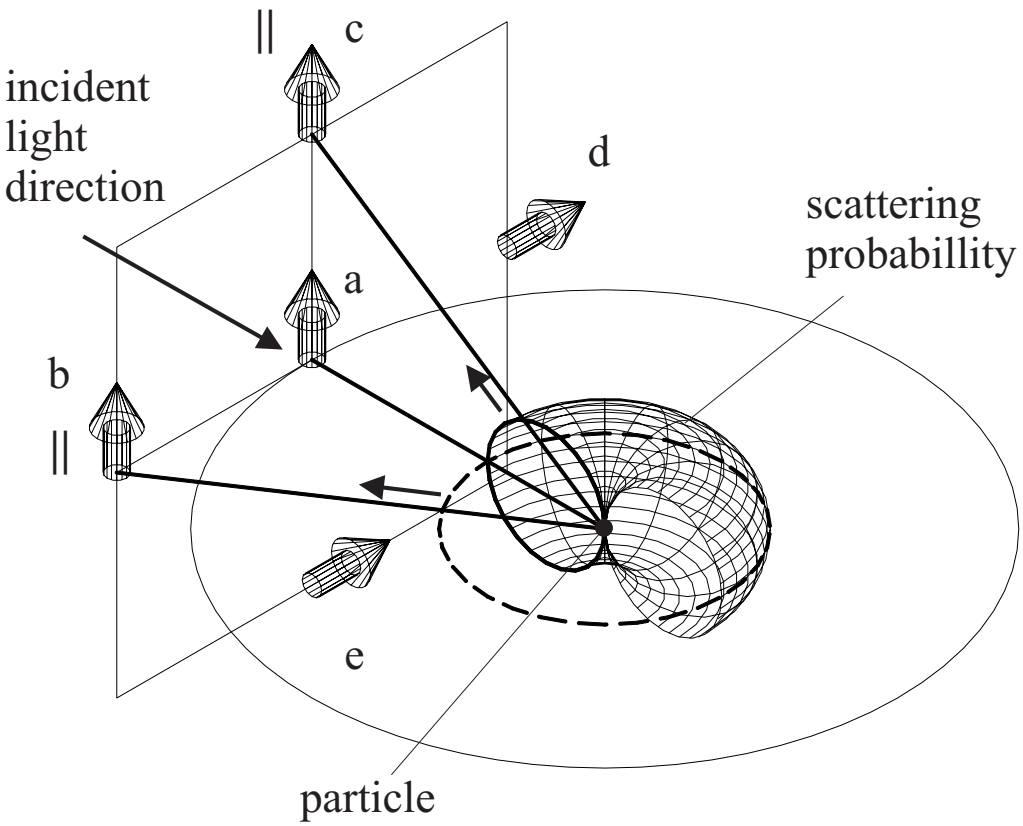
c
incident
light
direction
d
scattering
probabillity
a
b
e
particle

Figure 5 h)

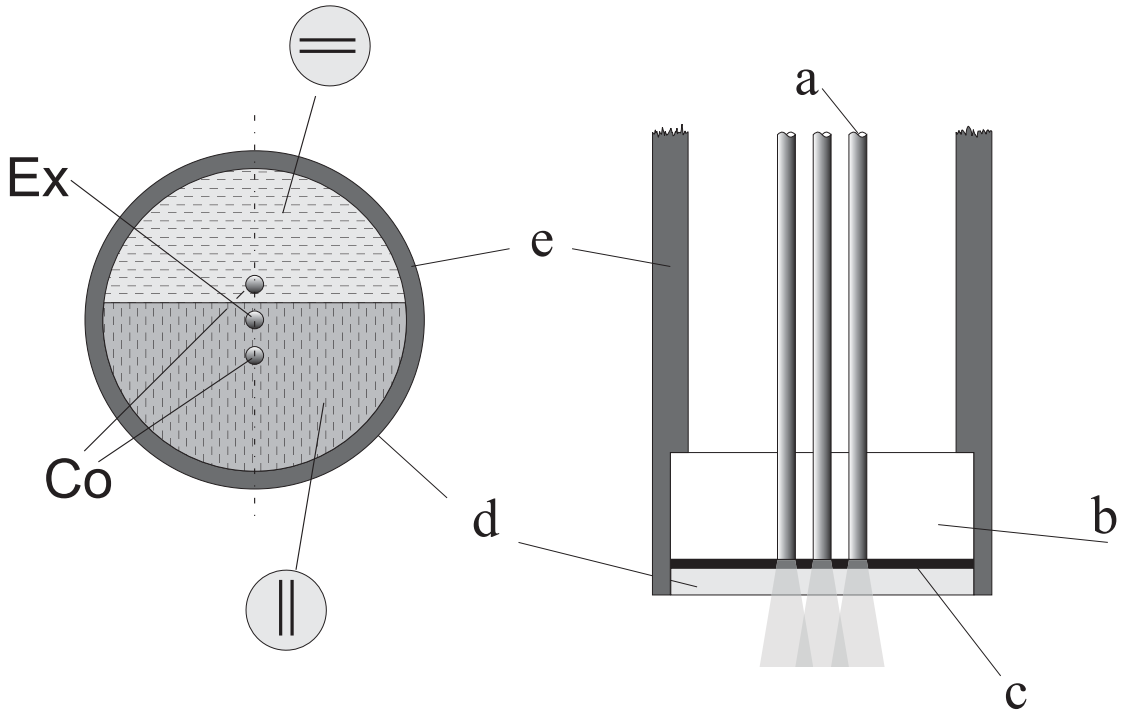

Figure 5 i)

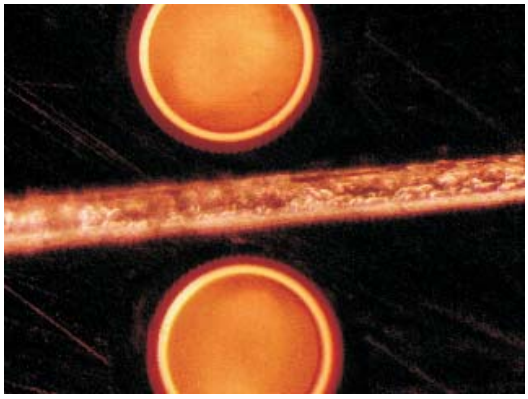

Figure 5 j)

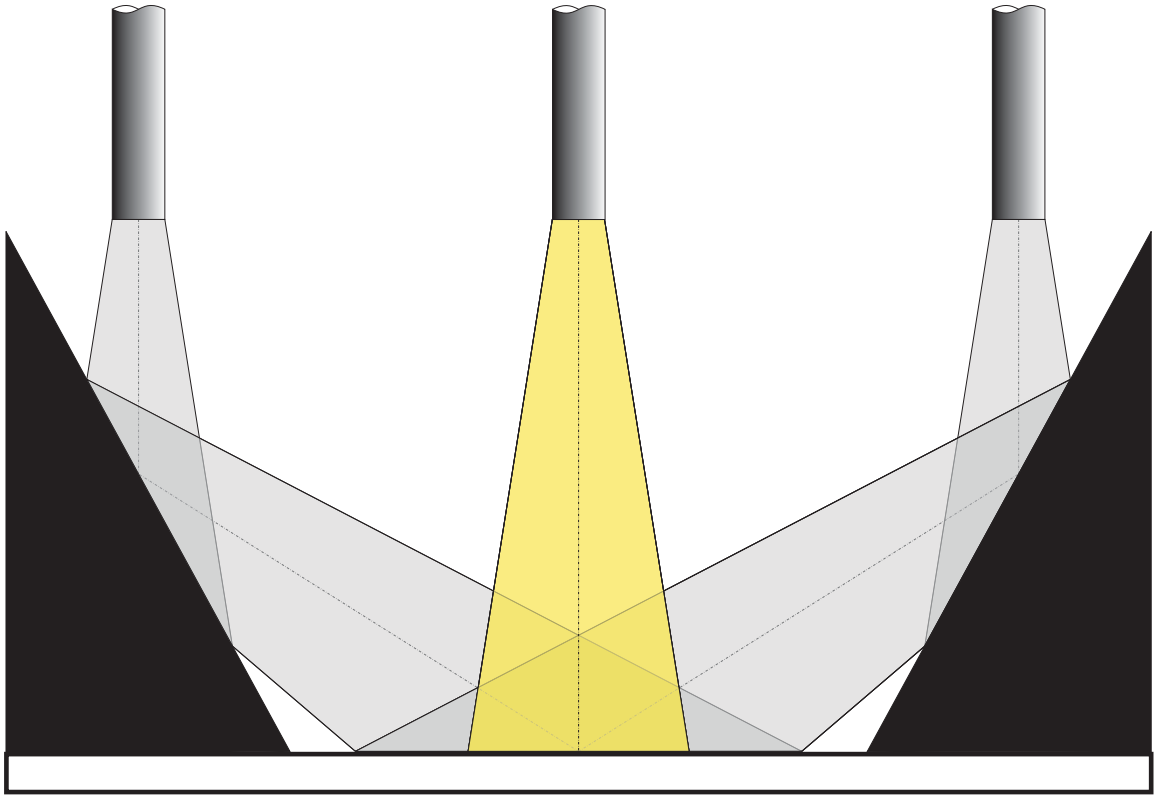

Figure 5 k)

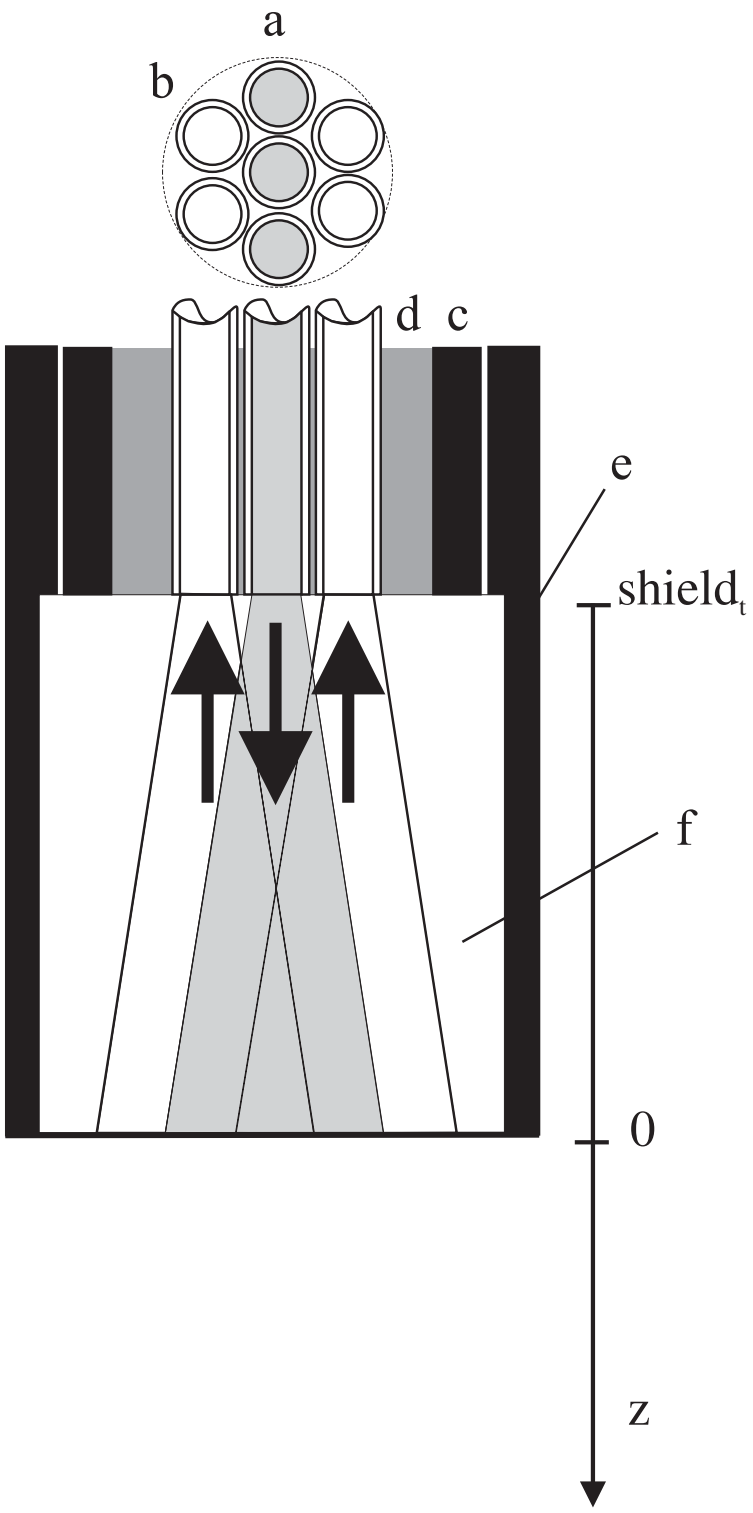

Figure 6 a)

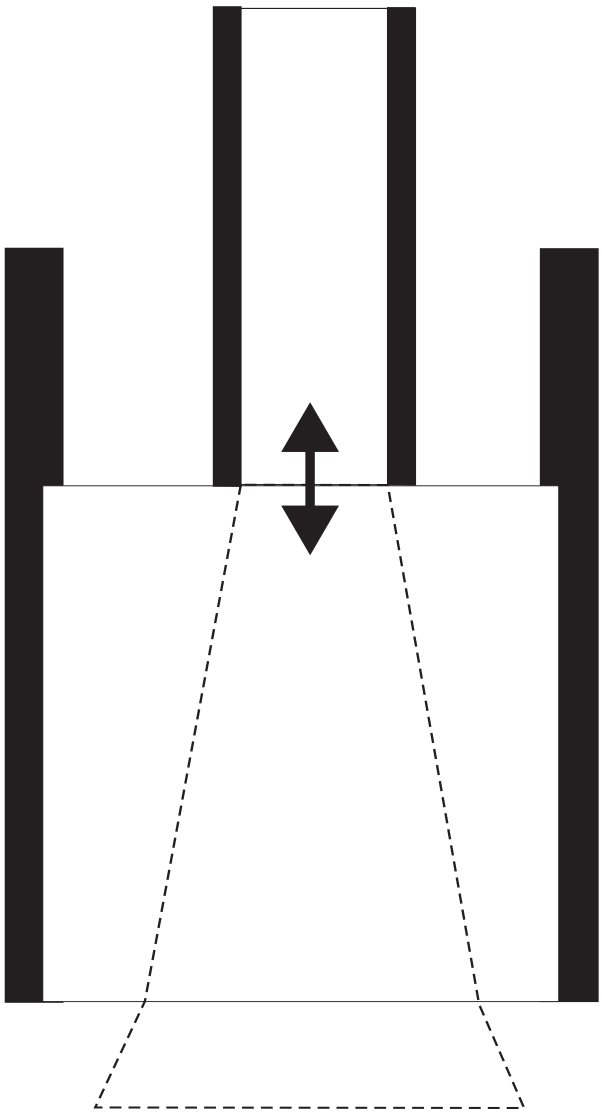

Figure 6 b)

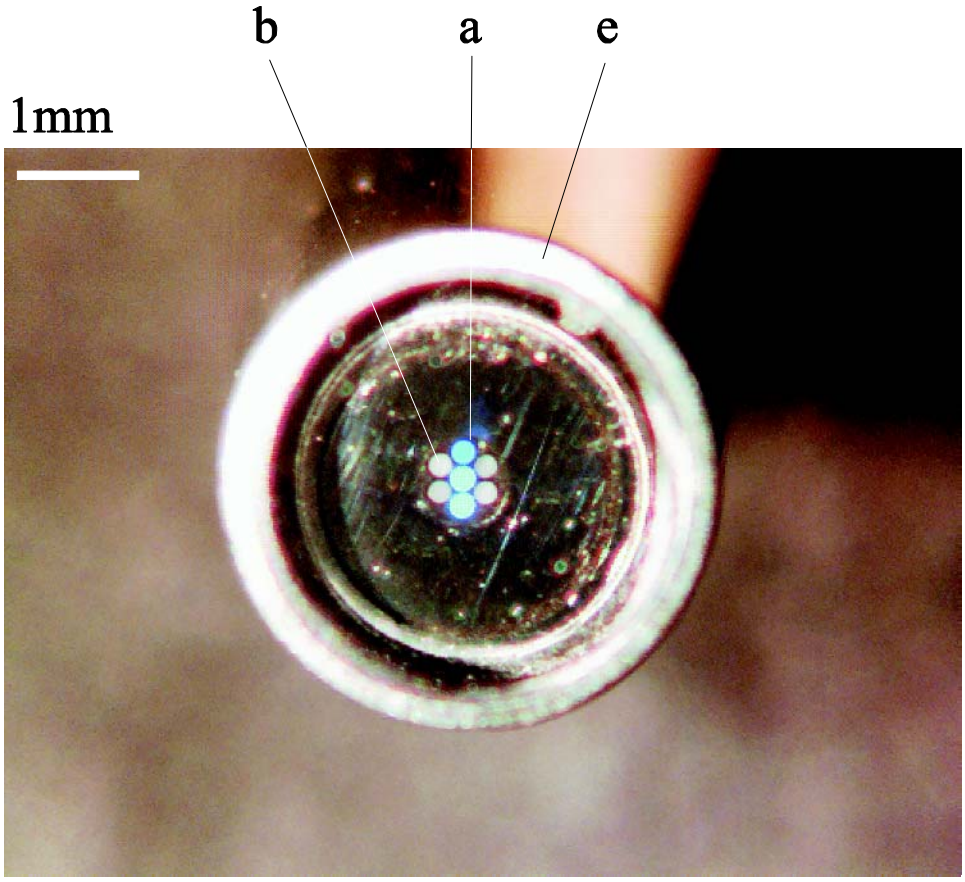

Figure 6 c)

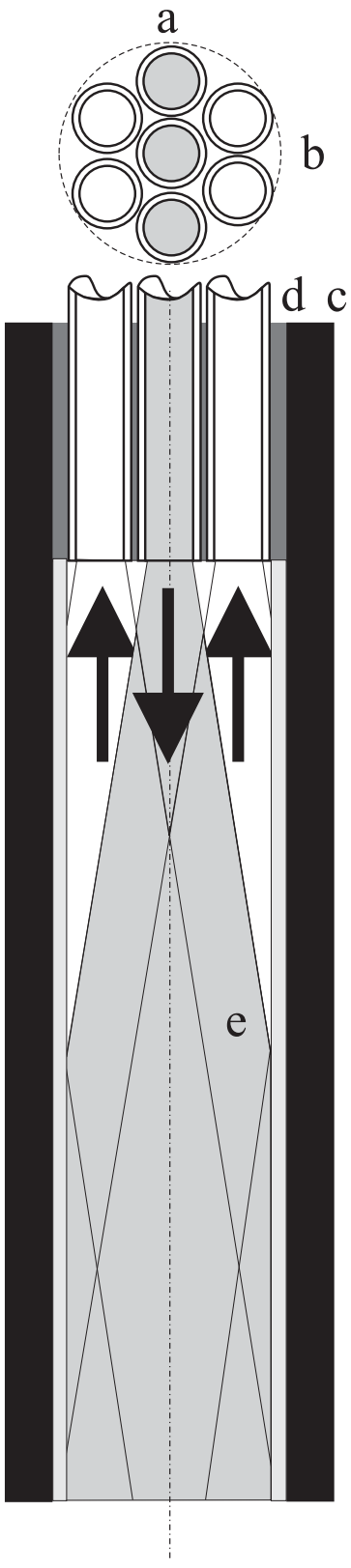

Figure 7 a)

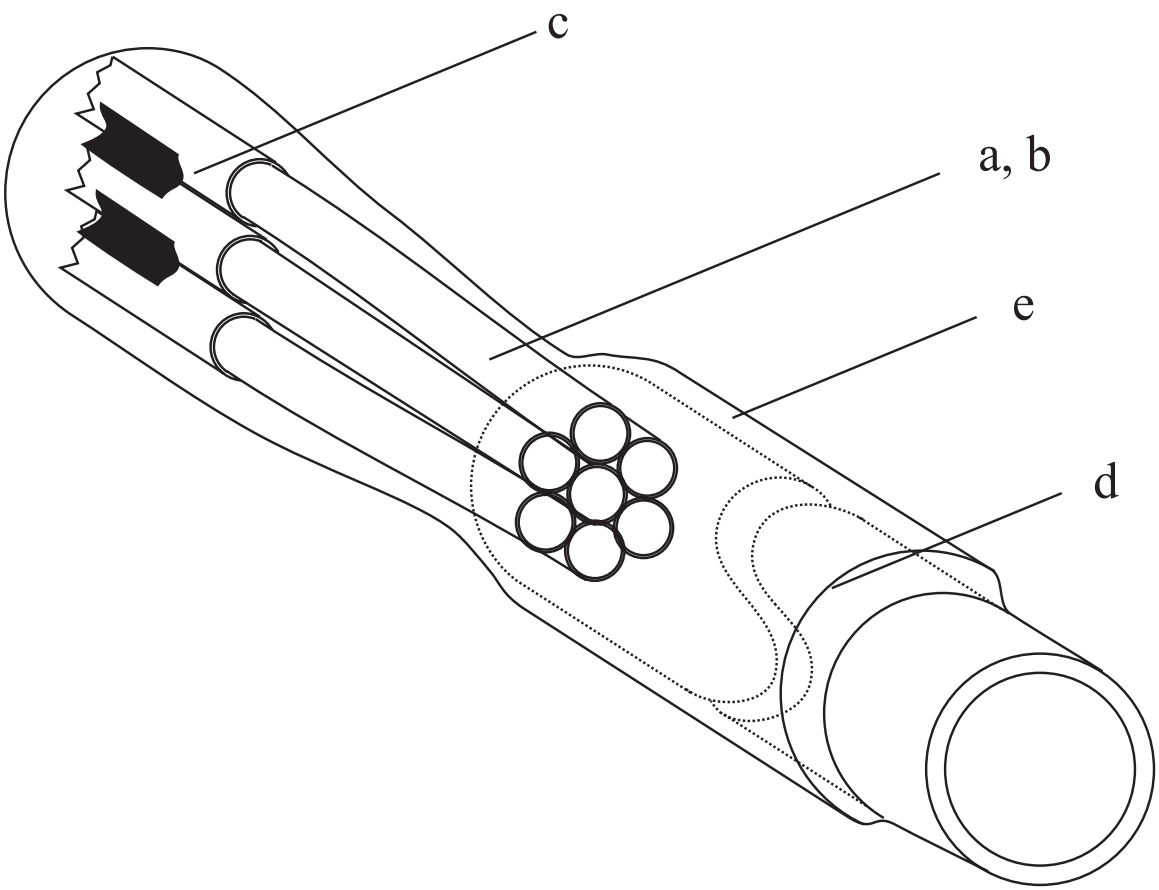

Figure 7 b)

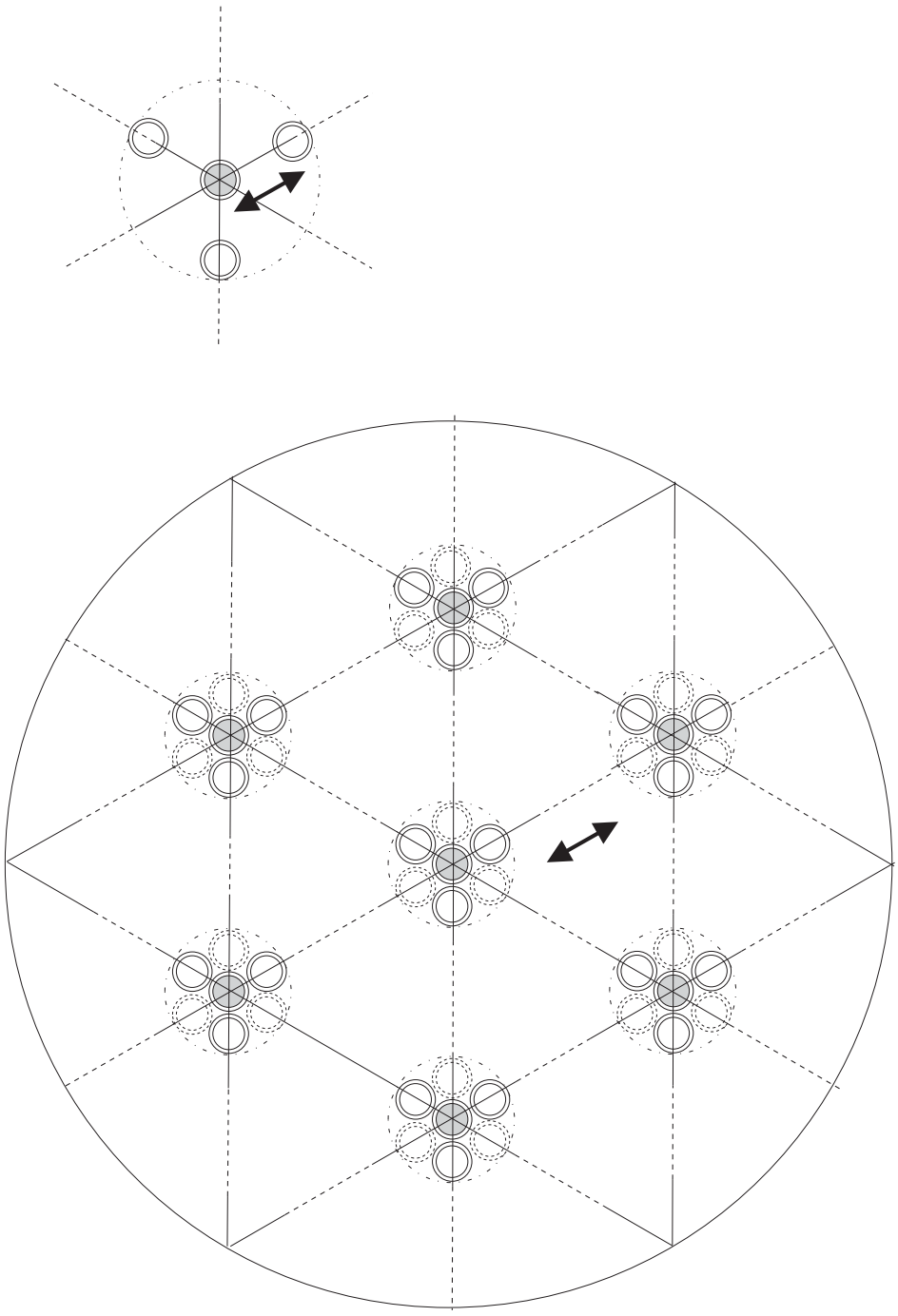

Figure 8 a)

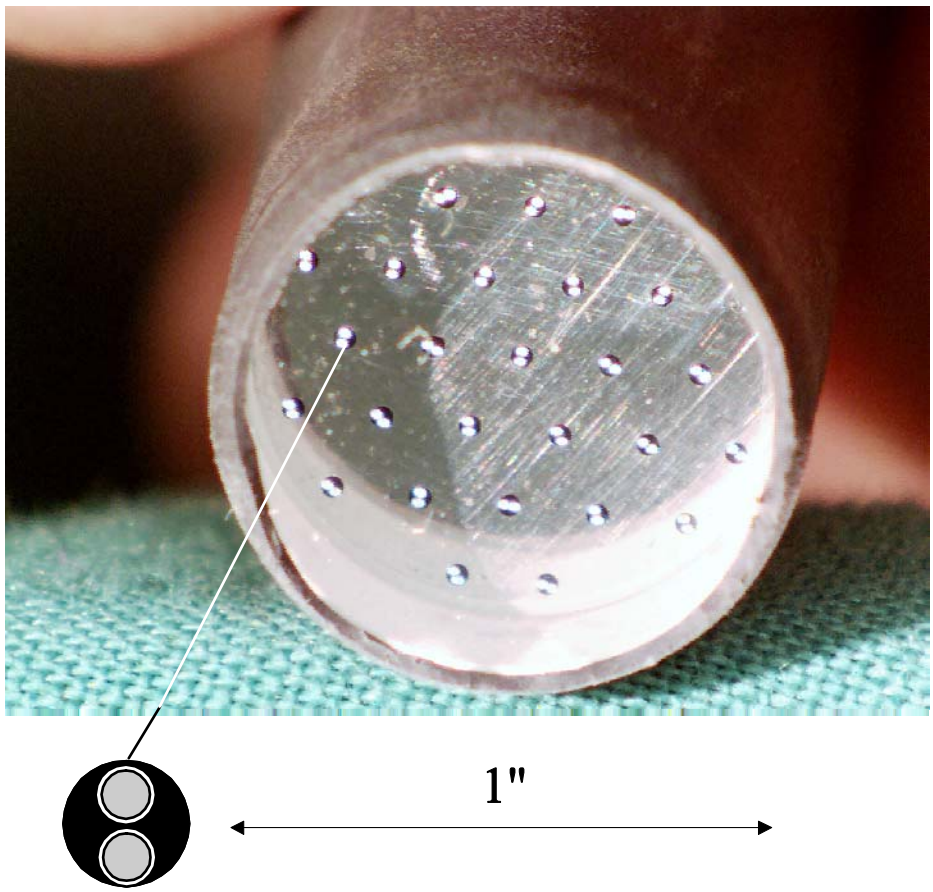

Figure 8 b)

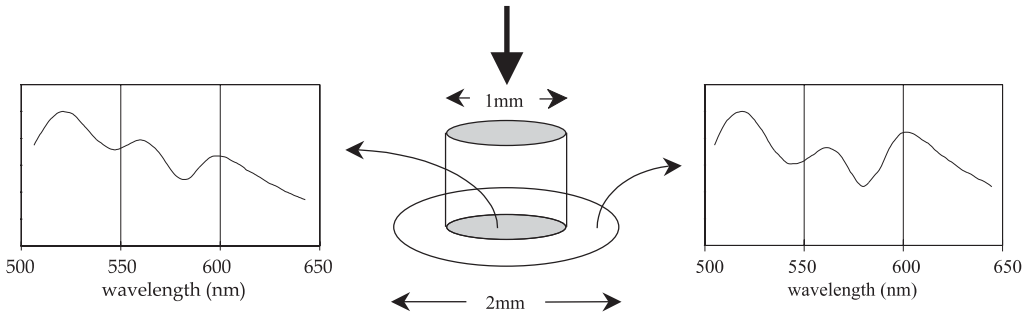
1mm
2mm
500
550
600
650
wavelength (nm)
500
550
600
650
wavelength (nm)

Figure 8 c)

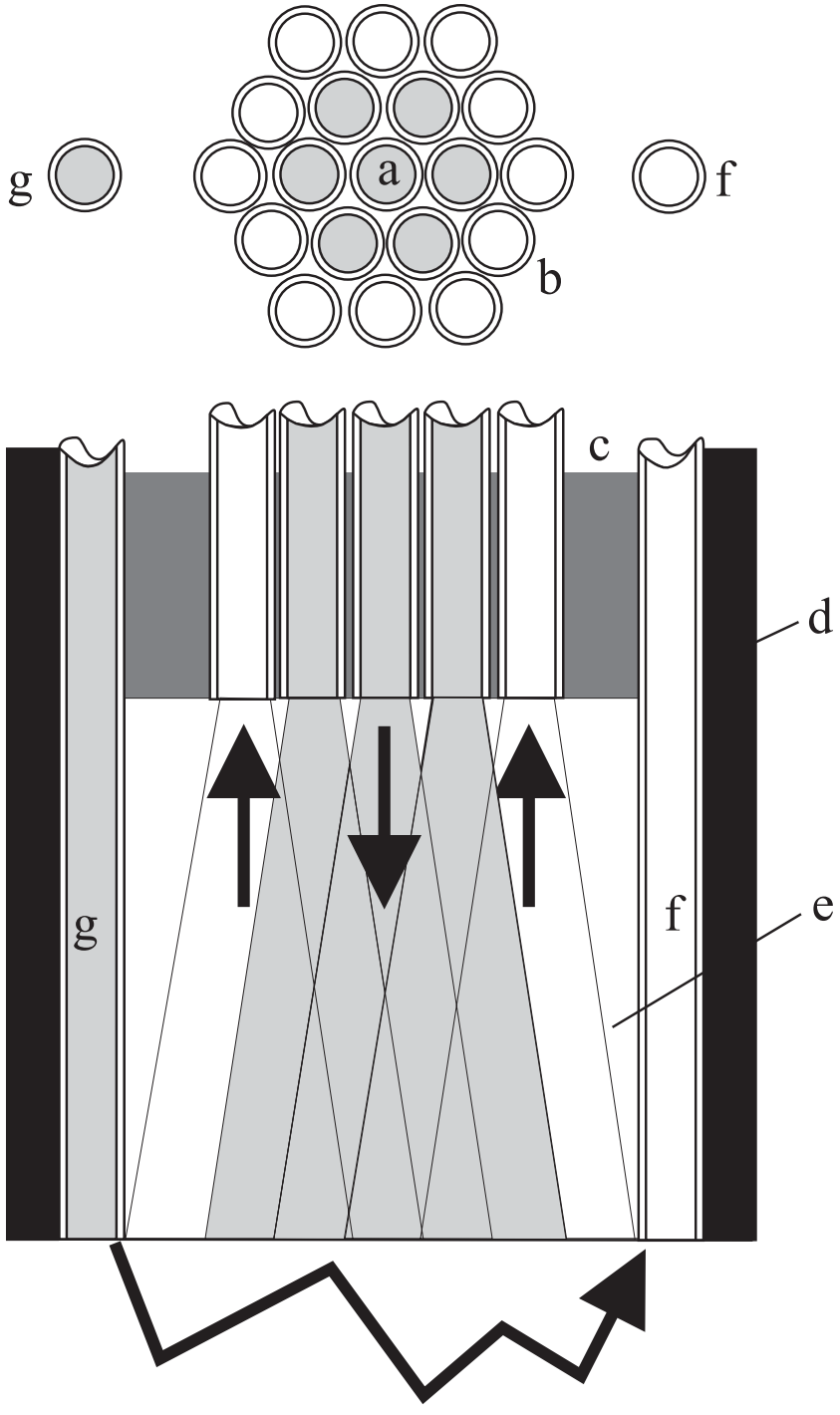

Figure 9 a)

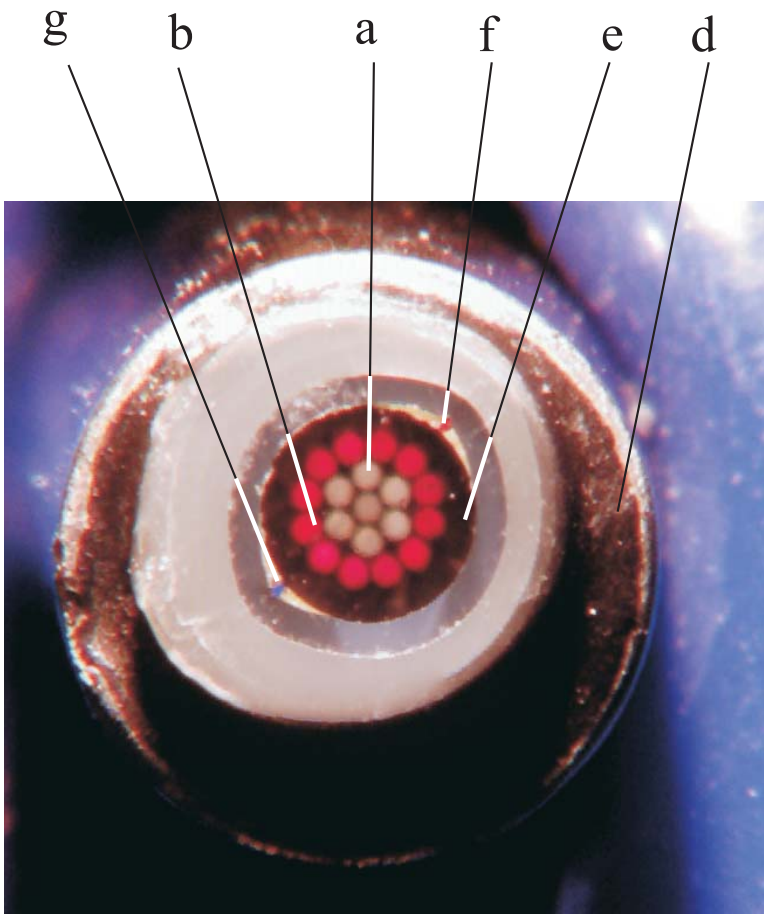

Figure 9 b)

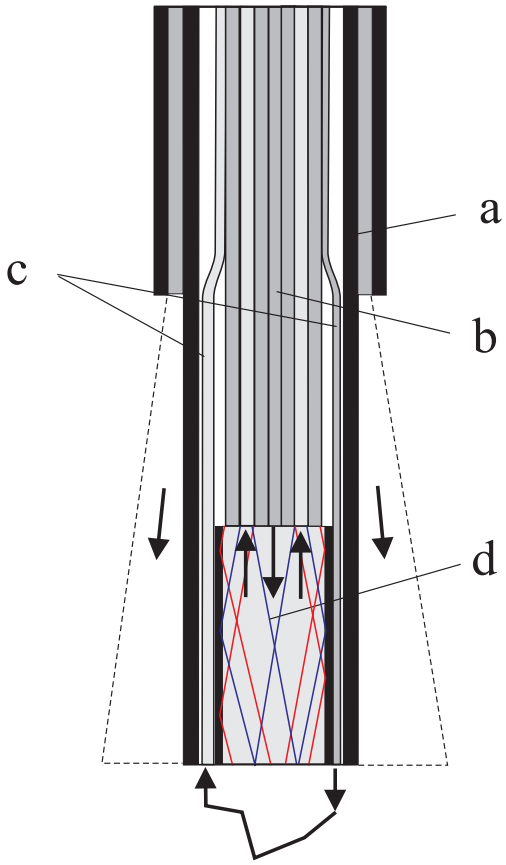

Figure 9 c)

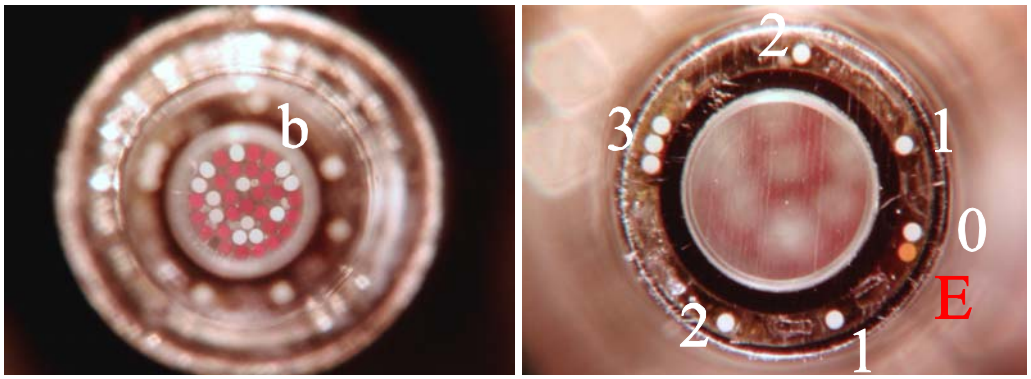

Figure 9 d)

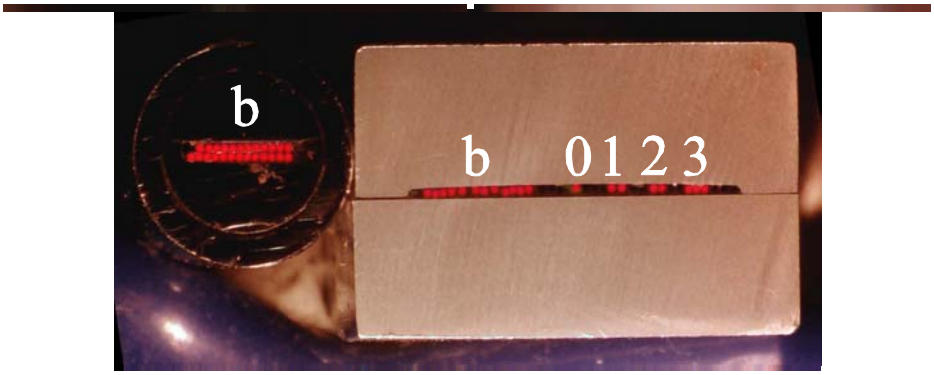

Figure 9 e)

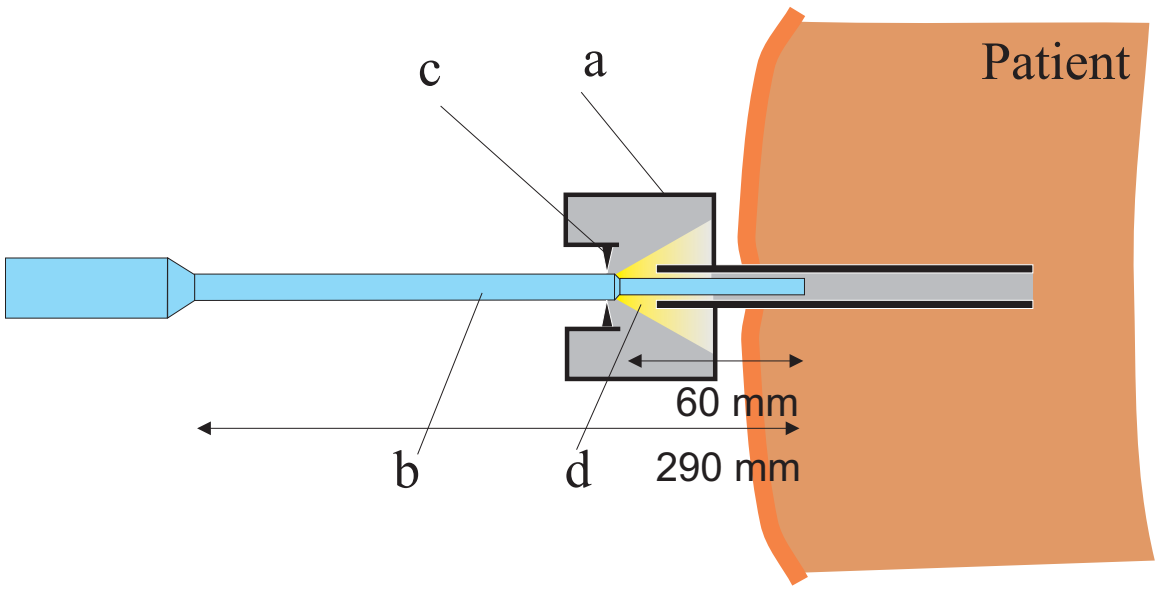

Figure 9 f)

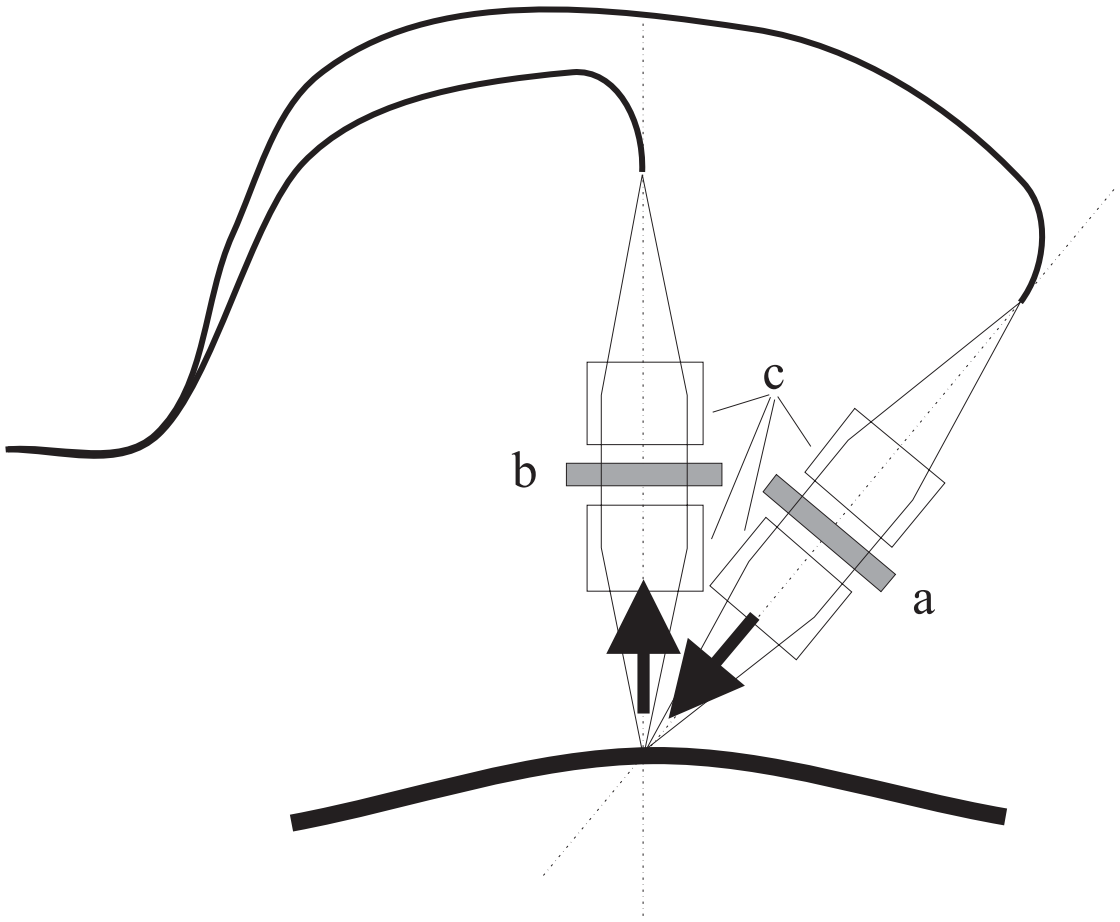

Figure 10 a)

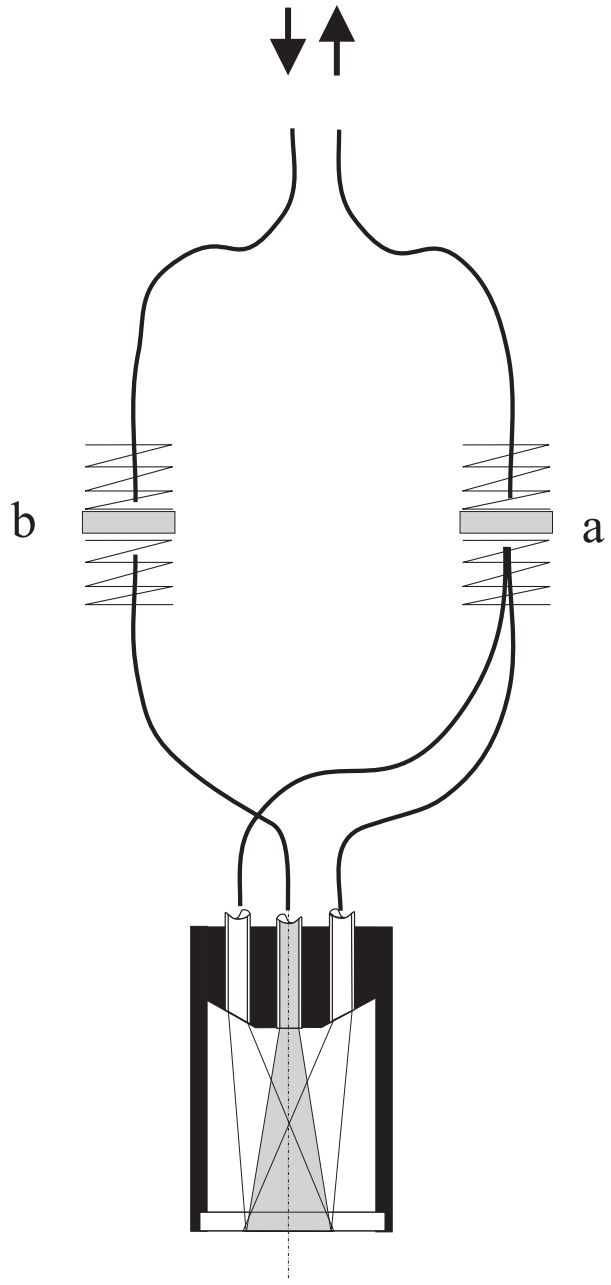

Figure 10 b)

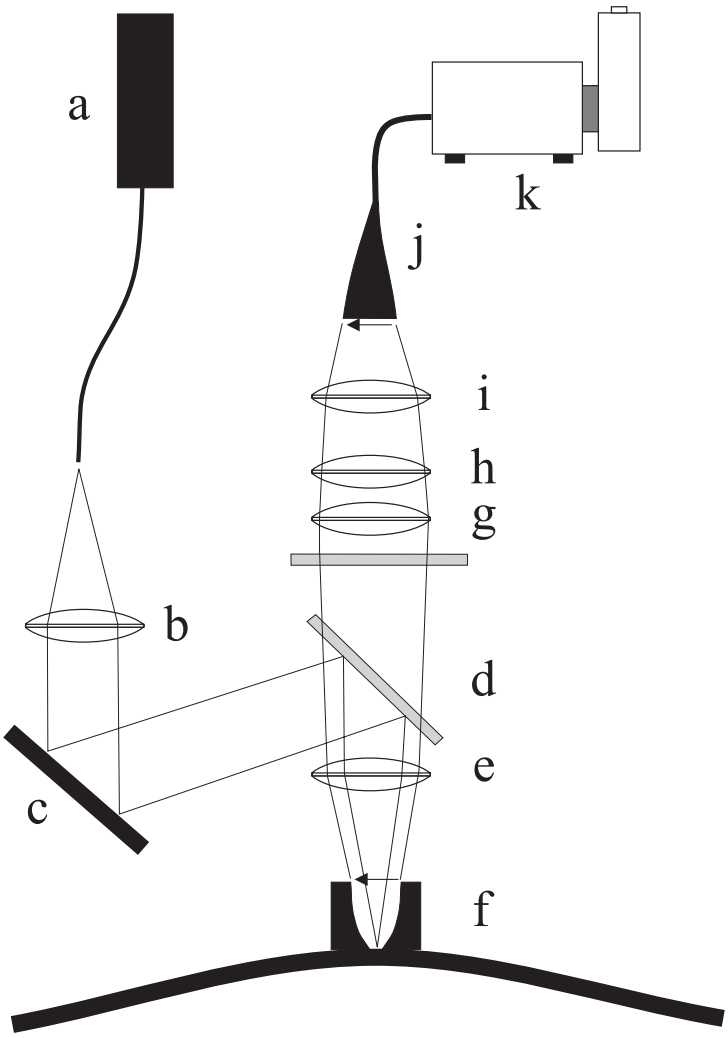

Figure 10 c)

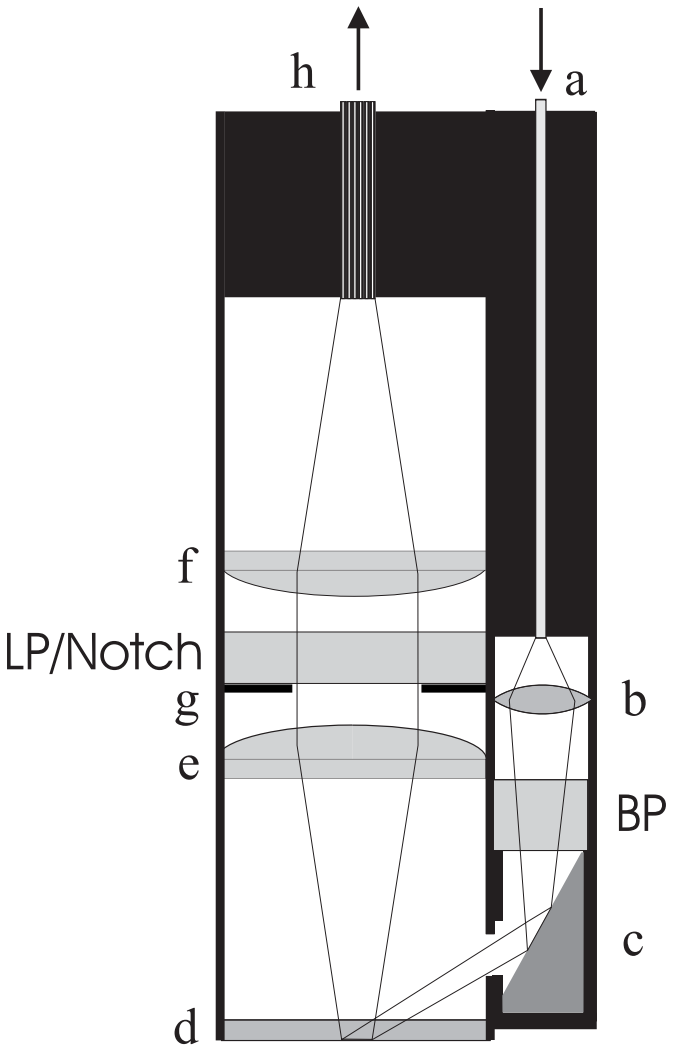

Figure 10 d)

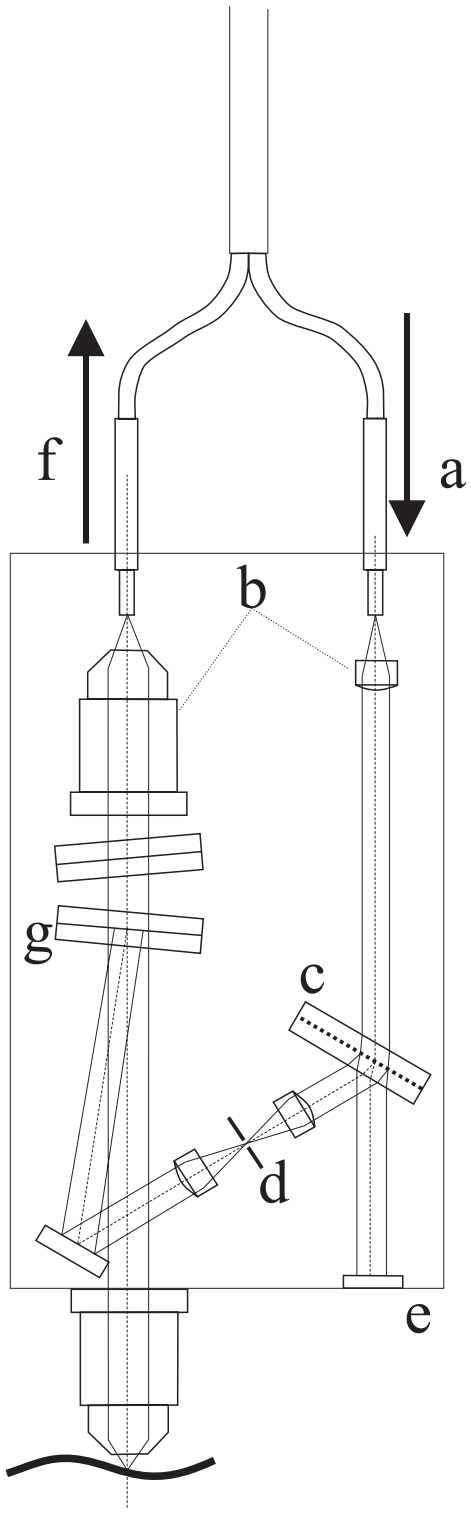

Figure 10 e)

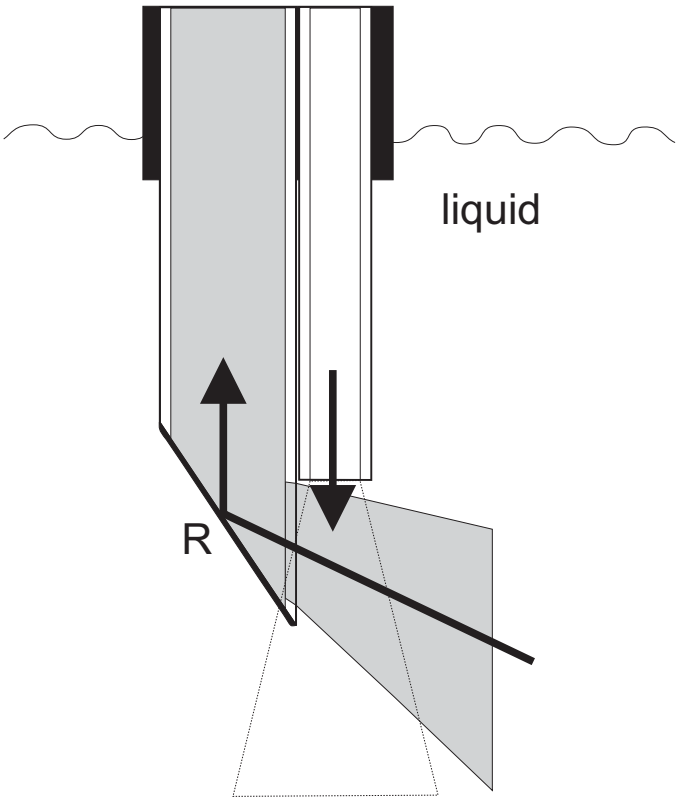

Figure 10 f)

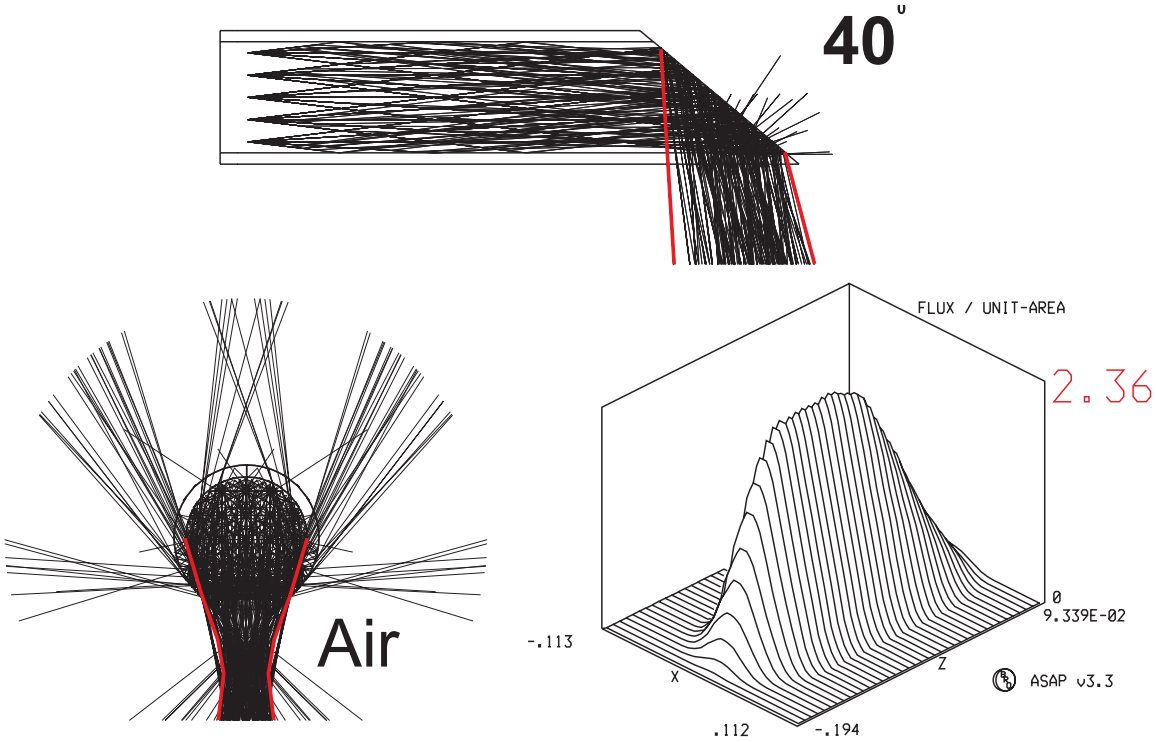

Figure 11 a)

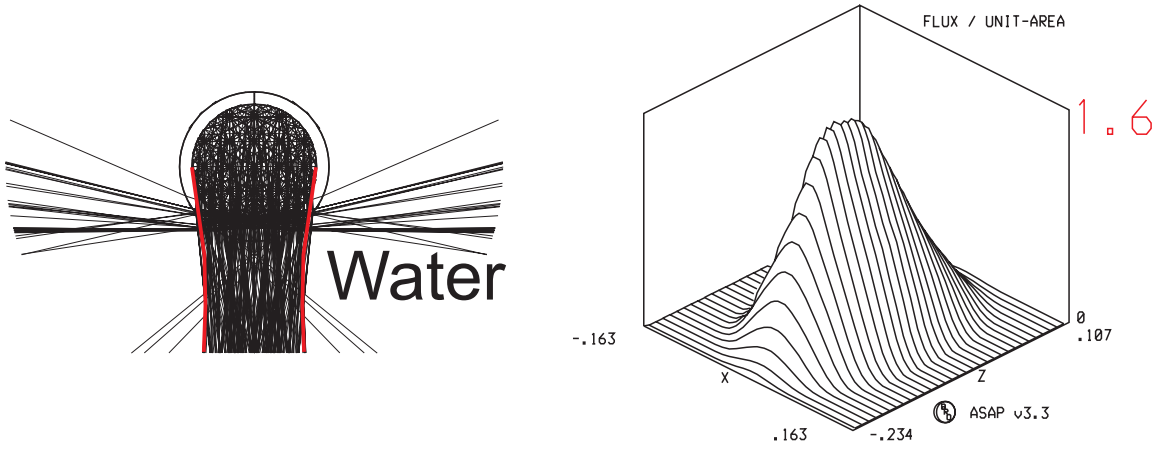

Figure 11 b)

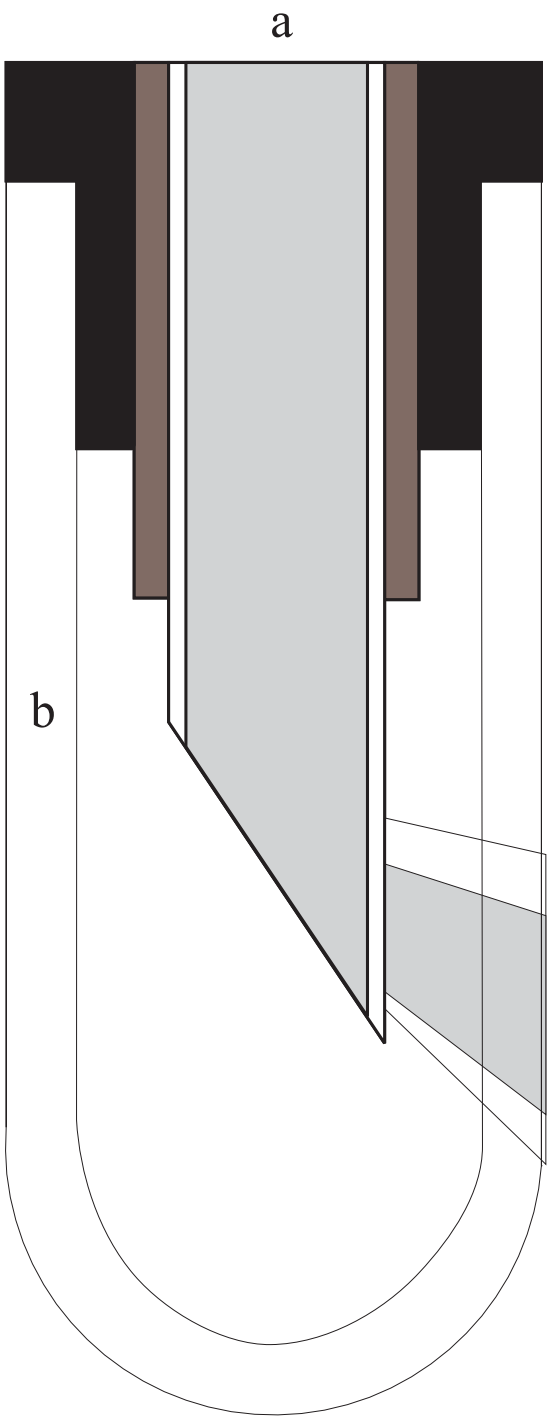

Figure 11 c)

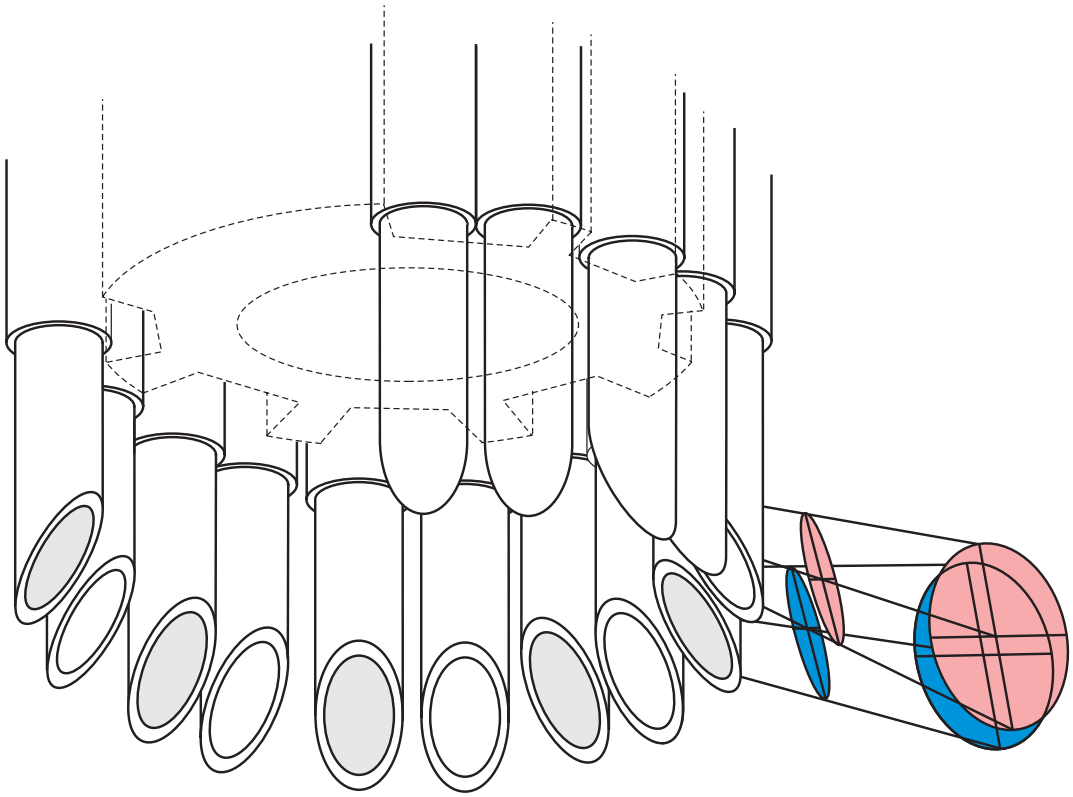

Figure 11 d)

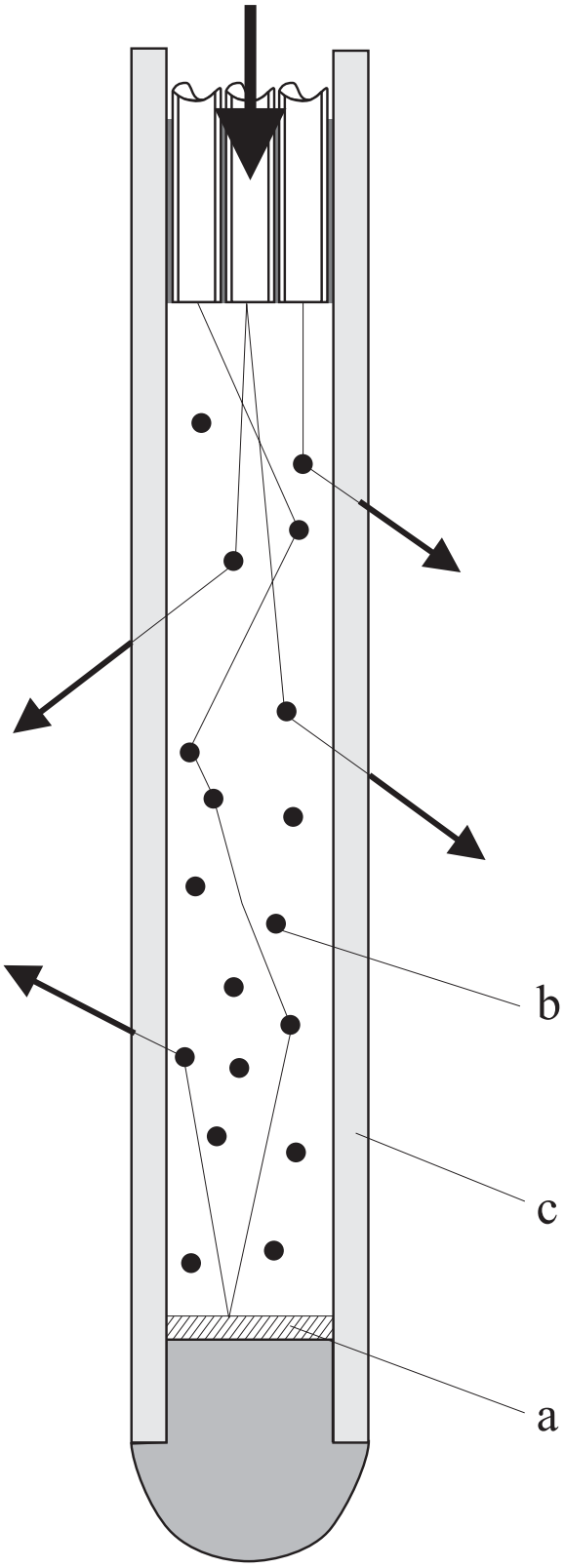

Figure 12 a)

Rare Earth Medical In
Lightstic
Length
Diameter
Wavelength
Serial Number
30 (mm)
0.065 (in)
365 (nm)
A0191.101
A0191.101

Figure 12 b)

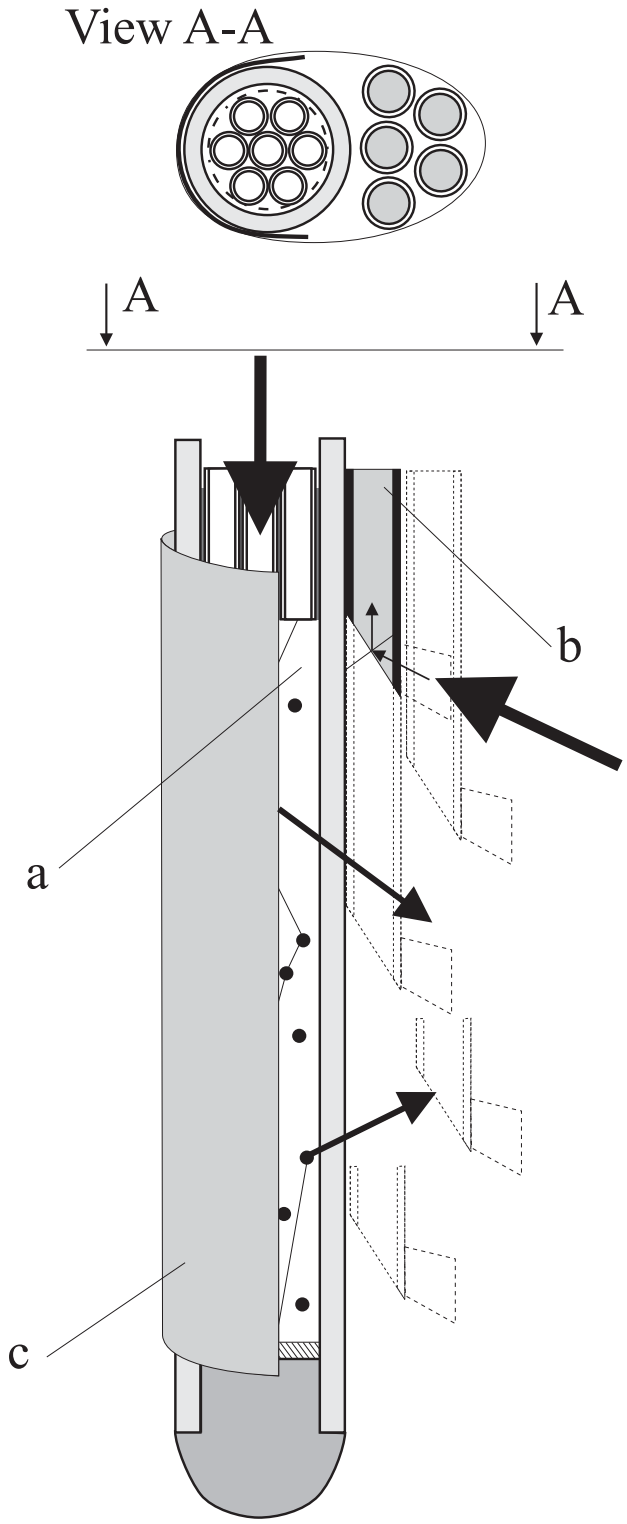

Figure 12 c)

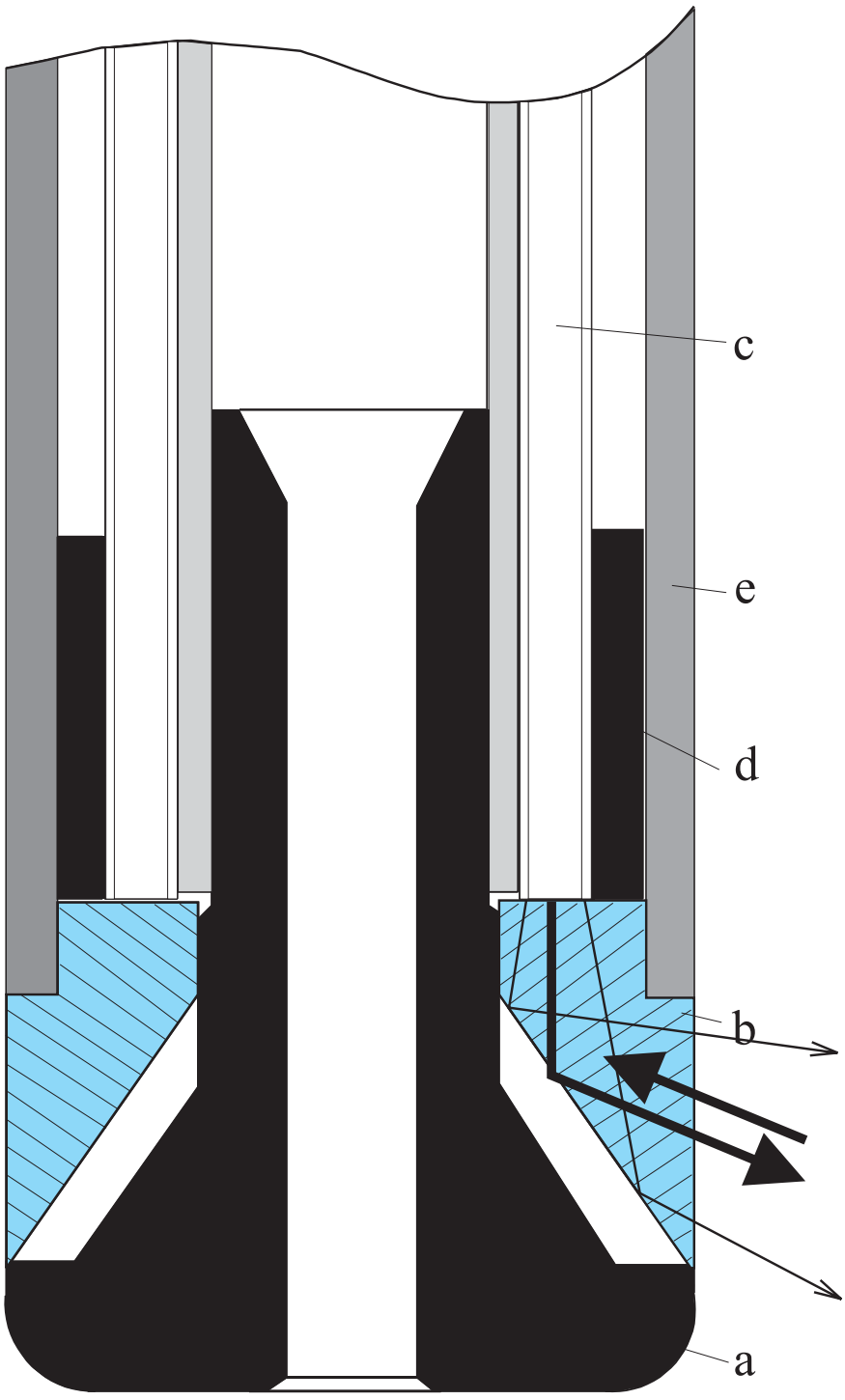

Figure 13 a)

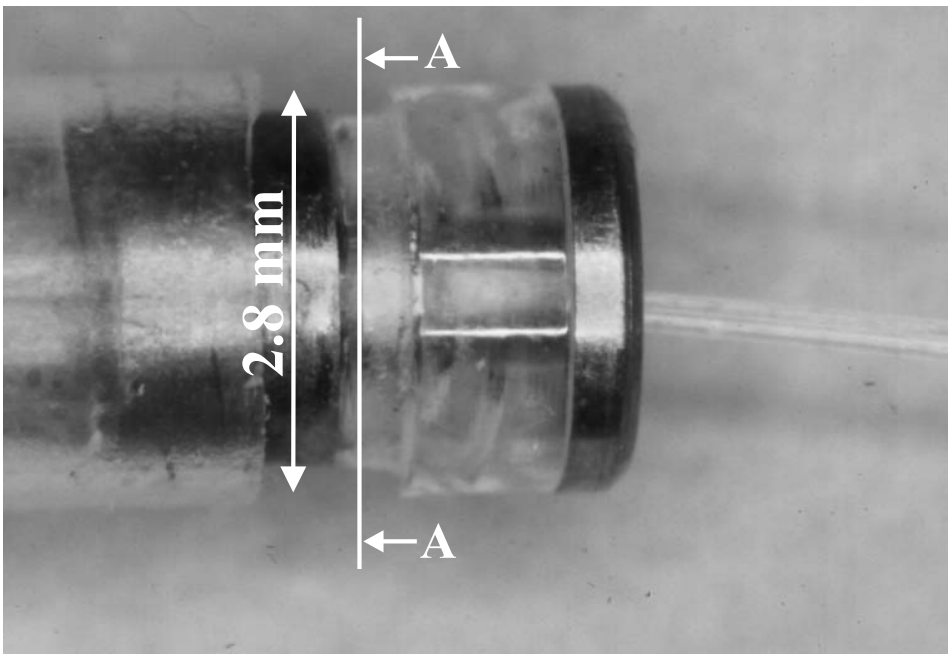

View A-A

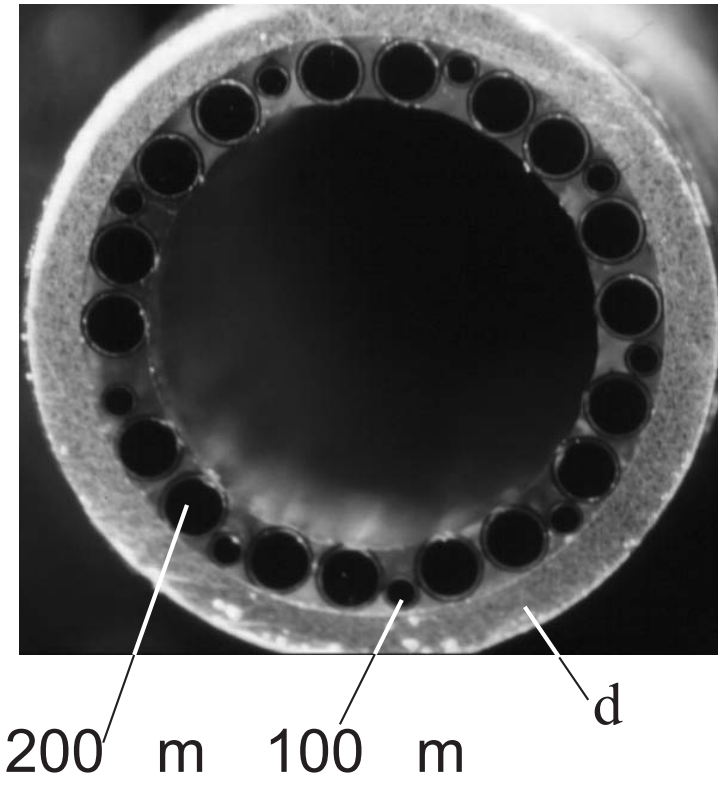

Figure 13 b)

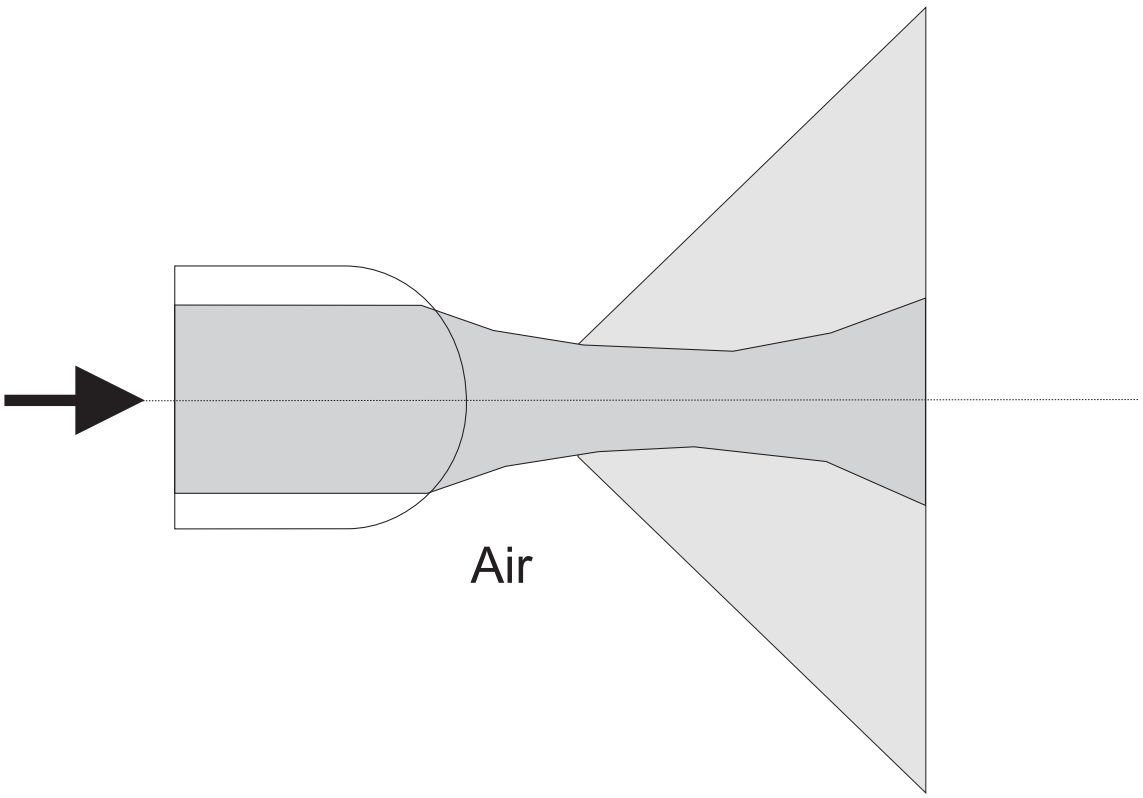

Figure 14 a)

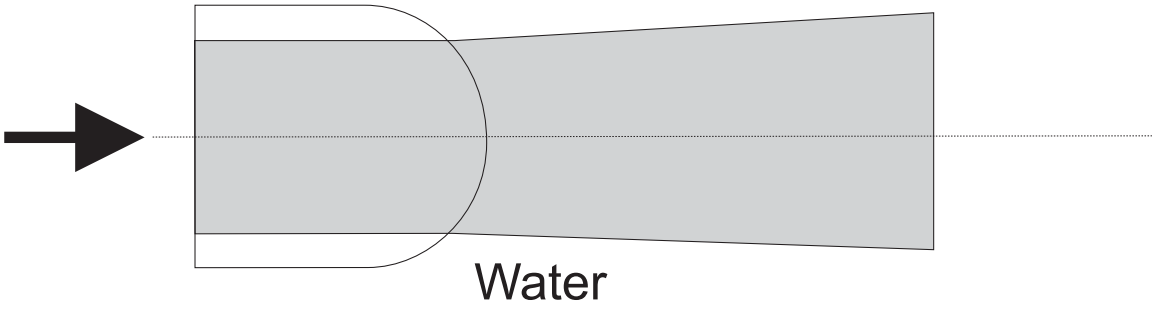

Figure 14 b)

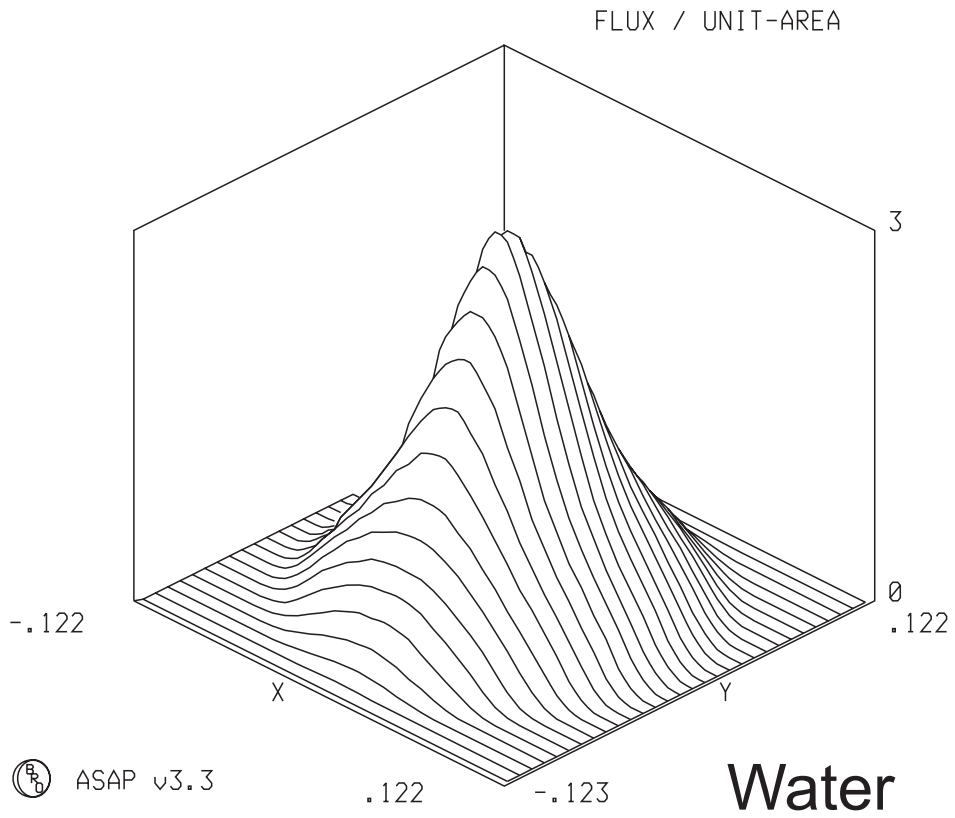

Figure 14 c)

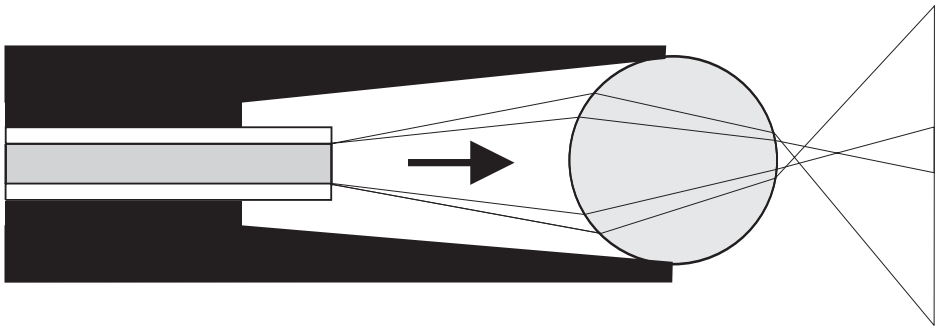

Figure 15 a)

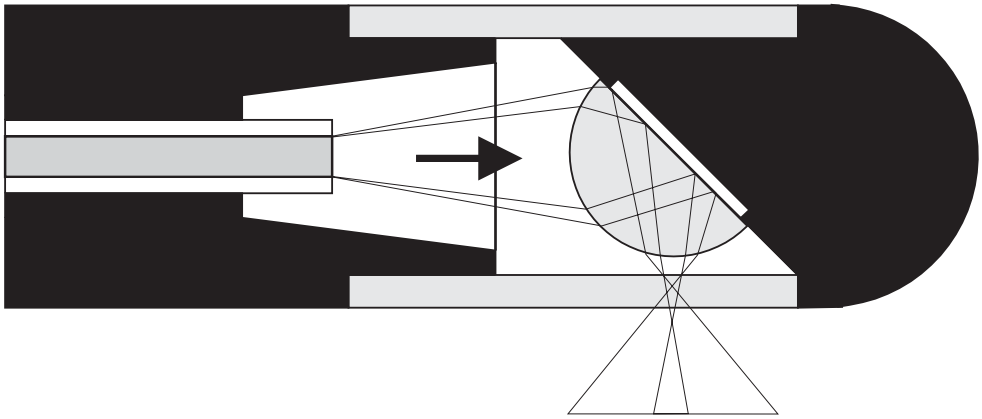

Figure 15 b)

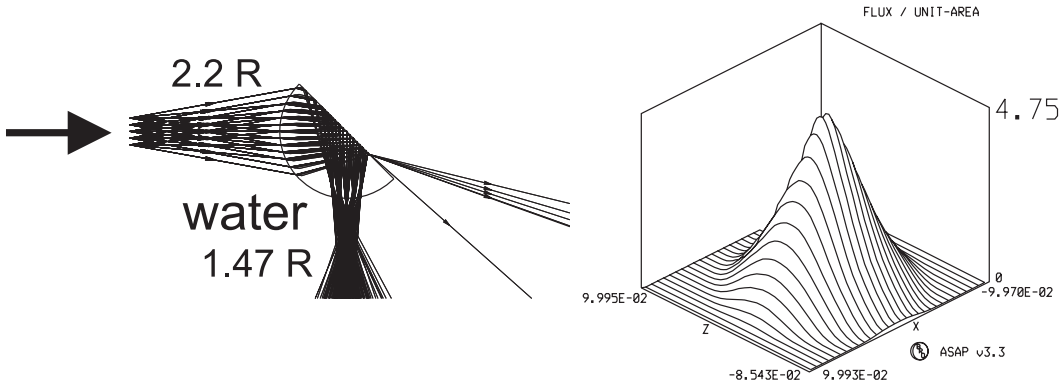

Figure 15 c)

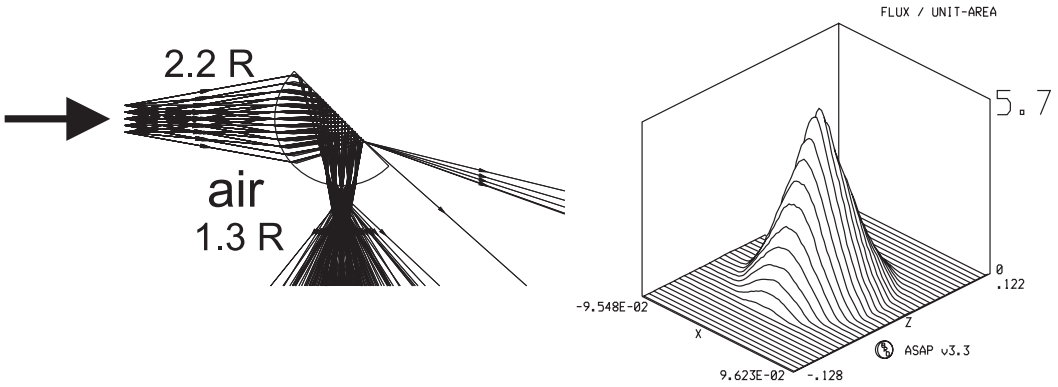

Figure 15 d)

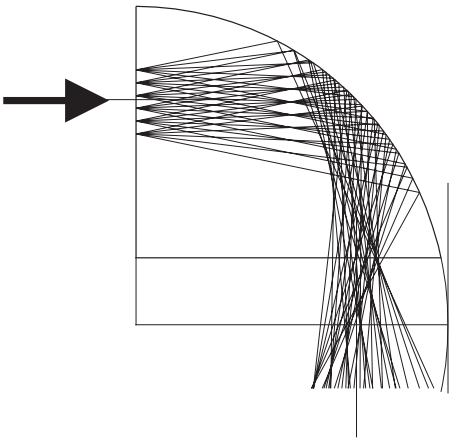

Figure 16 a)

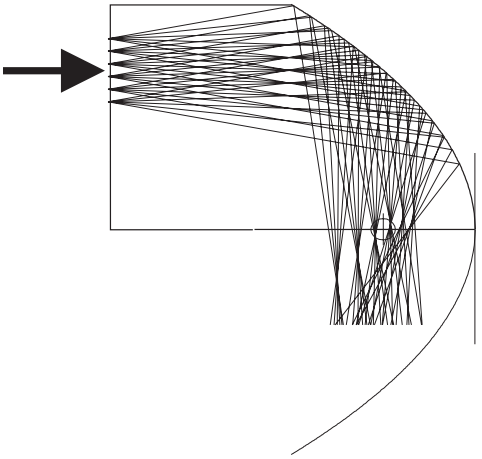

Figure 16 b)

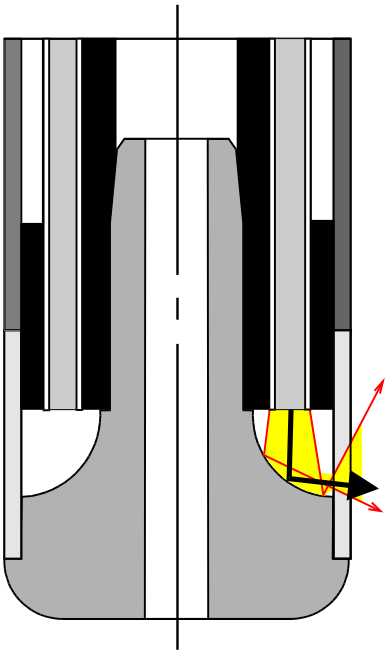

Figure 16 c)

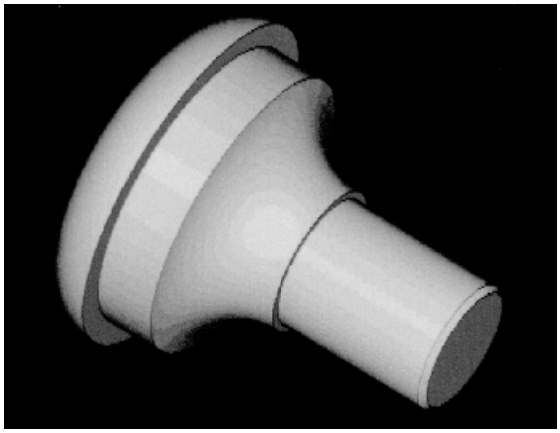

Figure 16 d)

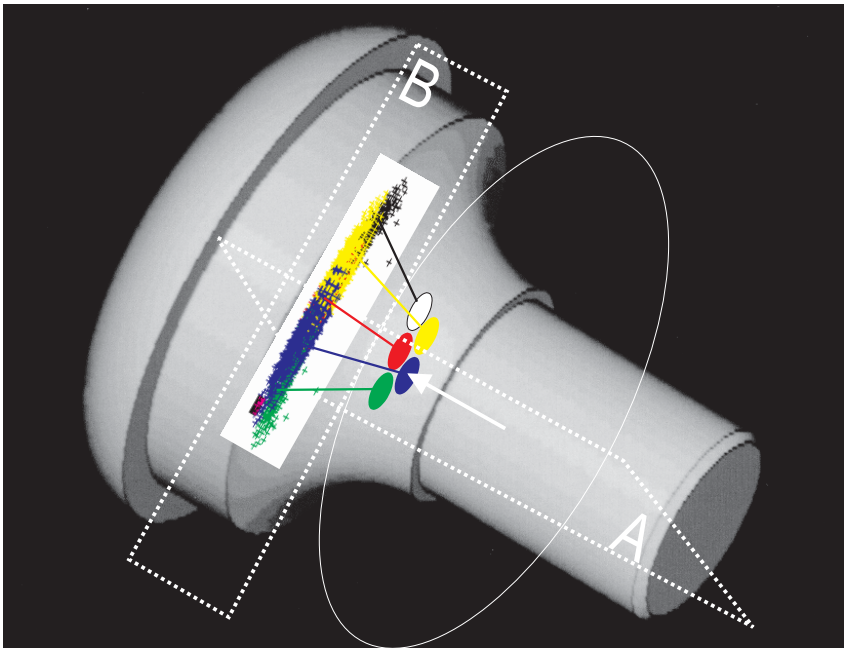

Figure 16 e)

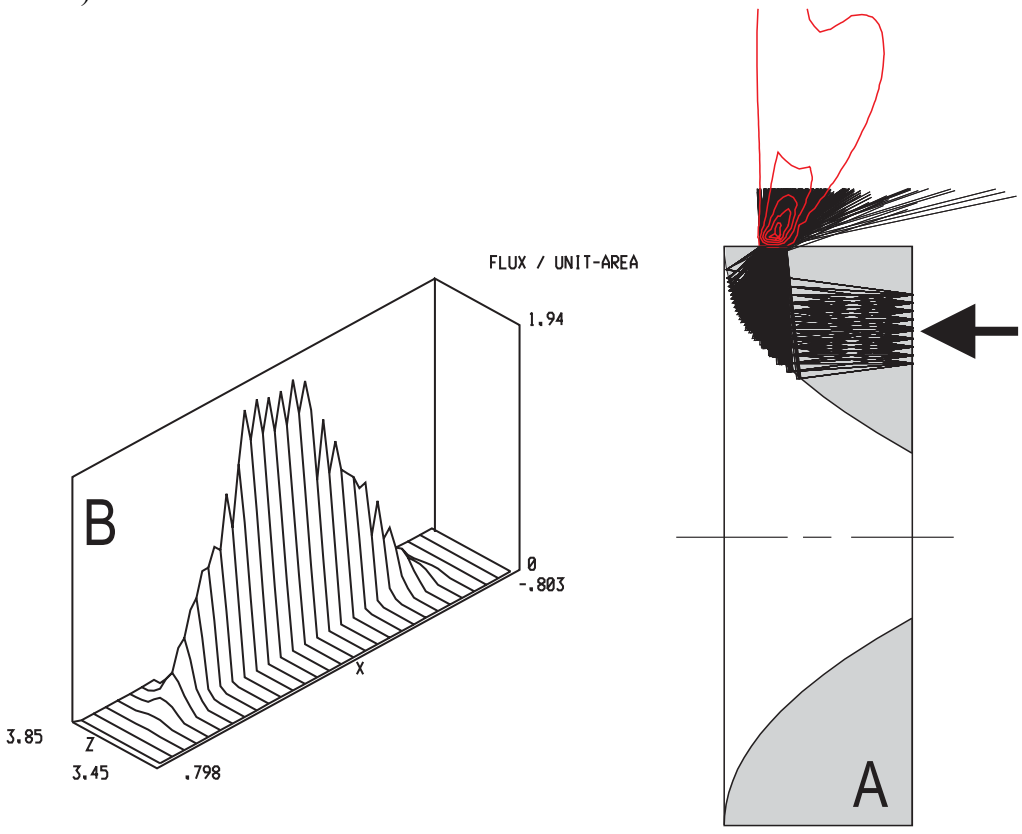

Figure 16 f)